HPT Annex 50

Heat Pumps in Multi-Family Buildings

Task 2.2: Acoustic characteristics of MFH air-to-water heat pumps with description of measures to reduce noise emissions

Country Report

AUSTRIA

Edited by AIT AUSTRIAN INSTITUTE OF TECHNOLOGY **(Ch. Reichl, A. Zottl)**

October 2021, Version 1.2 (FINAL)

Contents

1. Summary

Acoustic emissions are one of the most discussed topics when using air-to-water heat pumps. The topic therefore not only plays an important role in the development of heat pumps, but also in the installation and distribution to the end customer. The topic is also of great relevance for authorities and legislators (e.g. installation regulations or permits).

Currently, in the course of accredited tests of heat pumps, sound emissions are measured according to the principle of sound power measurement to assess the quality of a unit. This measurement gives an indication of the acoustic quality of a heat pump, but important parameters (e.g. tonal components in the noise emission), which are important for the psychoacoustic perception of sound emissions of an air-to-water heat pump, are not taken into account. In the research project "SilentAirHP", sound measurement methods are therefore being developed and tested, which allow a more precise sound characterisation. An overview of the most important results of this project is given here. The methods have been applied to heat pumps in the framework of the IEA HPT Annex 51 “Acoustic Signatures of Heat Pumps”. Also, results from these measurements are summarized here. Acoustic measurements have also been performed on the innovative heat pump prototype from the EU research project "GreenHP". These measurements are also discussed in this document. Finally, a 5 channel acoustic measurement technique is proposed and linked to a visualization tool to allow virtual heat pump placement accompanied by acoustic calculations. Acoustic sound field calculations are also briefly discussed.

Based on the results of this work in the Annex, recommendations for the design of MFH heat pumps will be derived and disseminated. Furthermore, measurement services are to be derived from the findings and presented for international discussion within the framework of the Annex. This should subsequently form a basis for standardization and ultimately lead to better testing standards. Dissemination of the results will take place by means of workshops with heat pump manufacturers in cooperation with the Heat Pump Association.

This report covers the analysis of Air-to-water heat pumps with special focus on acoustic characterisation. In addition to this experimental work a chapter discussing acoustic measures to reduce noise has been added. It covers an analysis of unit placement, indoor & outdoor sound propagation, the potential of sound absorption at nearby surfaces and a introduction to common “unclever” decisions in heat pump placement. The latter is additonaly discussed by introducing the HVAC Positioner and the related 5ch Acoustics system.

2. Introduction

The following sources of information have been made available for this report of Task 2.2 and are discussed in the following subsections:

- Development of methods and noise emission studies in the project SilentAirHP
- Findings of the IEA HPT Annex 51 “Acoustic Signatures of Heat Pumps”
- Acoustic measurements of the GreenHP developed as prototype in the EU FP7 project “GreenHP”
- Development of the measurement service “5ch Acoustics” as base for heat pump placement assistance and aurealization

- Method development “HVAC positioner” in the field of augemented reality with a focus on acoustics
- Sound field simulations for the selection of heat pump positions in multi-heat-pump environments
- Dome measurements of a commercial two fan heatpump
- Acoustic Measures to reduce noise

3. SilentAirHP

Air-to-water heat pumps (A/W heat pumps) have become increasingly popular in recent years due to their advantages such as small space requirements, comparatively low purchase costs, simple installation, etc. and are among the most sold heat pump systems for heating or cooling residential buildings in Europe. In addition to the annoying noise of the compressor, the high air volume flow required by the heat pump often causes annoying noise from the fan and evaporator. Especially during the transitional season, additional noise is generated due to icing of the evaporator. All these annoying noises often trigger neighbourhood conflicts with health, psychological and financial consequences, and can thus become a competitive disadvantage of the technology in the future and hinder its widespread use, especially in residential areas. The measures currently proposed in the literature, in the acoustic guidelines of heat pump associations, etc. to minimise the disturbing noise emissions include constructive, component-specific, control and active measures, whereby their effect on noise emissions is usually only assessed qualitatively. The simultaneous effects of these noise reduction measures on performance, COP (Coefficient of Performance), noise emission and psychoacoustic perception are currently not quantitatively evaluated, which means that the heat pump industry (in particular heat pump manufacturers, installers, planners) does not know which of the common measures is most optimal for the heat pump system as a whole.

SilentAirHP therefore aimed at developing advanced numerical and experimental methods for the quantitative evaluation of noise reducing measures for A/W-HP in order to support national manufacturers in the medium term in the new development or retrofitting of their A/W-HP. In order to achieve this goal, in the project acoustic measurement methods have been developed, which can distinguish and localise sound sources with frequency resolution. In parallel, overall system simulations have been carried out which take into account the sound emission (even during icing of the outdoor unit). These models are necessary in order to subsequently develop control engineering noise reduction measures. In addition, a modular L/W heat pump is being built, which is as close as possible to the industry, and which will be used for experimental investigations of noise reduction measures. Besides the quantification of selected "passive" measures, the use of anti-ice coatings for icing and defrosting, as well as noise cancelling as an "active" measure have been tested, adapted and evaluated in the project. Together with the Institute for Sound Research (ÖAW), selected sound reduction measures has also be psychoacoustically analysed and evaluated.

The project result comprise on the one hand a quantitatively evaluated catalogue of measures for known and novel noise reduction measures, and on the other hand a detailed system description of an A/W-HP, which for the first time took into account both the icing behaviour and the noise emissions.

The FFG project "SilentAirHP" involved a detailed evaluation of noise reduction measures for air-to-water heat pumps using the acoustic dome (see figure 3.1). The contributions to noise emission of

different typical components of heat pumps are investigated in detail. A catalogue of measures was developed and disseminated based on the findings.

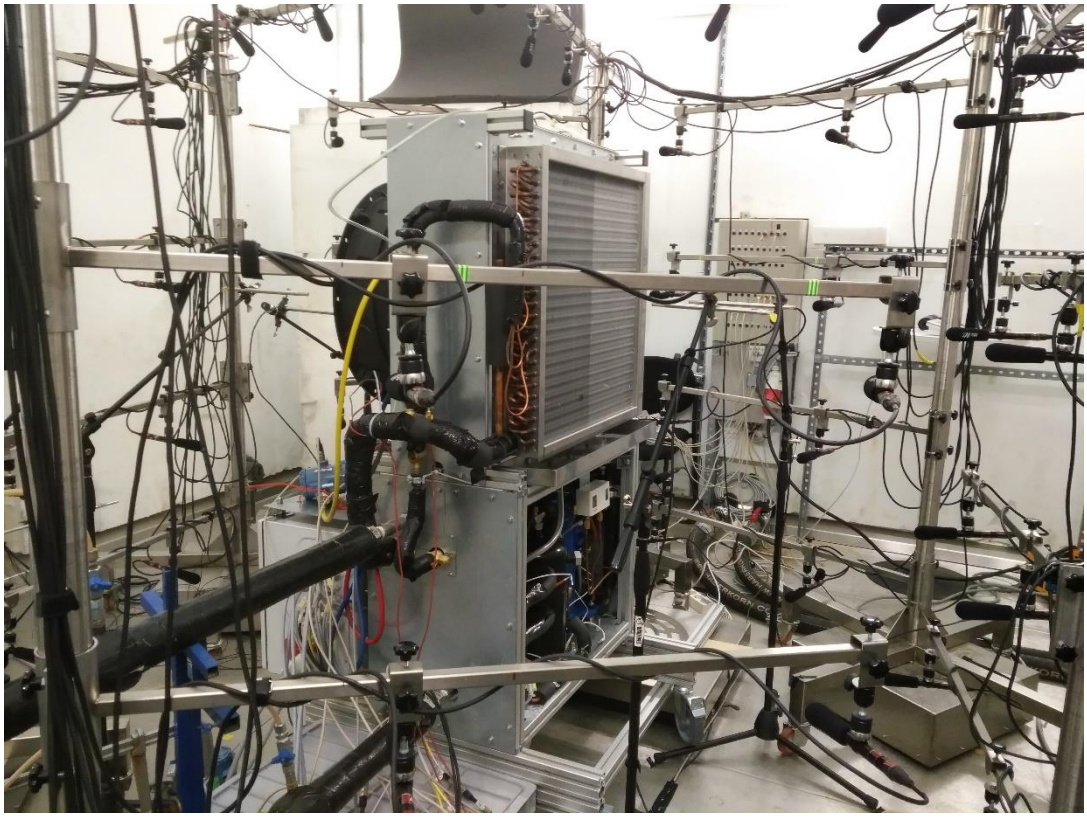

Figure 3.1: Messaufbau der SilentAirHP in der Klimakammer mit 64 Kanal Mikrofon-Dom, transienter Gewichtsbestimmung und synchroner Messung von Akustik und vier Vibrationssignalen.

Here, the icing of a heat exchanger of an air-to-water heat pump was chosen as an example for the consideration of emissions at component level. Figure 3.2 shows the calculated A-weighted sound power level of the air-to-water heat pump in state A7W35 over a period of 200 minutes. During this time defrosting takes place three times with a typical interval of normal operation of a little more than one hour. Defrosting is indicated by a decrease in electrical power consumption and sound power level. The small increase in electrical power and sound power level during defrosting is attributed to the operation in circuit reversal. The typical increase in sound power level during icing of the heat exchanger after a defrost is about 5 dB(A) in this mode.

The upper part of figure 3.3 shows the frequency-resolved sound power level in the time window around a defrost with a duration of about 330 seconds. During this time several light green and yellow "lines" are visible, corresponding to the increase and decrease of the frequency of the compressor and fan. The lower part of figure 3.3 shows the frequency-resolved sound pressure level at a selected microphone position. The range of 330 seconds again corresponds to the period of time when the four-way valve is switched to allow reverse operation to heat up the heat exchanger for defrosting. It is possible to follow various small acoustic bands that change their frequency (y-axis) due to changes in the speed of the fan and compressor: First the compressor and fan (1) stop, followed by the first switching of the 4-way valve (2); then the compressor restarts at reduced speed (3) in several stages for reverse operation and is stopped again (4); after the 4-way valve (5) is switched back, the compressor and fan are restarted to full speed (6), marking the start of normal operation. Comparing

the results of the 60 different microphones positioned around the heat pump during the tests, a sound pressure level range of 5 dB(A) can be established as a directional dependency of the sound emissions for the selected air-to-water heat pump. The acoustic measurements can also be combined with time-correlated vibration measurements - this provides information about the origin of acoustic emissions from propagation mechanisms [14], [15].

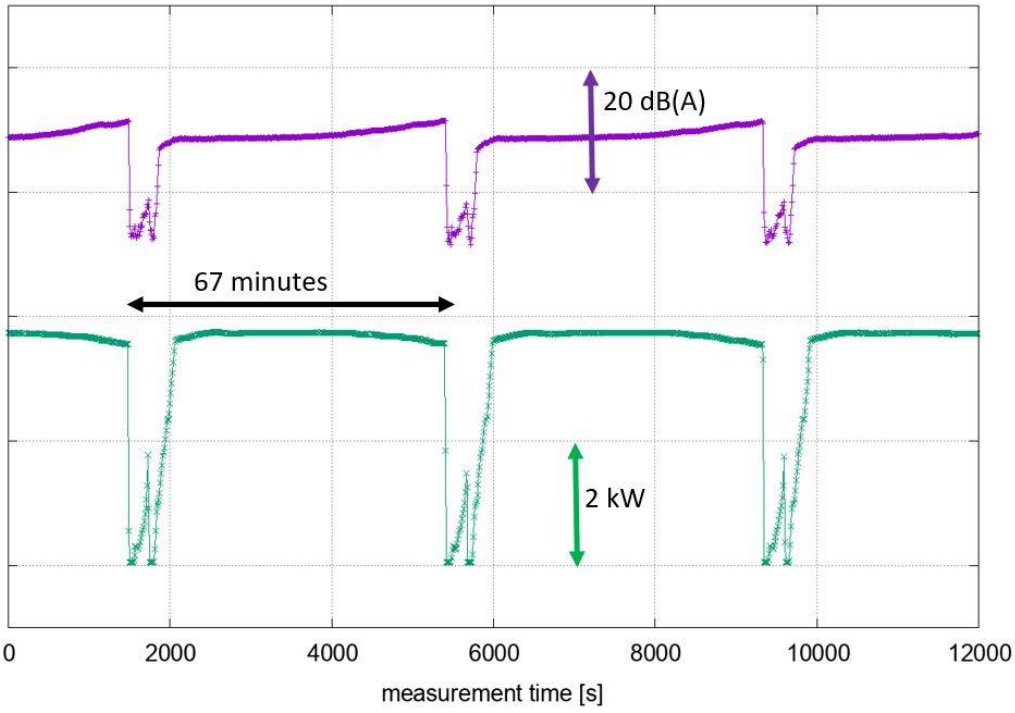

Figure 3.2: A-weighted sound pressure level and electrical power consumption of an air-to-water heat pump. Several defrost cycles are shown (source: AIT, Austria)

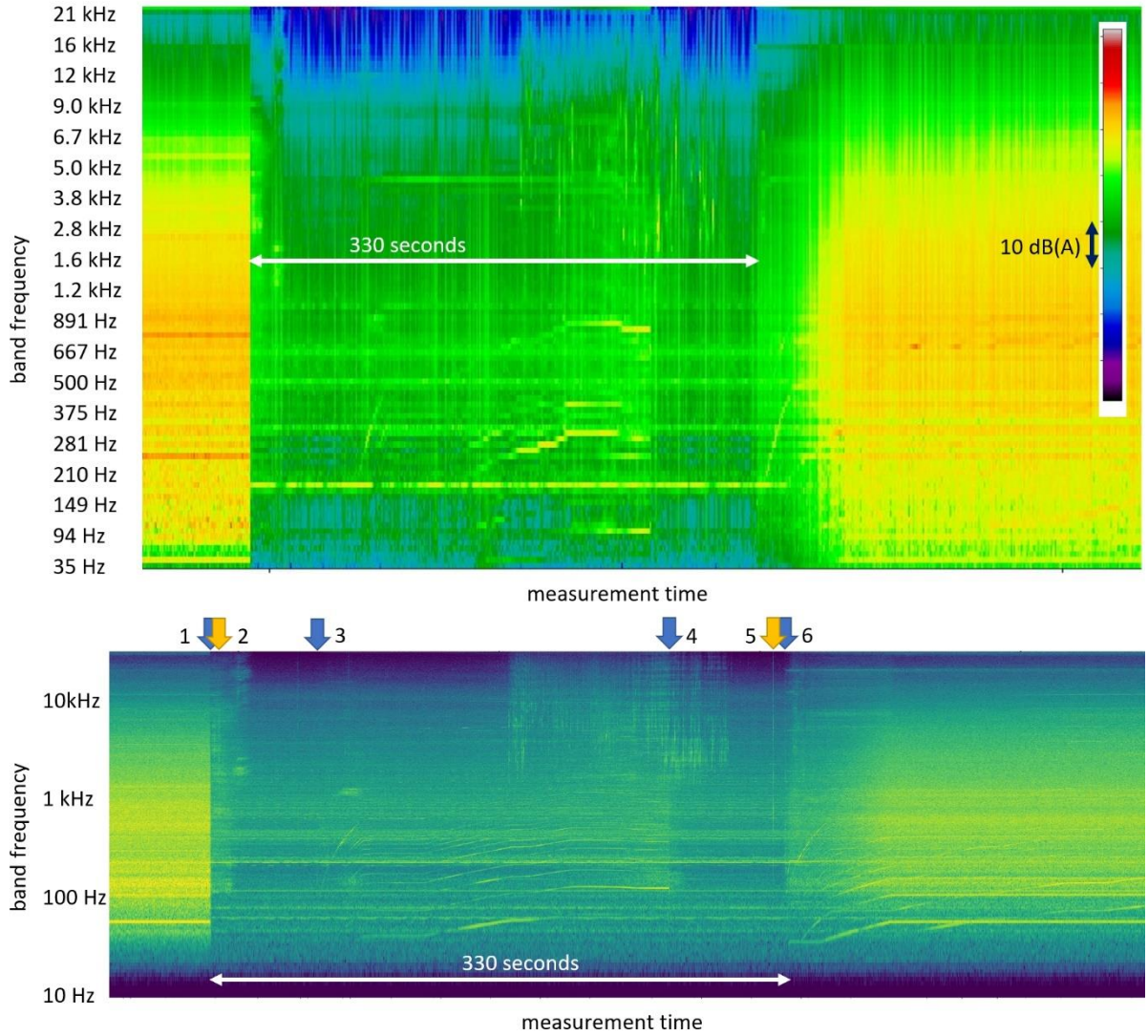

Figure 3.3: Frequency-resolved acoustic signature (in waterfall representation) during defrosting of an air-to-water heat pump. The upper picture shows the time-resolved acoustic signature in one-third octave band Representation. The lower picture shows the sound pressure level at a selected microphone position in narrow band representation (source: AIT, Austria).

The shown icing can also be examined in the context of simulation calculations. On the one hand this can be done in a complete system view (see figure 3.4). This Dymola/Modelica model [5], [6], [7], [8], [9] was supplemented with acoustic properties and allows the transient prediction of the acoustic emissions during operation in different states. The underlying library is freely available [9]. Figure 3.10 shows a good agreement of the measurement results at SilentAirHP (an Austrian heat pump research prototype [1], [10], [16]) with the simulations.

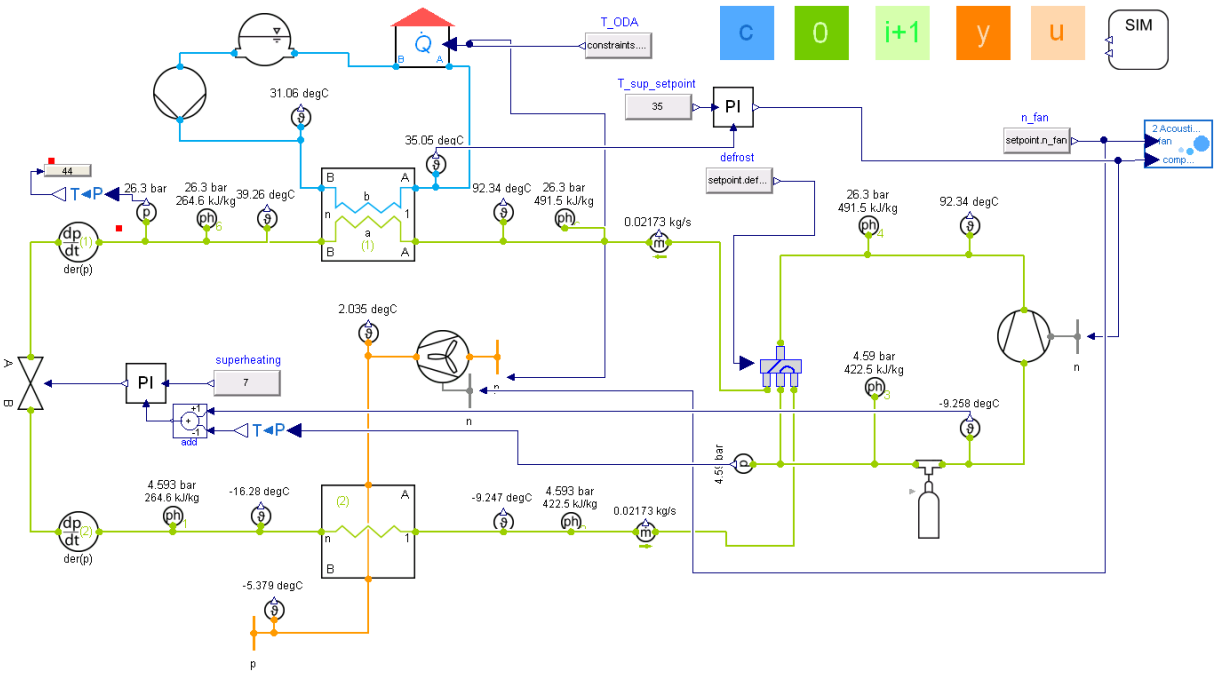

Figure 3.4: Simulation of SilentAirHP at design point A2W35 (Source: AIT, Austria)

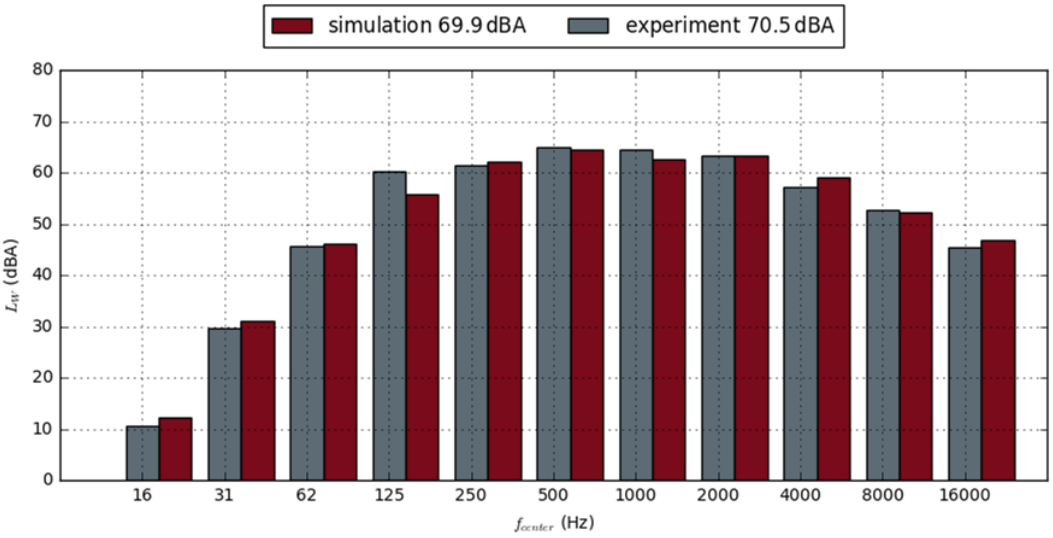

Figure 3.5: Comparison of experimental data of the SilentAirtHP with simulation results from the first test measurements in April 2017, where the individual components were measured and the total sound power level was compared. (Source: AIT, Austria)

On the other hand, the icing of a heat exchanger of an air-to-water heat pump can also be calculated and visualized by means of transient numerical flow simulation (CFD) [11], [12]. Figure 3.6 shows the temporal behaviour of the ice build-up of the SilentAirHP heat exchanger. Figure 3.6 on the right shows a schematic drawing of this heat pump design. Figure 3.7 shows velocities and pressures in a symmetrical section of the heat exchanger with increasing icing. Finally, figure 3.8 shows the ice build-up on evaporator fins in a general overview and a detailed view.

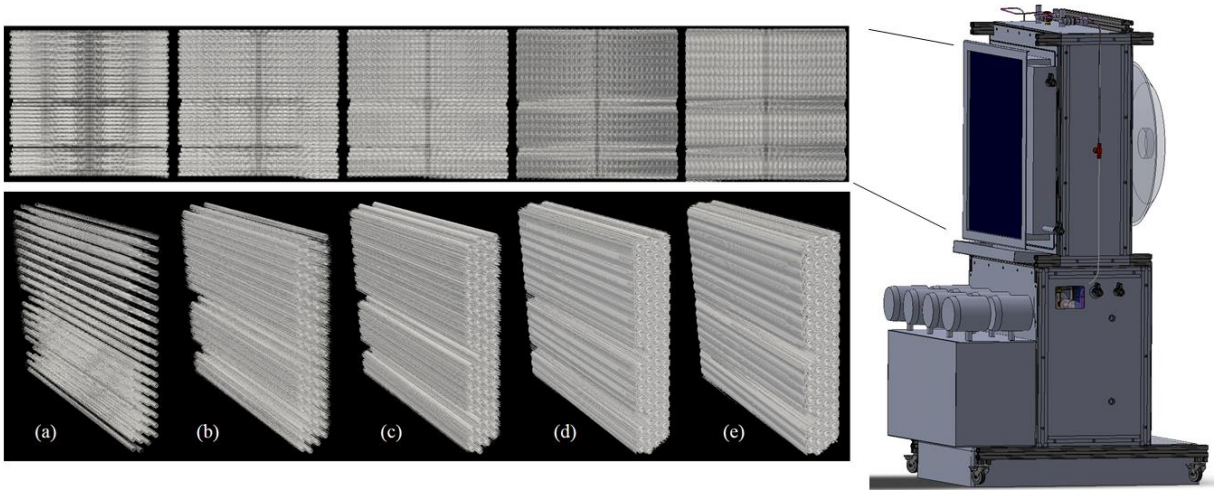

Figure 3.6: Temporal behaviour of ice build-up on the SilentAirHP heat exchanger. (Source: AIT, Austria)

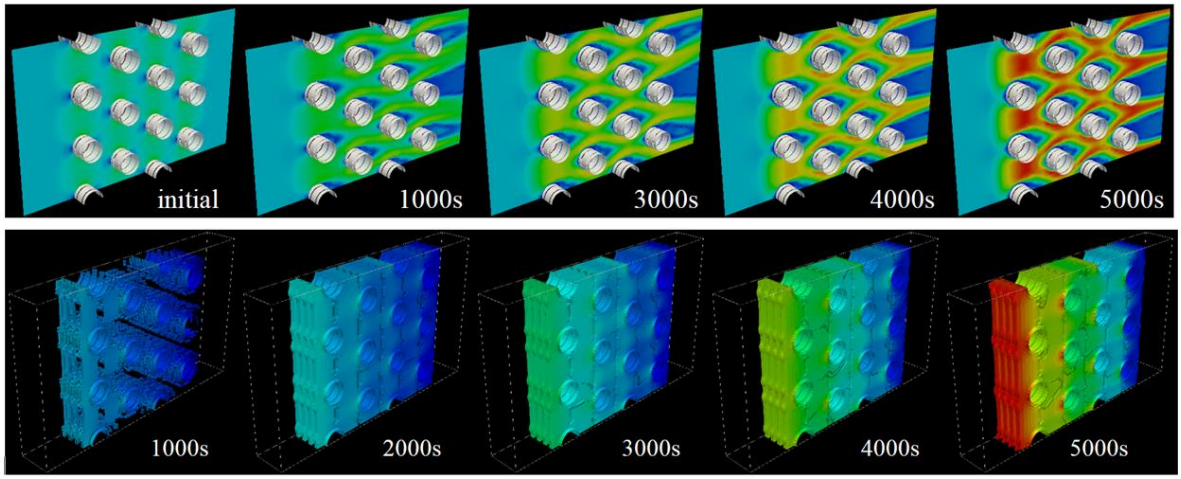

Figure 3.7: Temporal behaviour of the ice build-up on a small symmetrical section of the heat exchanger. Above is the flow velocity, below is the pressure loss during gradual icing. (Source: AIT, Austria)

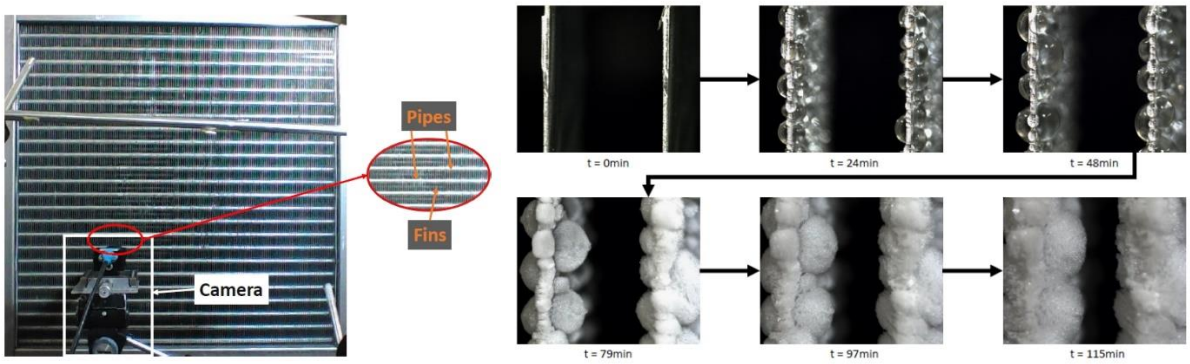

Figure 3.8: Surface of the SilentAirHP heat exchanger and the macro camera to visualise frost accumulation on the heat exchanger fins (left); frost accumulation on two fins of the SilentAirHP heat exchanger (right). (Source: AIT, Austria)

As an example for the evaluation of noise measures, their mechanism of action and the effect found with the SilentAirHP, the following table is shown her including resuts derived from the SilentAirHP.

Action		Effect Mechanism	Influence on the Sound Power Level
Constructional measures on the A/W-WP			
1	Encapsulation of the compressor	particularly effective when installed outdoors	Uncapsulated compressor not available
2	Structure-borne noise insulation of the compressor		Has not been examined
2a	Airborne sound insulation of the compressor	Attachment of an acoustic compressor hood	Reduction: <1 dB (A)
3	Structure-borne noise insulation of the fan	Less structure-borne noise transmission to the housing and channels	Has not been examined
4	Improvement of the flow near the fan	Diffusor	Reduction: 2 dB (A)
4	Sound absorbing duct insulation	Insulation material	Reduction: <4 dB (A) at maximum fan speed
6	Square duct deflections with additional lining	Use the deflection as a reflection silencer. Pay attention to the large channel width and prefer radiation upwards	Reduction: 2 dB (A)
7a	Absorption silencer	Deflection splitter silencer	Reduction: 2.5 dB (A)[1]
7b	Absorption silencer	Deflection	Reduction: 2.5 dB (A)[2]
8	Avoidance of channel resonances	Matching the length and cross section of the channels	Has not been examined
9	Baffle plates in bends	Less turbulence and less pressure loss	Has not been examined
Component-specific measures			
10	Low noise compressor	Noise reduction at the source	The compressor was not replaced
11	Low-noise fan type	Reduction of fan noise	Reduction: 8 dB (A)[3]
12	Clearing of the fan blades	Less structure-borne noise radiation through the wings	See 11
13	Optimization of the operating point of the fan	Reduction of fan noise through better flow conditions	See 4
14	Optimization of the evaporator	Reduction of pressure loss through the evaporator	Depending on the fan characteristic (eg 5 dB (A) if the pressure loss is halved)

[1] FC050@594rpm,6.67V 60.25 dBA // Ref FC050@594rpm,6.67V 62.55 dBA
[2] FC050@594rpm,6.67V 60.15 dBA // Ref FC050@594rpm,6.67V 62.55 dBA
[3] ZN050@537rpm,4.79V 54.58 dBA // FC050@594rpm,6.67V 62.55 dBA // Data for the same volume flow

15	Anti-ice coatings	Delay in ice build-up, change in defrost behavior of the heat exchanger	No change in sound power[4]
Control measures			
16	Optimization of the fan speed	With various circuits or with pre-resistors, a simple speed reduction is possible if required	Depending on the fan characteristic (eg: 5 dB (A) when reduced by 100 rpm)
17	Control optimization	Fewer on / off switching operations and shorter operating times at night, partial load operation during the night	With A2W35 and night reduction (12h): 10 dB (A), day 4.5 dB (A) more.[5]
18	Abtaustrategien	Changed ice formation behavior	"Defrosting noise level" < "operational level"
Active measures			
19	Active Noise Cancelling (ANC)	Active generation of counter sound	1-dimensional sound fields combated well with counter-sound (~ 7dBA reduction), 3-dimensional fields in the wake of the fan hardly influenceable

[1] FC050@594rpm,6.67V 60.25 dBA // Ref FC050@594rpm,6.67V 62.55 dBA
[2] FC050@594rpm,6.67V 60.15 dBA // Ref FC050@594rpm,6.67V 62.55 dBA
[3] ZN050@537rpm,4.79V 54.58 dBA // FC050@594rpm,6.67V 62.55 dBA // Data for the same volume flow
[4] 10% extension of the icing period
[5] With A2W35, partial load all day with 69 dB(A) or night: 58.8 dB(A) and day 73.5 dB(A)

The detailed SilentAirHP final report can be downloaded in English language at the IEA HPT Annex 51 website:

https://heatpumpingtechnologies.org/annex51/wp-content/uploads/sites/59/2020/11/silentairhpfinalreport.pdf

4. IEA HPT Annex51 Heatpump Measurements

Three heat pumps (an air-to-water heat pump (see figure 4.1), an exhaust-air heat pump water heater (HPWH) and an air-to-air heat pump) were on tour through Europe at the participating institutes, their last tests will be carried out in 2020.

The results of the air-to-water heat pump measurement campaign show similar results in most cases in the participating laboratories. The differences that may occur are acceptable given the variety of test environments and acoustic test methods (see Figure 4.2). When a larger difference occurred, it was often due to a difficulty in adjusting the operating conditions rather than an acoustic test sample. One laboratory carried out measurements with a dodecagonal frame [3], around the outdoor unit with 55 microphones. The data from 12 microphones (see figure 4.1 on the right) allow the relative directivity diagram to be displayed, which is shown in figure 4.3 (left) as an A-weighted total level. The

[4] 10% extension of the icing period
[5] With A2W35, partial load all day with 69 dB(A) or night: 58.8 dB(A) and day 73.5 dB(A)

directivity diagram in Figure 4.3 (right) shows the directivity of the unit's acoustic radiation for each octave band in dB(A).

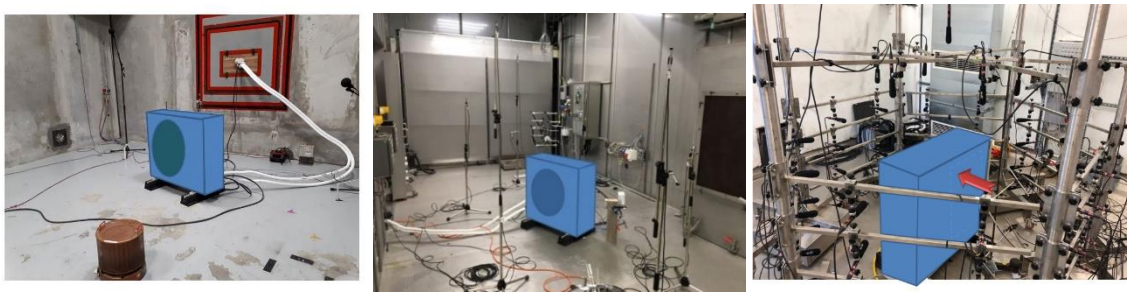

Figure 4.1: Examples of heat pump installation in a reverberation room (left) and in climate chambers (centre and right). A setup with microphone array is shown in the right picture. Source: CETIAT, France (left), ISE, Germany (middle) and AIT, Austria (right).

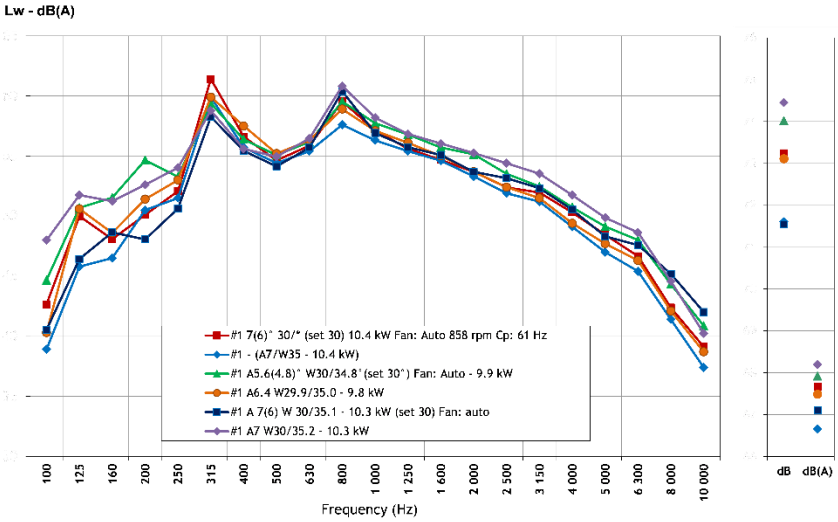

Figure 4.2: Frequency spectrum of the A-weighted sound pressure level for standard conditions according to EN 14511 (#1) with the results of 6 laboratories (source: CETIAT, France)

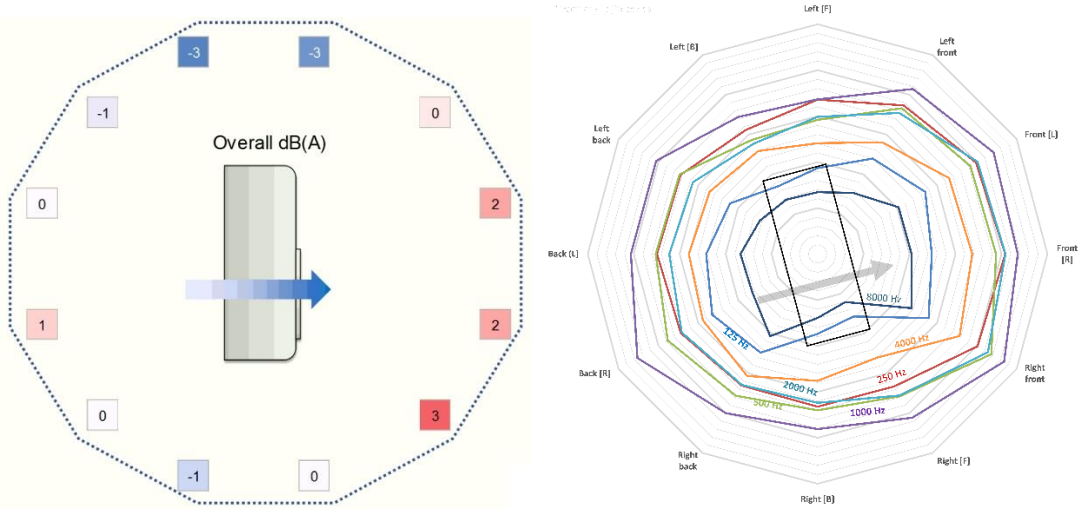

Figure 4.3: Polar pattern of the total A-weighted sound pressure level measured at a height of 75 cm (left) and the polar pattern for the different A-weighted octave bands (right) (source: AIT, Austria)

For the EN 14511 at maximum frequency condition, the air and water temperature conditions remain the same, but both the compressor and the fan run at their maximum frequency (see figure 4.4). For this test, results are more scattered, even for capacity, e.g. lab D measuring an unexpected 7.1 kW. The spectrums are not identical, except for labs A and D which are very close, the other being above (lab. F) or highly above (lab. C).

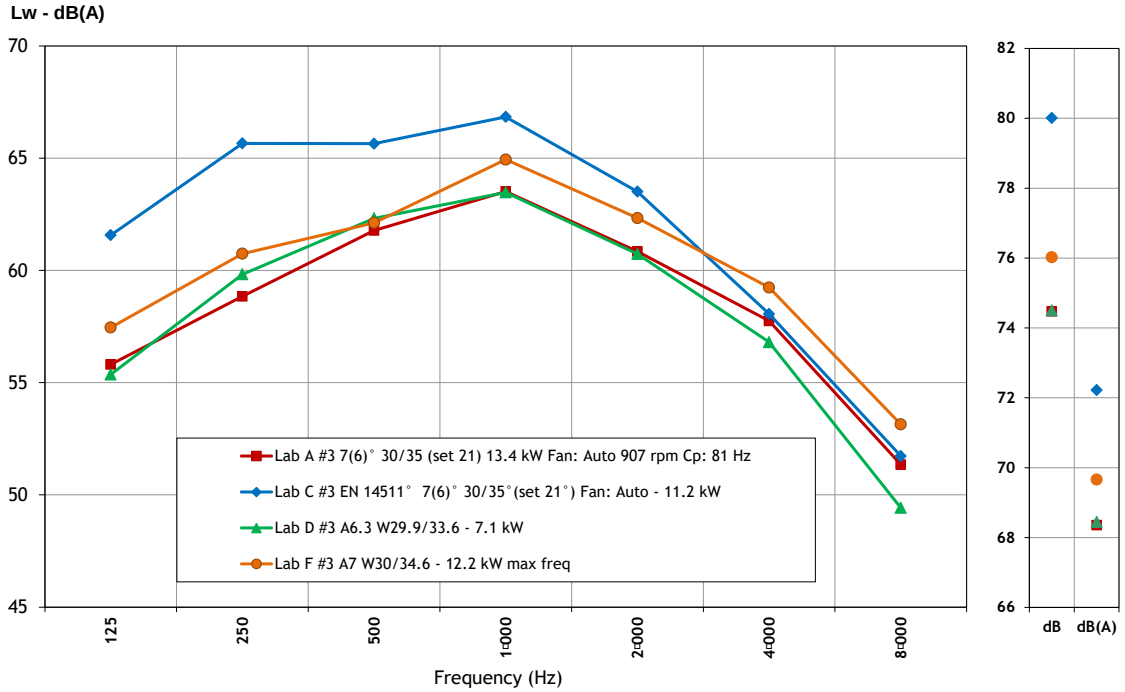

Figure 4.4: sound power levels in octave bands at EN 14511 and max. frequency. (Source: IEA HPT Annex 51 D2.2)

The 1/3 oct. band spectrum of lab A may give an explanation (see Fogire 4.5). The fan and compressor run at higher rotation speeds giving a higher sound level, easy to see on the major part of the spectrum. The peaks observed for the EN 14511 operating conditions at 315 and 800 Hz, totally disappear, these resonances probably being due to frequency coincidences in the unit.

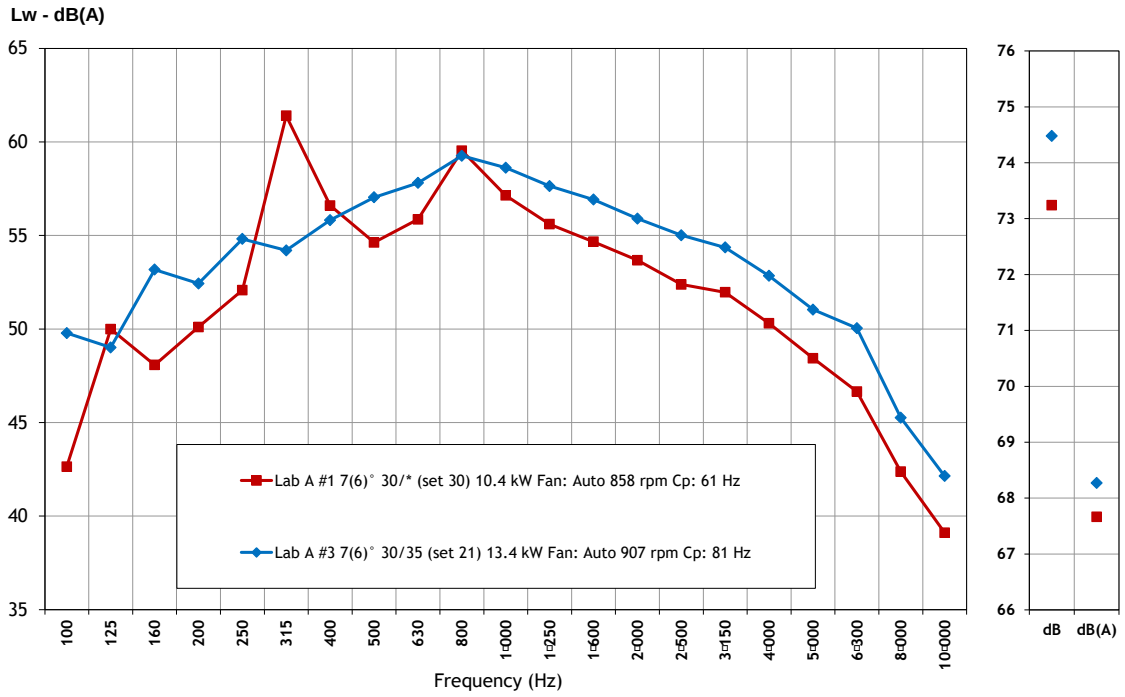

Figure 4.5: sound power levels for EN 14511 max freq. (1/3 octave bands) for lab A (Source: IEA HPT Annex 51 D2.2)

The part load conditions of EN 14825 is important as it allows giving the capacity to get during the acoustic operating condition according to EN 12102-1 – Annex A.4, but with a different setting in water temperature (see Figure 4.6 and Figure 4.7)

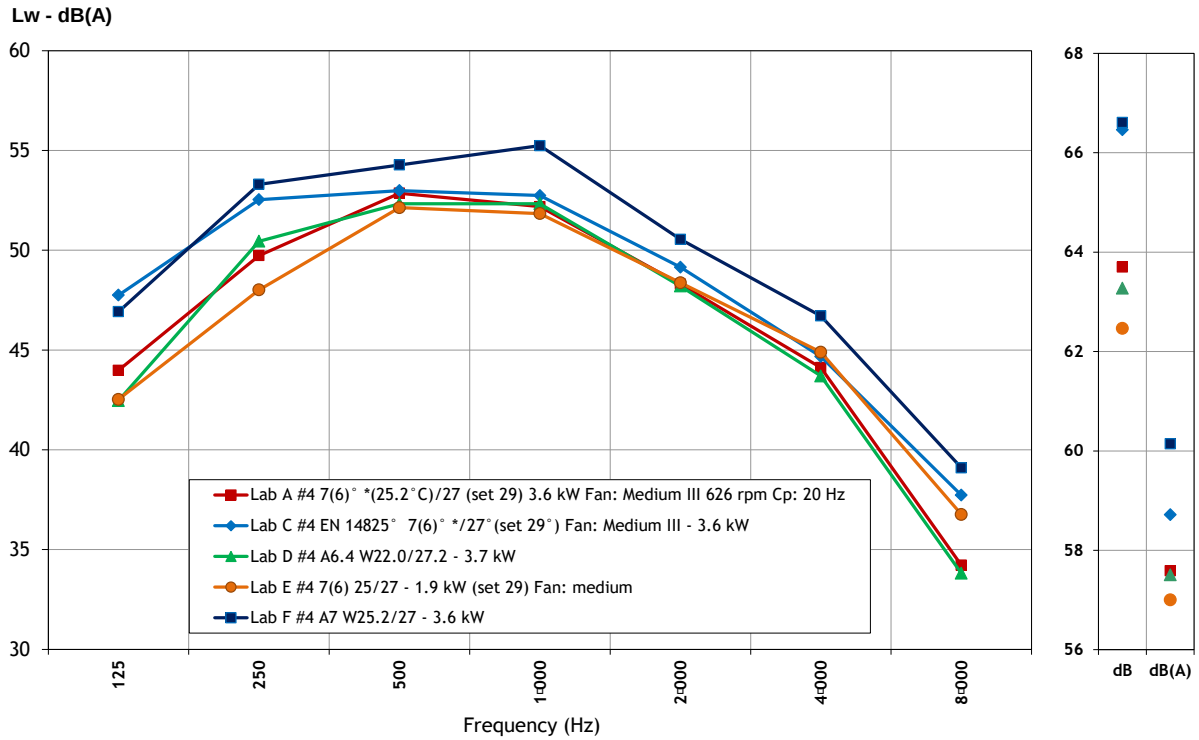

Figure 4.6: sound power levels for EN 14825 point C (octave bands) (Source: IEA HPT Annex 51 D2.2)

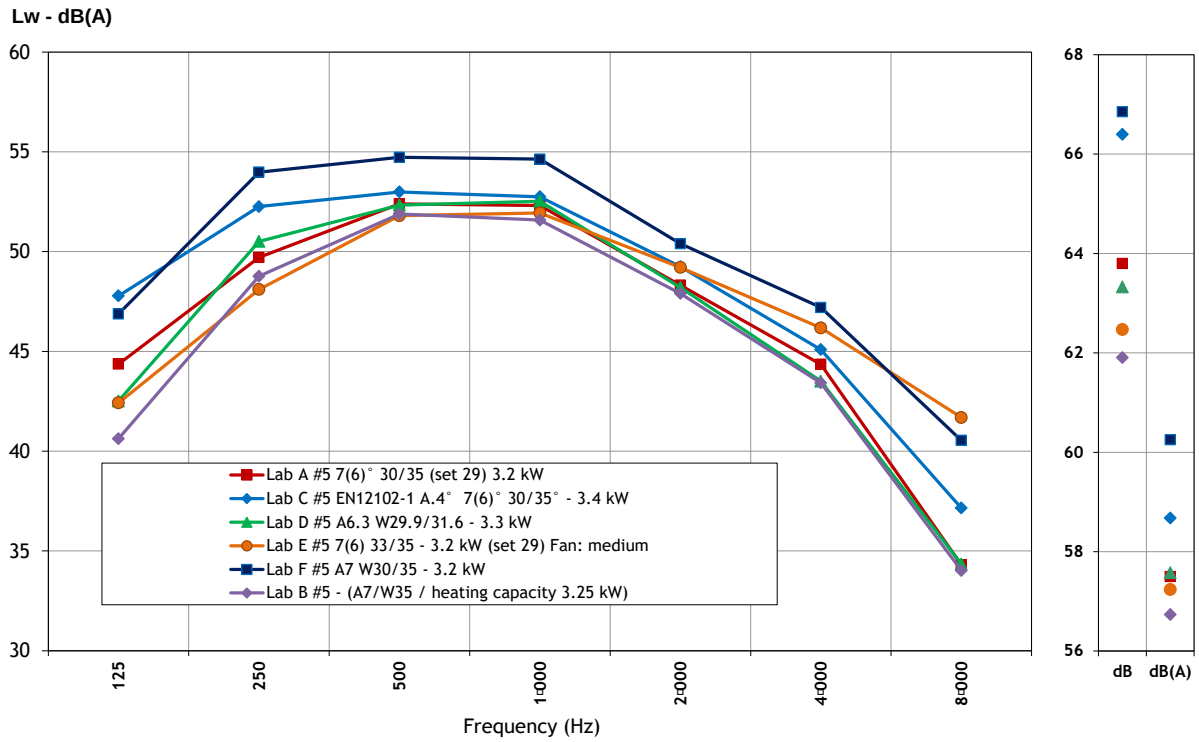

Figure 4.7: sound power levels for EN 12102-1 (octave bands) (Source: IEA HPT Annex 51 D2.2)

For EN 14825 point C, (see Figure 4.6), the results are again very scattered, with higher sound level on all spectrum for lab F and high level at low frequencies for lab C. Otherwise, despite some significant differences in the spectrum, the overall value is close for labs A, D and E.

The approach to obtain results within EN 12102-1 (see Figure 4.7) is often not well understood by the EN 12102-1 users. And in fact, the $\Delta T = 5K$ is not fulfilled by all laboratories. For those who implement it, with capacity close to the one measured for EN 14825 point C, the spectrums are not so close, with more than 1 dB(A) overall difference between lab A and C. Lab F continues to find higher values in average.

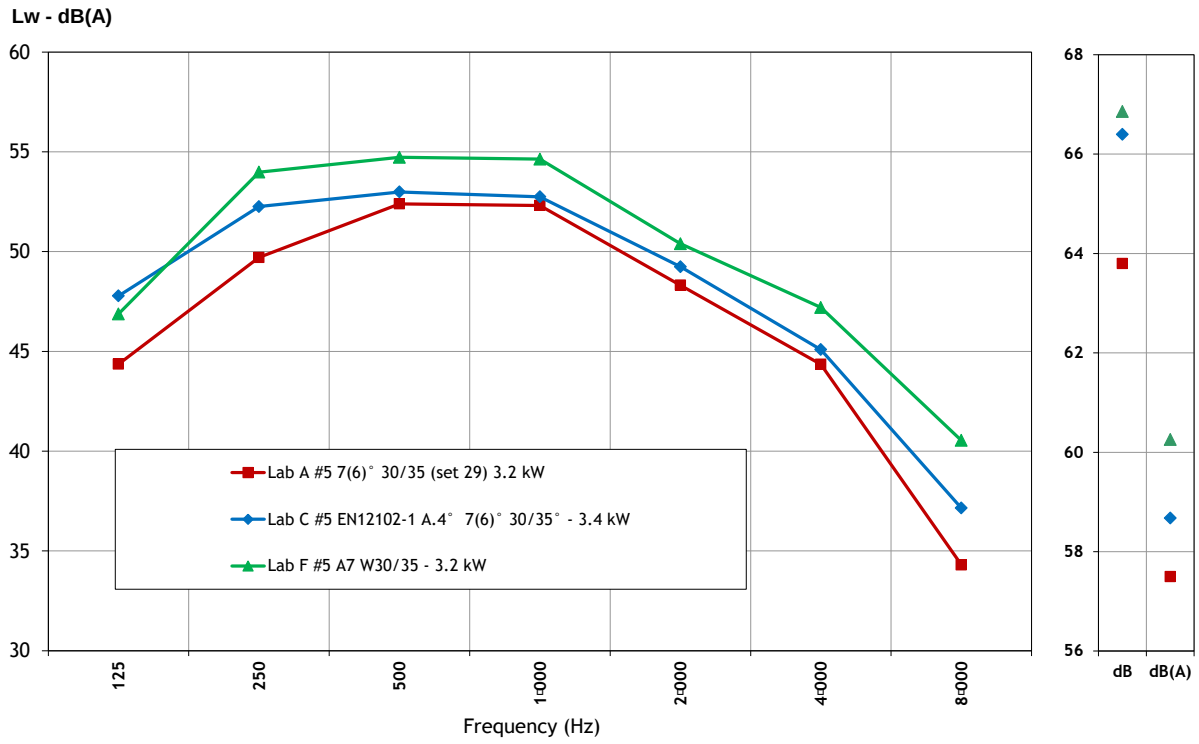

Figure 4.8: sound power levels for EN 12102-1 with 30/35 °C on the water side (octave bands) (Source: IEA HPT Annex 51 D2.2)

The difference between sound power levels during EN 14825 (C) and EN 12102-1 conditions are given in Figure 4.9. Its shows that results are really close (except 8 kHz for Lab E), at least for this unit, meaning that laboratories at least performed both tests in a similar way.

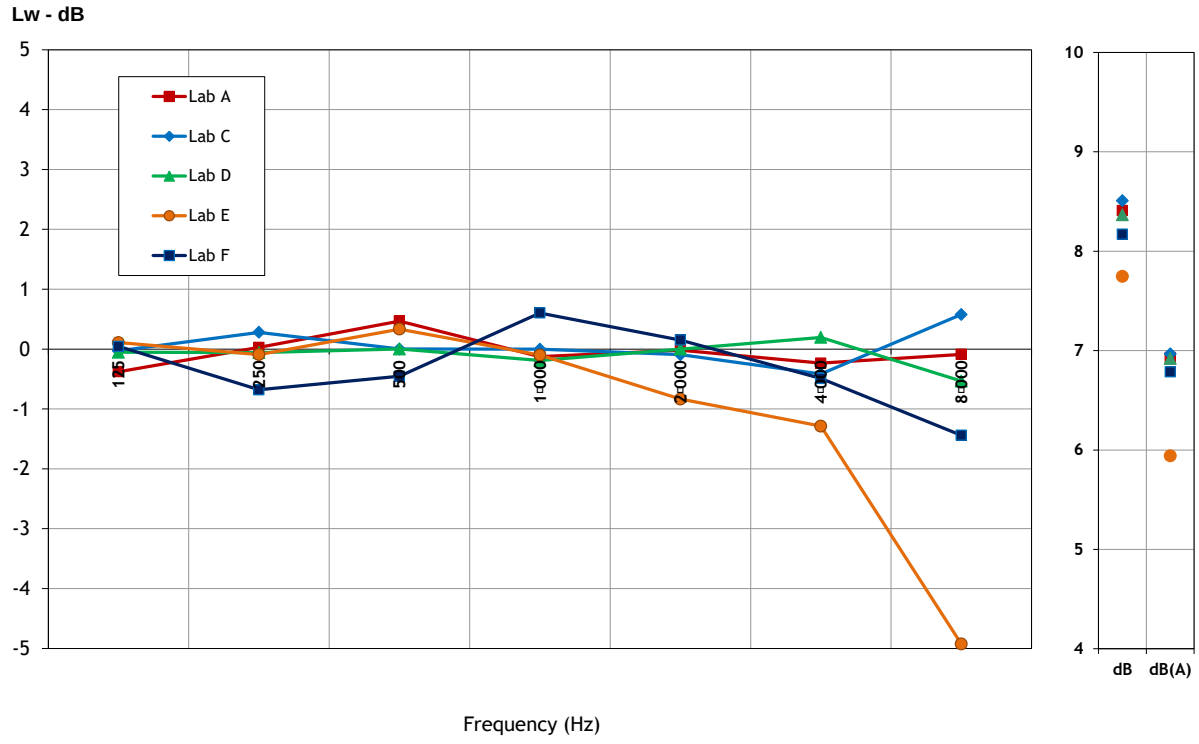

Figure 4.9: comparison for EN 14825 and EN 12102-1 (Source: IEA HPT Annex 51 D2.2)

But the conditions of EN 12102-1 are not perfectly fulfilled as the conditions of operations are not exactly those required by the standard: the ΔT being not 30-35°C, or the capacity being (slightly or more) different between the part load point C and EN 12102-1 Annex 4. To conclude, it appears that the setting of the EN 12102-1 is not clearly understood and had to be changed in some ways: it can be a better description in the standard or more, another setting for the "acoustic" condition.

The condition D of EN 14825 is performed for an outdoor temperature of 12 °C. The same conclusions can be stated than above with very close results for labs A, D then E, including spectrum values, but much higher sound level for lab F (looks like an offset), and lab C, again higher sound levels in the low frequency range.

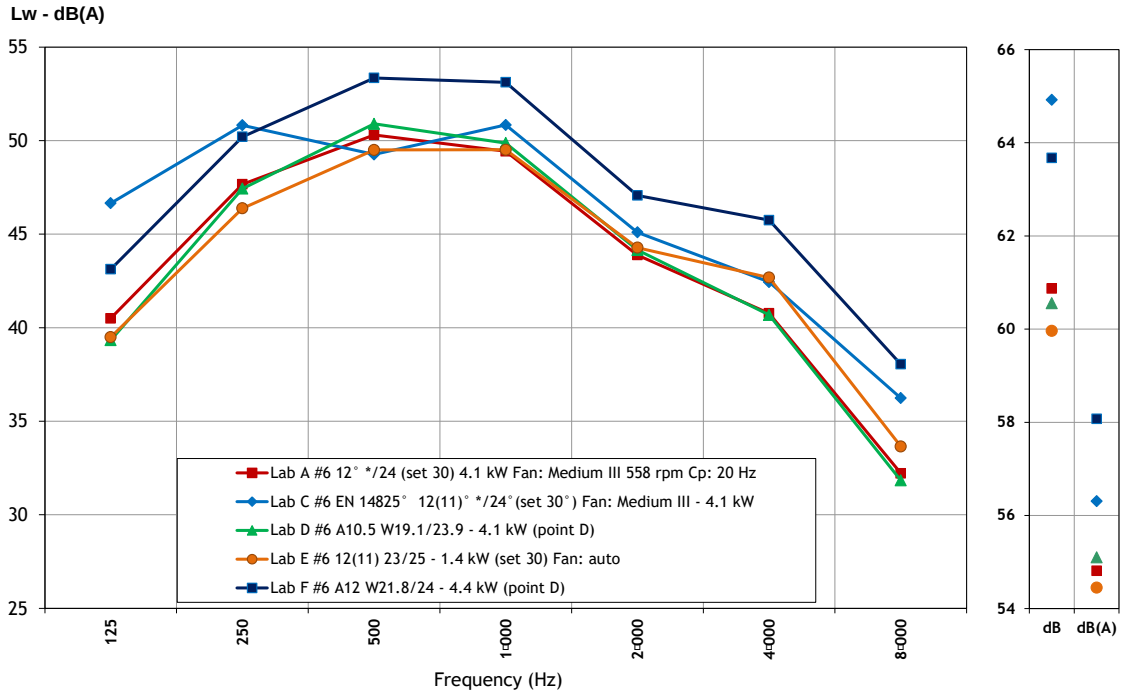

Figure 4.10: comparison at EN 14825 condition D (Source: IEA HPT Annex 51 D2.2)

This operating point gives capacities close to 4.1 kW for all laboratories (except E, but it is probably a typing mistake).

Note: for this temperature and higher ones, in the real life, the unit may have a cycling behavior, with ON/OFF operation.

For the EN 14825 condition E at 2°C outdoor air temperature, all results seem to be more consistent especially at high frequencies while some scattering remains on low and medium frequencies. Unfortunately, operating conditions and resulting measured heating capacities among the laboratories are also different. A clear conclusion is then not possible, especially without recorded data in rotation speeds of fan and compressor.

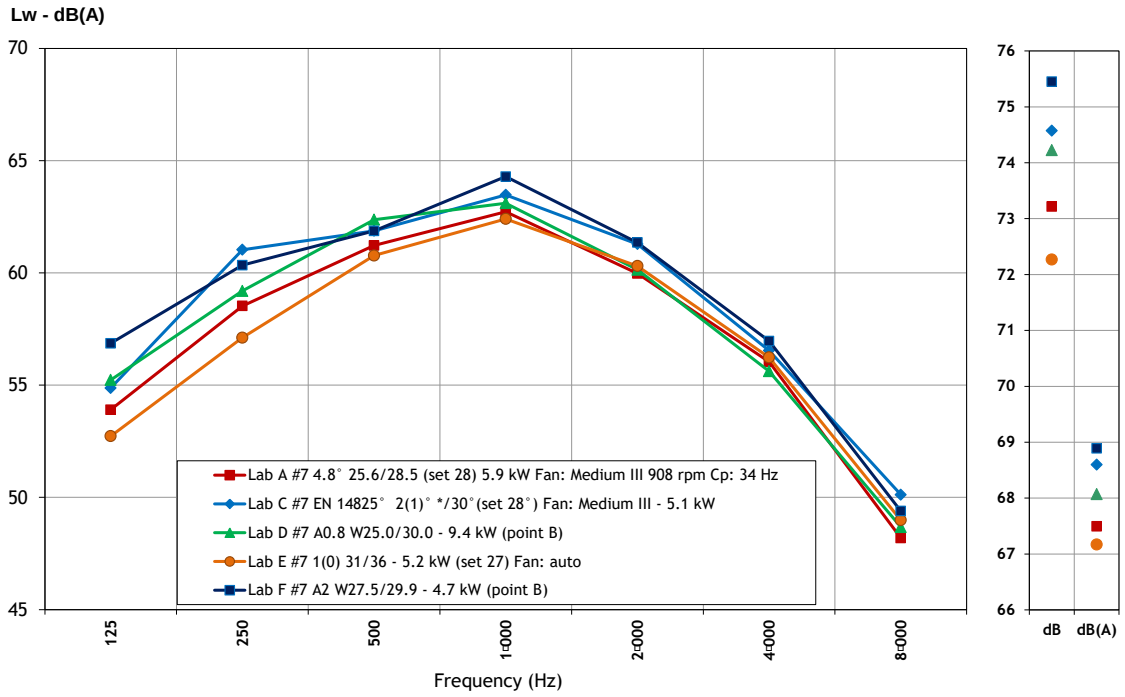

Figure 4.11: comparison for EN 14825 point B (Source: IEA HPT Annex 51 D2.2)

Note: at this outdoor air temperature, one laboratory observed a frosting/defrosting cycle

For the operating condition EN14825 condition A/F at -7 °C of outdoor air, the rotation speed of compressor is first set according to the instructions (#8) and then set at its maximum frequency (#9).

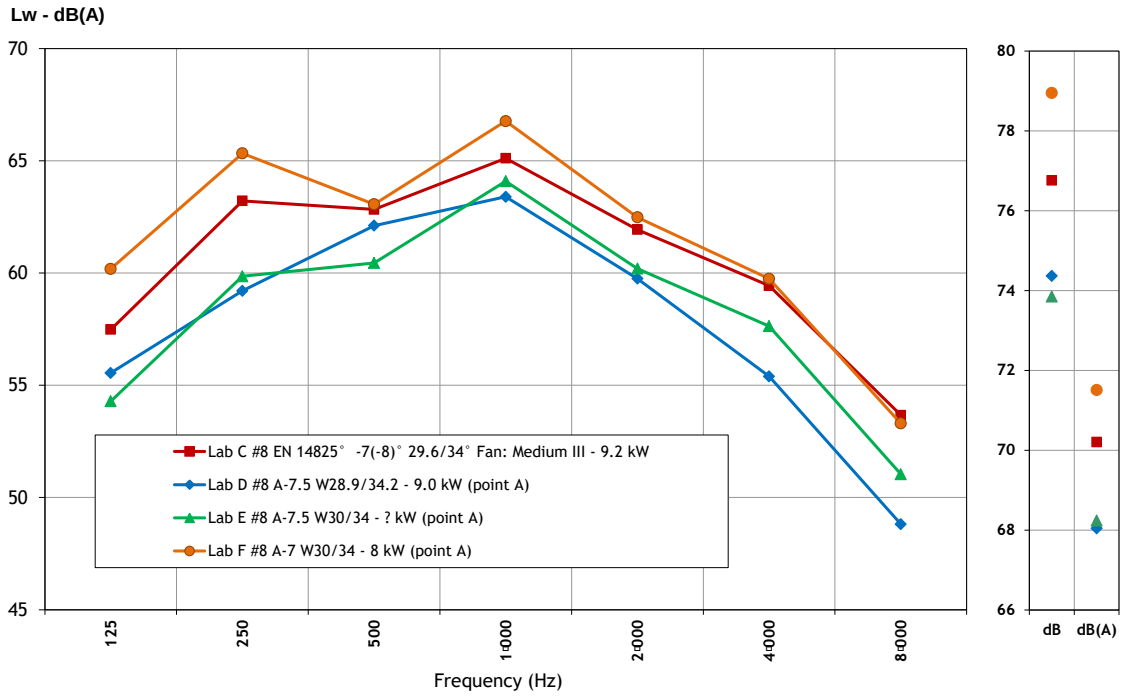

Figure 4.12: comparison at EN 14825 condition A (Source: IEA HPT Annex 51 D2.2)

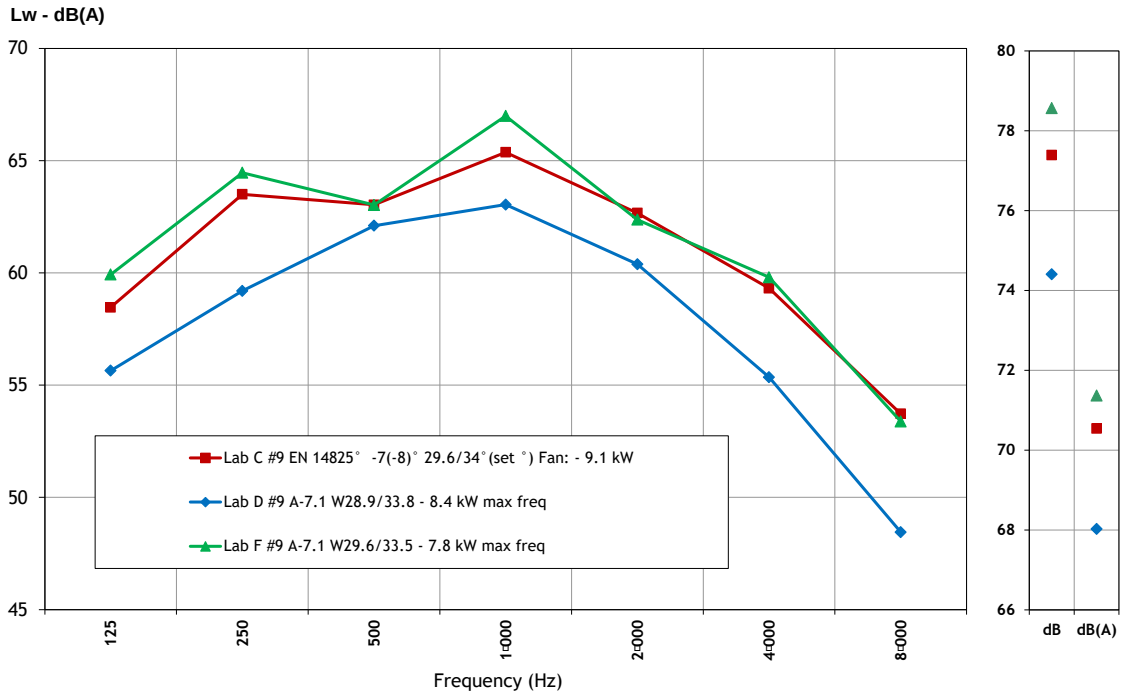

Figure 4.13: comparison at EN 14825 condition A and max frequency compressor (Source: IEA HPT Annex 51 D2.2)

Figure 4.12 and Figure 4.13 lead to the same conclusions: with lab C and F as louder than the others, when lab D and E are very close, even if the measured heating capacities are not so close.

At a low outdoor air temperature of condition E, only 4 laboratories were able to perform the acoustic test. From these tests, two sets of results are identified.

- Labs C and F which applied different acoustic methods obtained very similar sound levels, the spectrum in 1/3 oct. bands speak for themselves, although the capacity is 8.4 vs 7.5 kW.
- Labs D and E again found lower sound levels than labs D and E for which the spectrums remains in the vicinity… but the capacities are again very different (5.9 vs 8.4 kW).

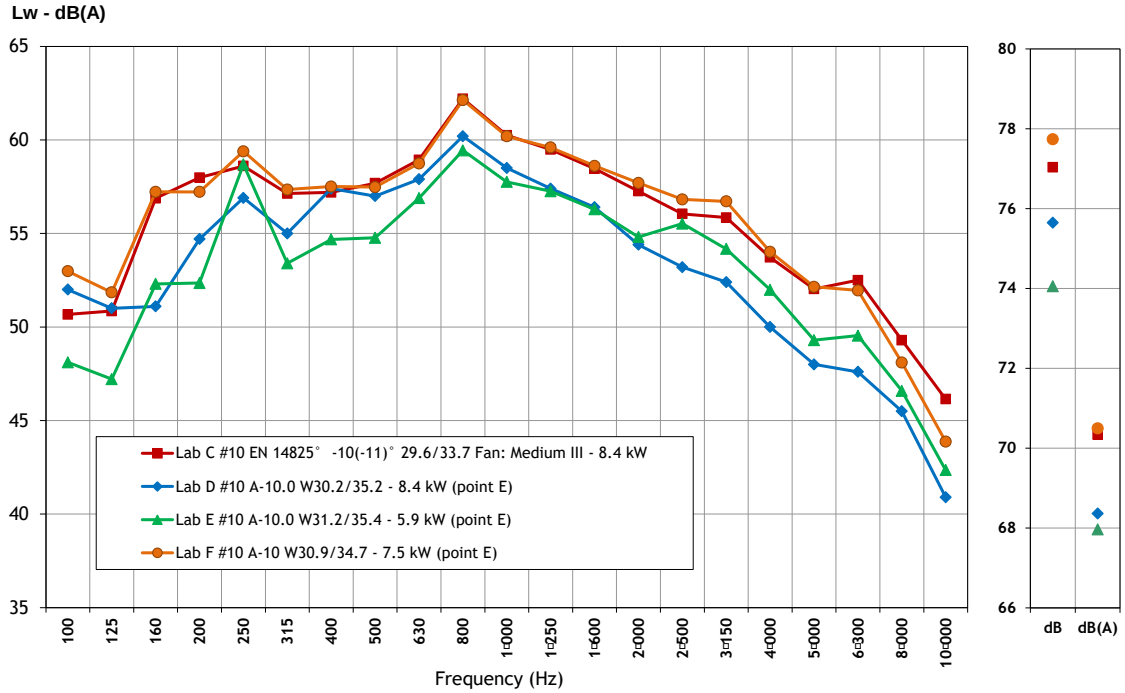

Figure 4.14: comparison at EN 14825 condition E (Source: IEA HPT Annex 51 D2.2)

An overview on the influence of operating conditions on the sound power level can be done, by looking at the rotation speeds of fan and compressor, as laboratory A measured their value, unfortunately not for the lowest ambient temperature. Fortunately, these conditions lead to high capacities of the unit which were already described by #3 (EN 14511 max. frequency).

Fehler! Verweisquelle konnte nicht gefunden werden. clearly shows that different operating conditions lead as expected to variable sound power levels and different spectrum shapes. In the present case, the standard rating condition (configuration #1) exhibits a peak at 315 Hz band which disappears when the compressor and the fan are boosted at their maximum frequency; the modal coincidences do not exist anymore. In spite of an average difference of 1.5 to 2.5 dB over the spectrum, the overall value only differs by 0.8 dB(A), due to the peaks removal.

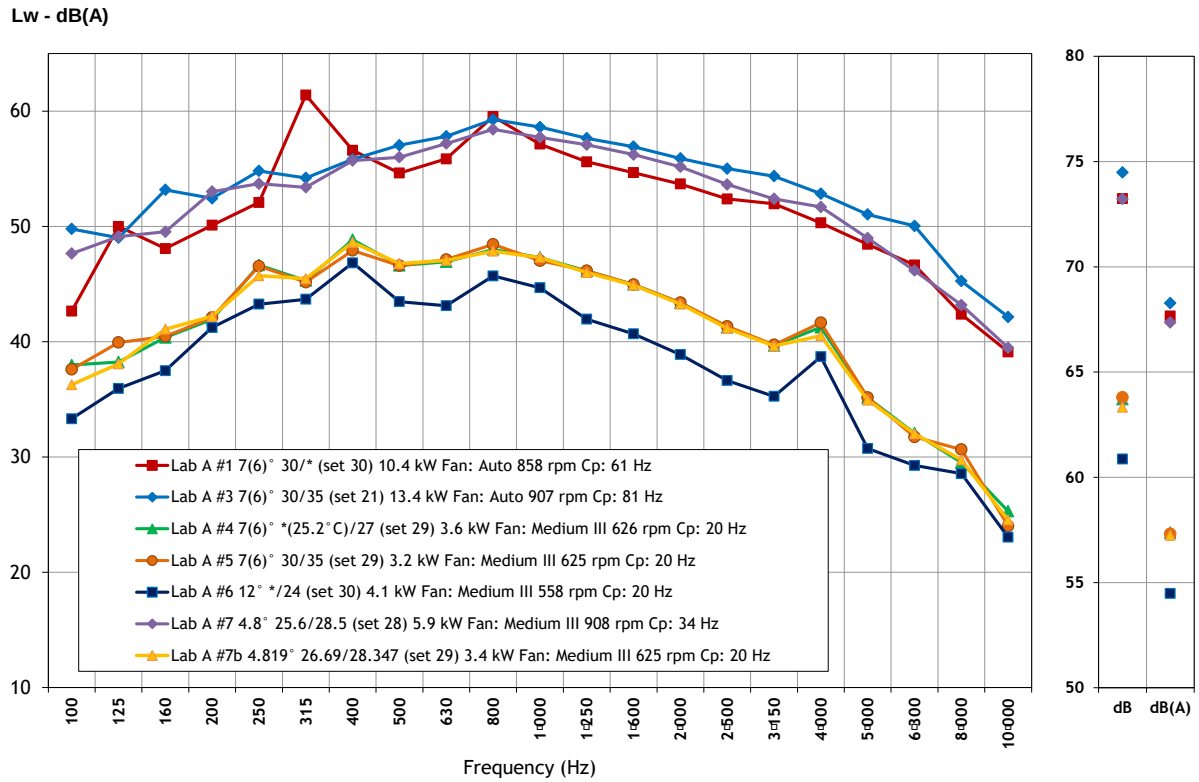

Figure 4.15: influence of operating conditions on the sound level (Source: IEA HPT Annex 51 D2.2)

10 dB(A) respectively compared to the standard rating conditions EN 14511 (#1). The heating capacity is then clearly lower, so does the fan rotation speed.

In a general approach, the noise level is the highest for high capacities and the lowest for small capacities, but it is not possible to find a relation for this unit between the noise level and the heating capacity. As an example, **Fehler! Verweisquelle konnte nicht gefunden werden.** shows that configuration #5 is louder by 2.8 dB(A) than #6, due to the higher fan rotation speed (625 vs 558 rpm), despite a lower capacity.

Although the two configurations have the same fan rotation speed (908 rpm), configuration #3 is louder by 1.3 dB in average than #7, because compressor rotation frequency is 81 Hz instead of 34 Hz.

When the heating capacity increases (ex. for conditions with negative ambient air temperature), the sound level is close to the ones observed at the maximum heating capacity or at the max frequencies of both fan and compressor.

From measurements of another laboratory, a similar increase of sound power level is observed on Figure 4.16 for the configuration #7 (EN 14825 point B) condition, with a smaller effect on the overall increase, which is around 2 dB(A). Almost all octave bands increase, except 4 and 8 kHz. Octave 125 Hz and 250 Hz increase a lot but do not really contribute to the overall value, which is mainly driven by the medium frequency bands.

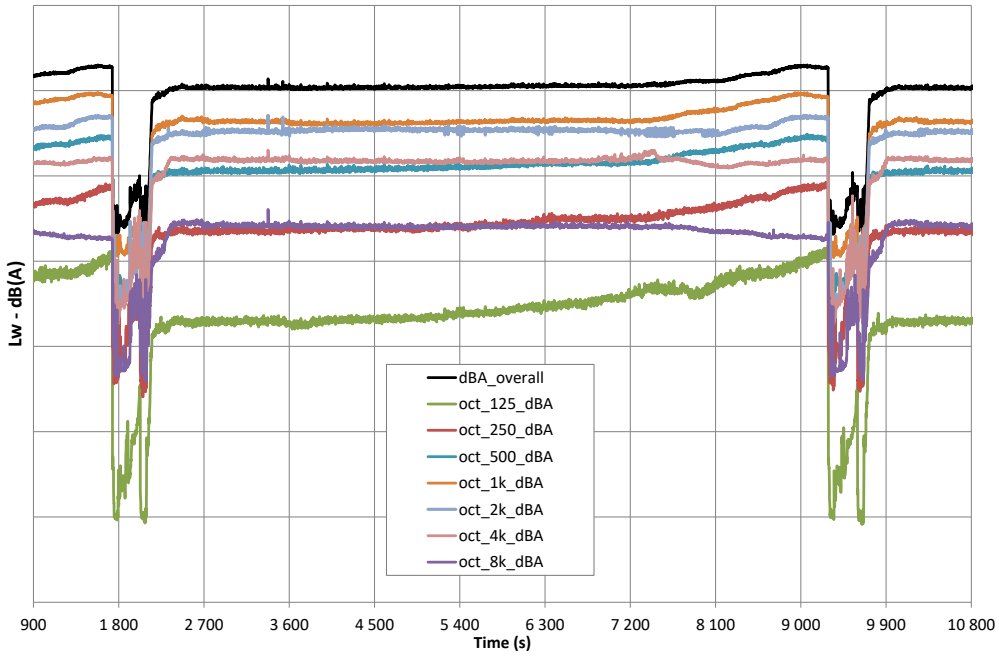

Figure 4.16: Time dependent A-weighted sound power levels (in octave bands) between two defrosting phases configuration #3: EN 14511 frequency max (Source: IEA HPT Annex 51 D2.2)

Figure 4.17**Fehler! Verweisquelle konnte nicht gefunden werden.** shows the spectrums at time H and D (cf. arrows on Figure 4.16**Fehler! Verweisquelle konnte nicht gefunden werden.**), for #3 (EN 14511 max frequency) condition, and for #7 (EN 14825 point B at +2°C). The frosting induces an increase of the low and medium frequencies by 3 to 5 dB (consistent with the observations of lab 1).

Figure 4.18 shows the same quantities as Figure 4.16, but for negative outdoor air temperatures, leading to different behaviors of the sound power level. These levels are steadier, without noticeable increase before the defrosting starts, even though some accidents on frequency band may occur, but without larger influence on the overall level (see changes at 1800 s). However, this overall level quickly reaches the same magnitude than the one observed at the end of heating of Figure 4.16**Fehler! Verweisquelle konnte nicht gefunden werden.**- arrow "D").

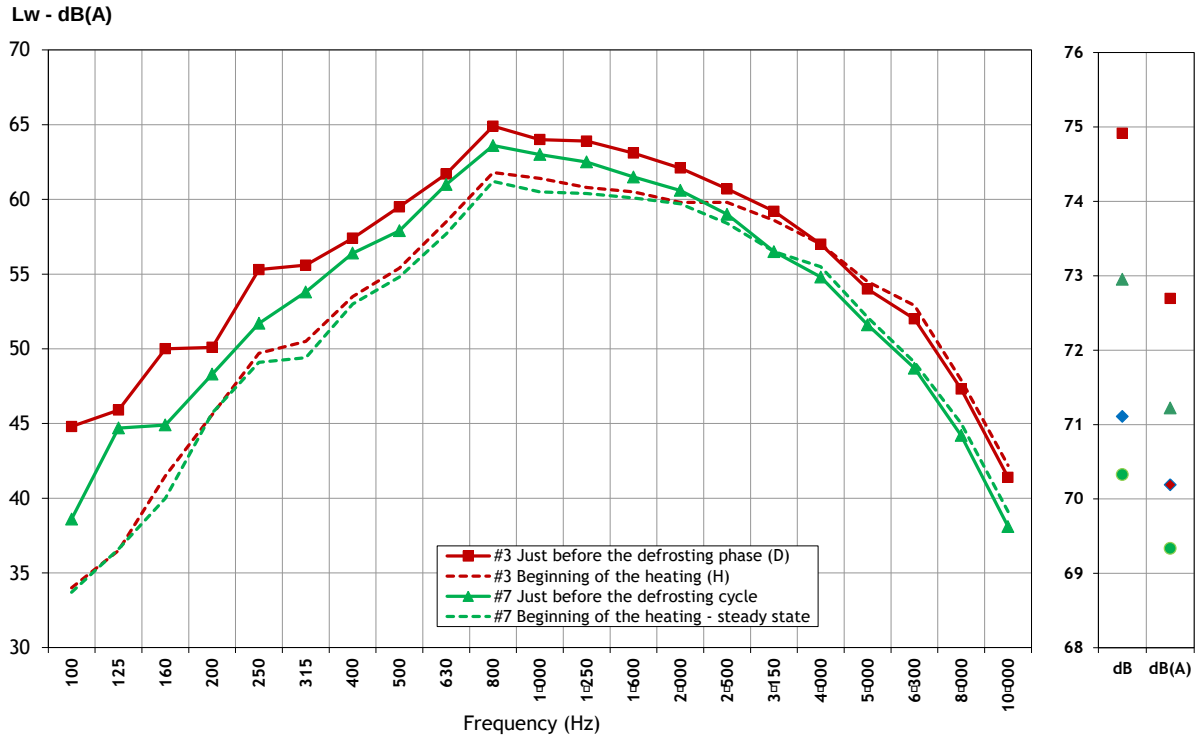

Figure 4.17: averaged sound power levels for the 3 phases of frosting, defrosting (related to Figure 4.16). (Source: IEA HPT Annex 51 D2.2)

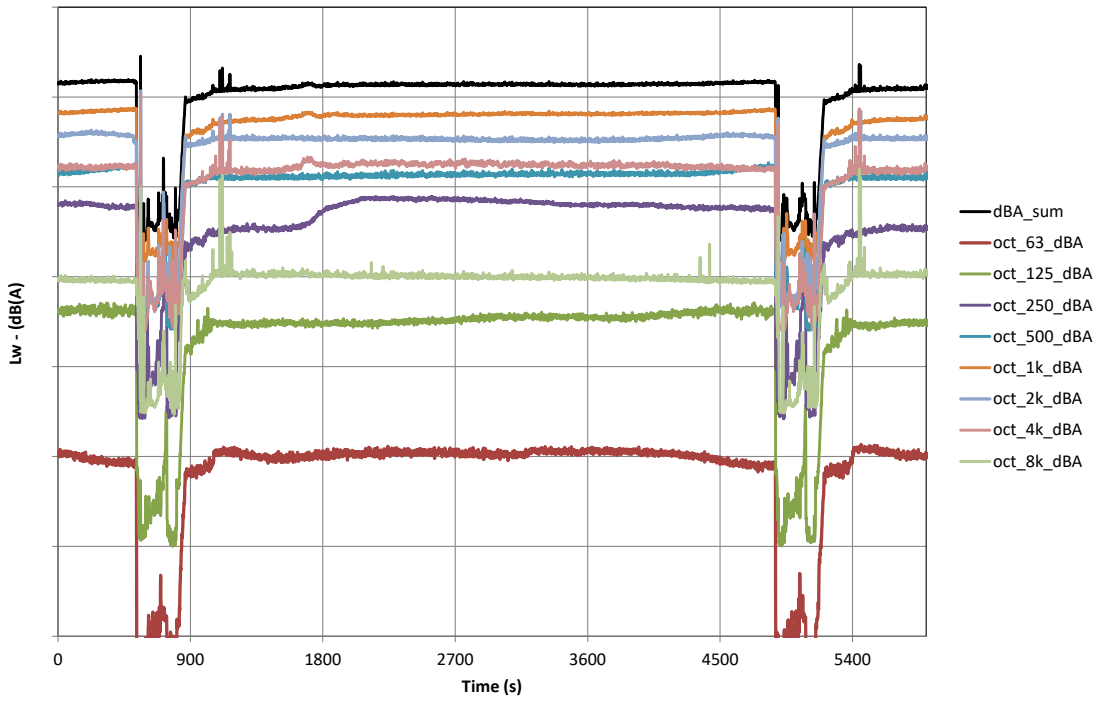

*Figure 4.18: Time dependent A-weighted sound power levels (in octave bands) between two defrosting phases. Configuration #8: EN 14825 -7(-8) */34 (Source: IEA HPT Annex 51 D2.2)*

The detailed report can be downloaded at the IEA HPT Annex 51 website:

https://heatpumpingtechnologies.org/annex51/wp-content/uploads/sites/59/2021/10/iea-hpt-annex-51-d22.pdf

5. GreenHP

The EU Project GreenHP culminated in providing an air-to-water HP (see figure 5.1 ff.), which was acoustically characterized.

5.1. Measurements of the full assembly in the climate chamber

An acoustic dome (see figure 5.1) was setup with 64 microphones surrounding the GreenHP (see figure 5.2 – 5.4). Measurements have been performed without (see figure 5.5) and with several acoustic shieldings (for example see figure 5.6 – 5.8). Acoustic shieldings investigated included “Foamed plastic bags” and “aluminium coated felt”. Measurements have also been performed with inversed fan rotation. Fan speed has been varied using the reference values 61%-62%. Measurements without sound absorbers have been performed at fan speeds between 60%-90%. The climatic chamber was operated at a temperature of 7°C and a relative humidity of 87%.

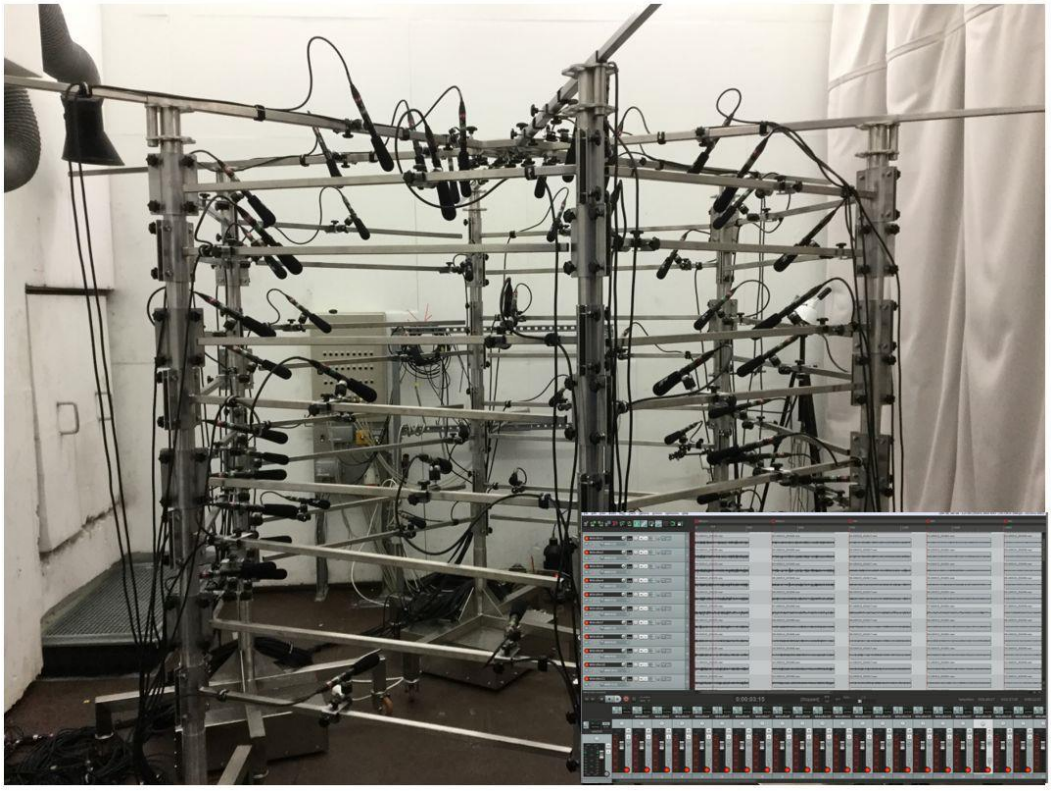

Figure 5.1: Up op 64 microphones are placed around a sound emitting object forming an acoustic “dome”. In this case a six-fold symmetrical setup has been constructed. The right lower part of the image shows the some of the wave-signals recorded during a typical test.

Figure 5.2: Acoustic Dome surrounding the GreenHP (view to the upper part)

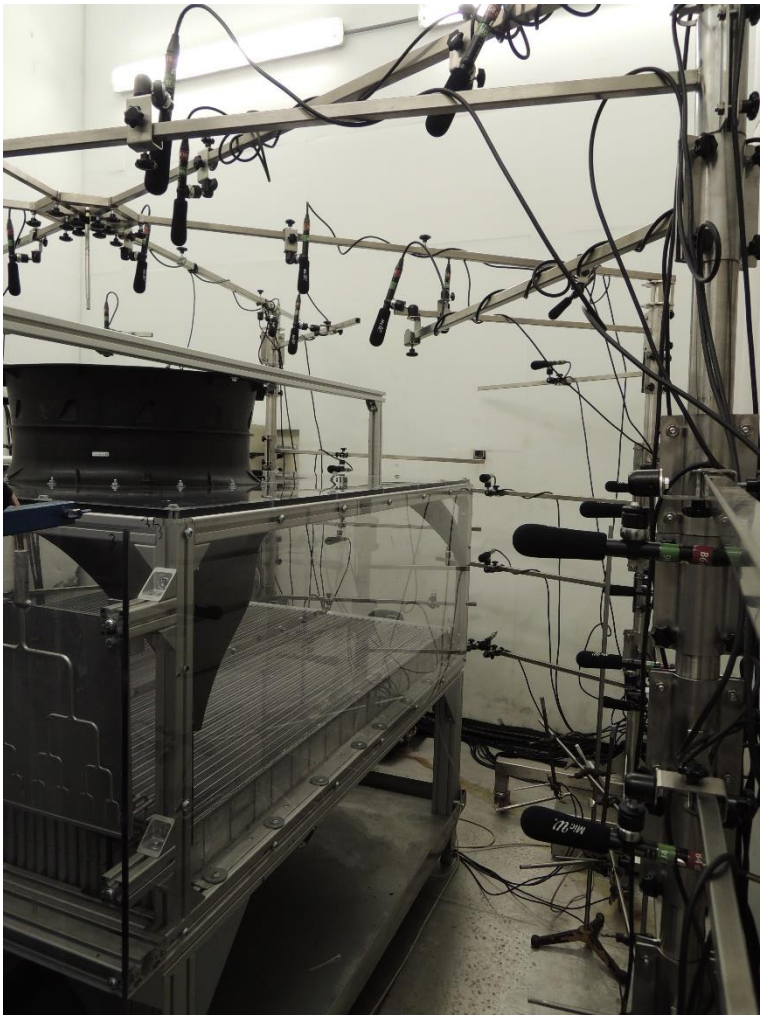

Figure 5.3: Acoustic Dome surrounding the GreenHP (view to the side part)

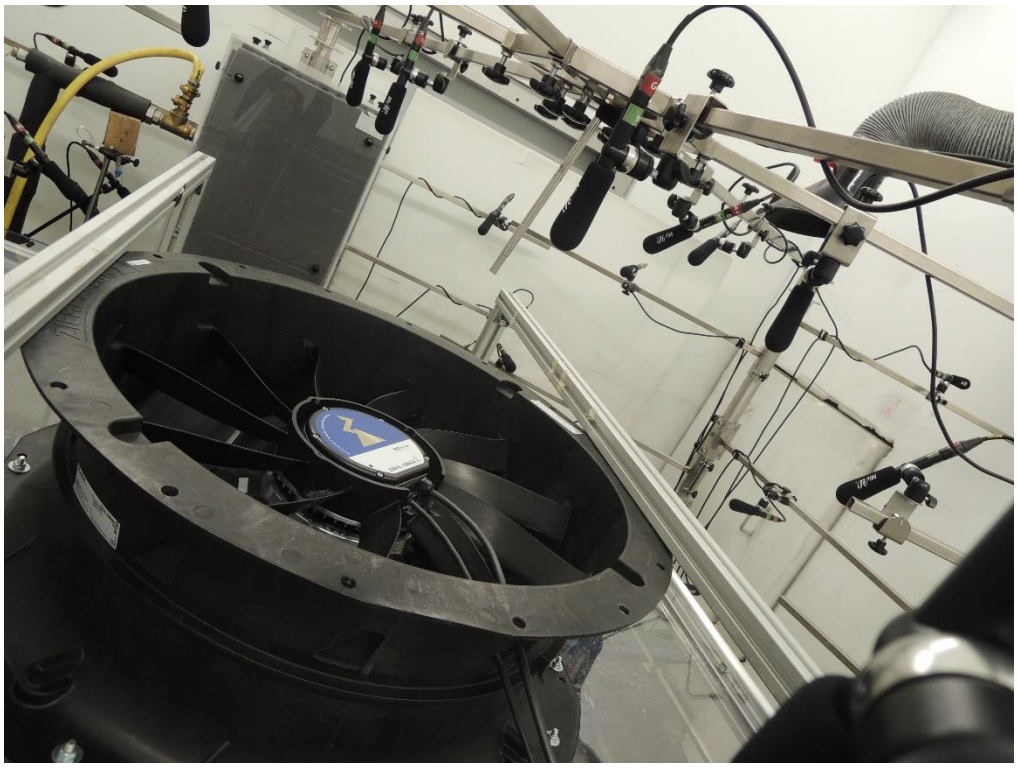

Figure 5.4: Microphone placement in the vicinity of the fan

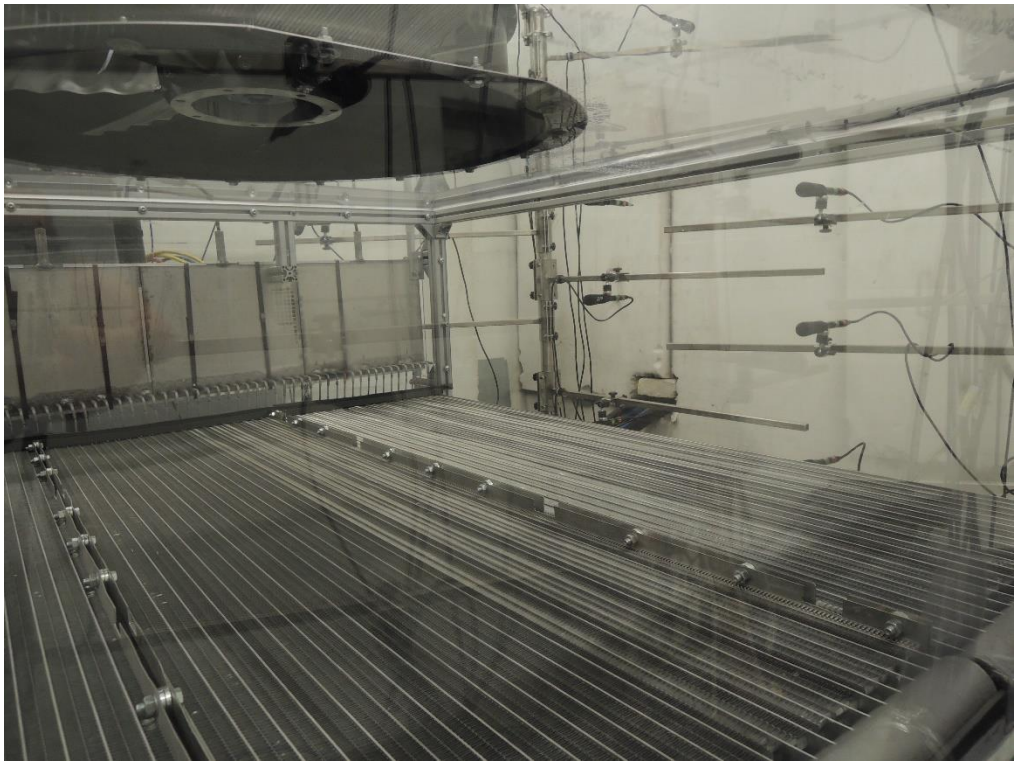

Figure 5.5: View to the space between fan and heat exchanger - microphone placement at the outside can be seen

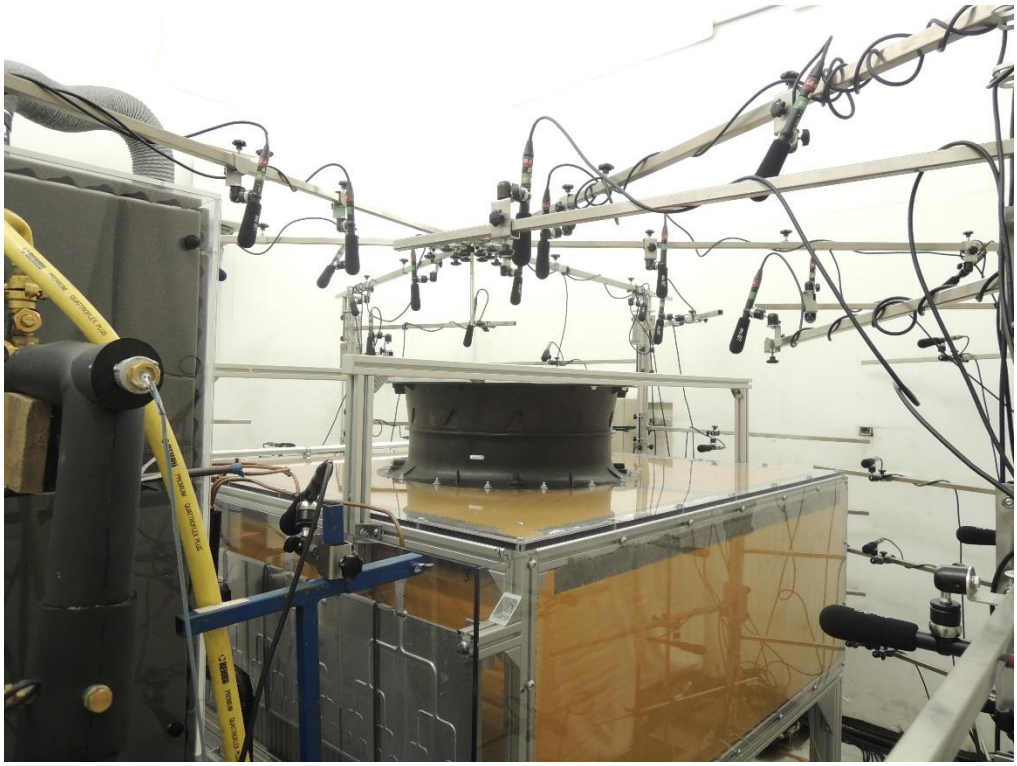

Figure 5.6: GreenHP with mounted sound absorbers (outside view)

Figure 5.7: GreenHP with mounted sound absorbers (inner view towards the fan)

Figure 5.8: GreenHP with mounted sound absorbers (inner view towards the fan, detail)

During the measurements two sorts of images have been recorded (see figure 5.9 / 5.10 and figure series 5.11) to later evaluate the icing progress during operation. An overview is given by the first image capturing device (see figure 5.9 for the initial condition and figure 5.10 for advanced frosting of the full heat exchanger). In figure 5.11 the frosting of the heat exchanger captured by the detail camera is shown in a time frame of around 4 hours) at a detail location. A location, where severe icing occurred, has been selected for positioning of this second camera.

Figure 5.9: Icing of the GreenHP heat exchanger (enlarged view, without ice)

Figure 5.10: Icing of the GreenHP heat exchanger (enlarged view, with ice)

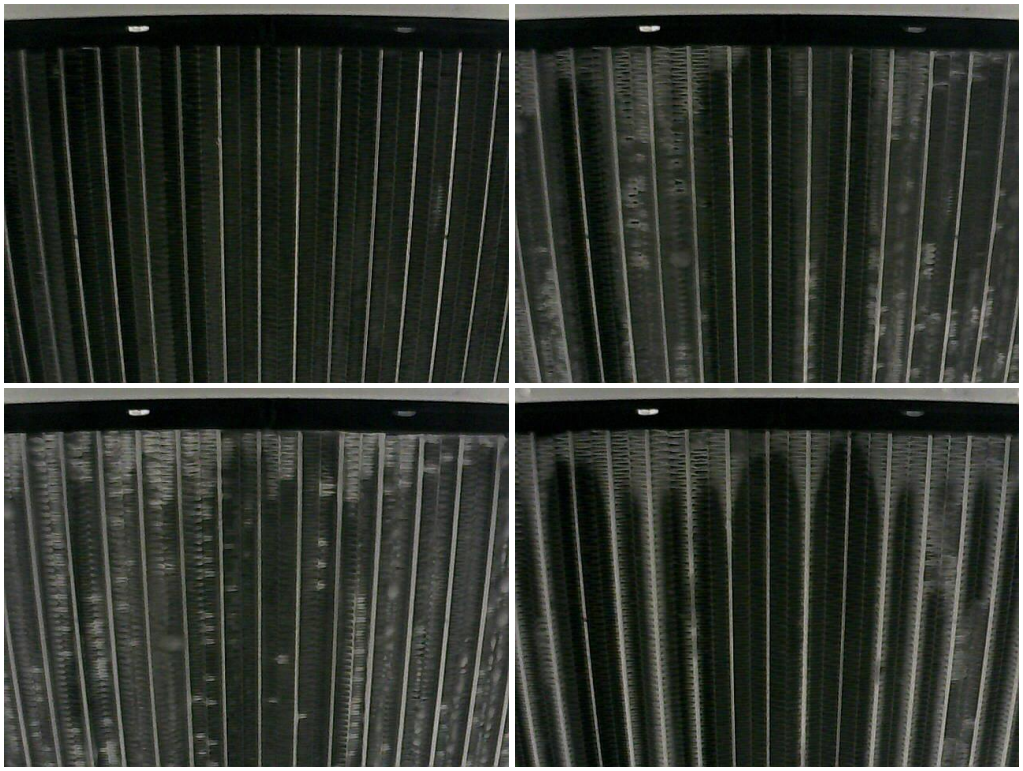

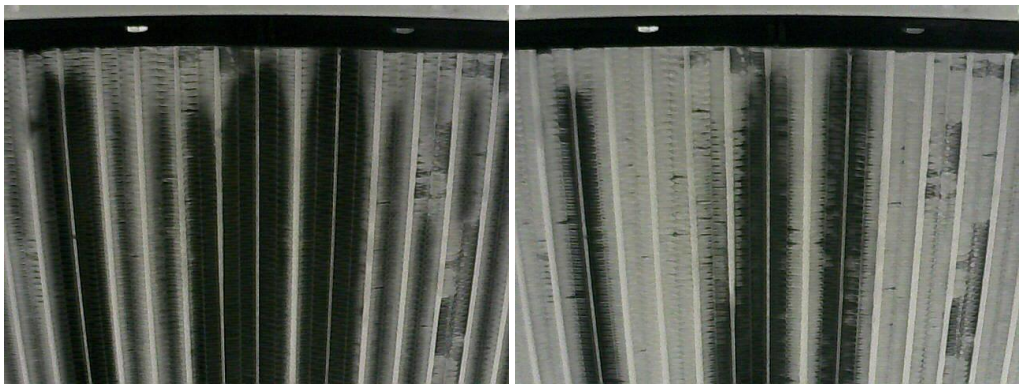

Figure 5.11: Icing of the GreenHP heat exchanger (8:55, 9:54, 10:53, 11:51, 12:33 and 13:09)

5.2. Acoustical optimization of the fan blades

Deliverable 7.1 in the FP7 GreenHP project covers the acoustical optimization of the fan blades as an example for component improvement dedicated to noise reduction:

The fan blades resulting from the CFD optimization process with the given parametrization have been optimized subsequently for acoustical purposes. The fact that the blades are forward swept in the radially outward region is known to be favorable not only for the stall margin, but also from an acoustical point of view. The blade tip regions are equipped with winglets, and the blade trailing edge is serrated in order to reduce trailing edge boundary layer noise, has already been proposed. In the GreenHP project, a new technology was investigated in order to reduce tonal noise. In the present investigation, prototypes have been built with a wavy structure on the blade. In the leading edge region, this wavy structure has a similar effect to the leading edge bumps. Concerning the trailing edge, the serrated trailing edge effect is recovered. In addition, the wavy structure on the blade surface leads to noise reduction due to the scattering of the emitted sound.

Figure 5.11: Fan prototypes for EC090 drive (left) and EC116 drive (right) with tonal noise reduction technique (from the FP7_GreenHP Project, Deliverable 7.1)

In Figure 5.11, the prototypes with the wavy structure are depicted. They have been generated by superposing a sinusoidal wavy component to the circumferential position of the blade sections of the previously described fans for the EC090 and the EC116 drive.

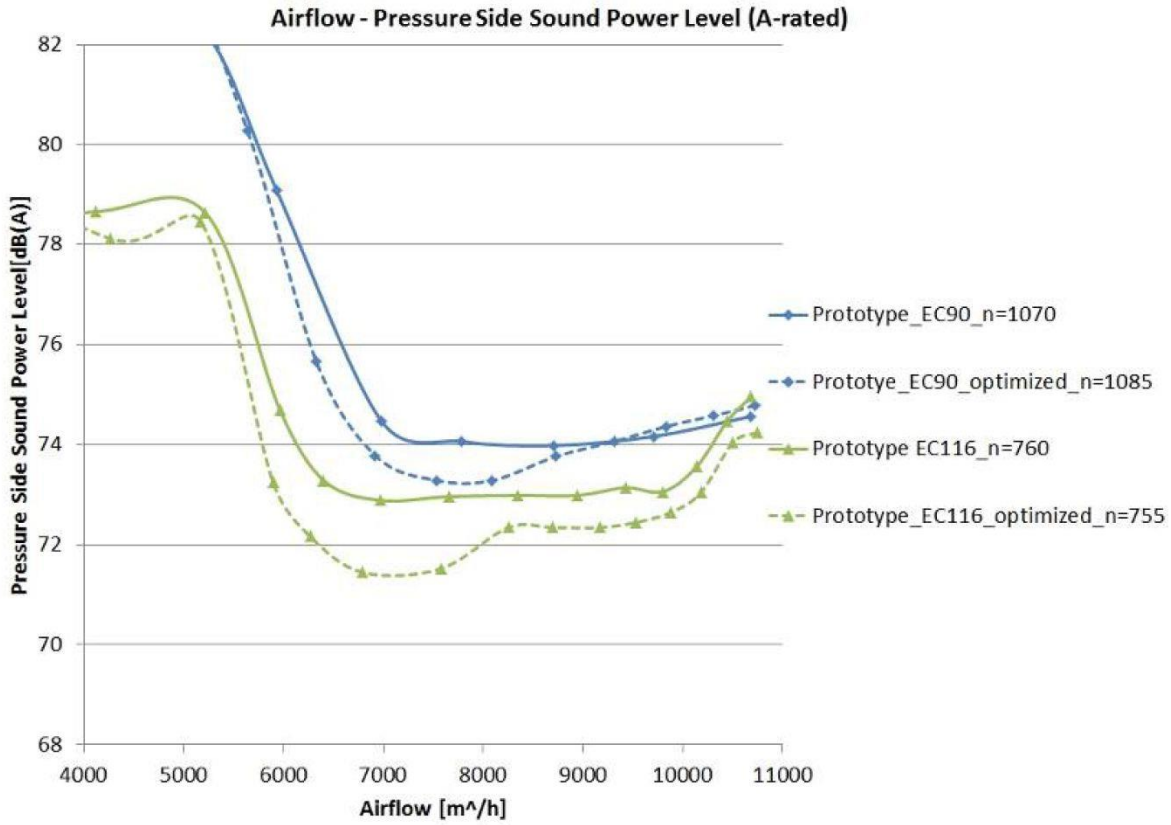

Figure 5.12: Experimental results for the tonal noise optimization technique (from the FP7_GreenHP Project, Deliverable 7.1)

Experimental results for the acoustical behavior of these fans designs are shown in Figure 5.12. Both for the EC090 fan and the EC116 fan, a significant acoustical improvement can be observed using this approach.

Optimization of sound emission is one of the most important issues in the fan-development within heat pumps. There is much knowledge about sound reduction of fans (winglets, profile, serrated trailing edge), which is applied to the fan design for the GreenHP project. In this work, additionally the influence of adjacent parts like the additional diffuser to sound emissions and the important directivity patterns has been worked out. Optimized versions of the diffusor with sound absorbing materials have been tested. The results are shown in figure 5.13, 5.14 and 5.15. It is obvious, that diffusor as well as the on-top diffusor lead to noise reduction. Additionally, the directivity pattern of the noise becomes more attractive in both cases, as the sound radiated to the sides, where potentially people may be situated, is considerably reduced.

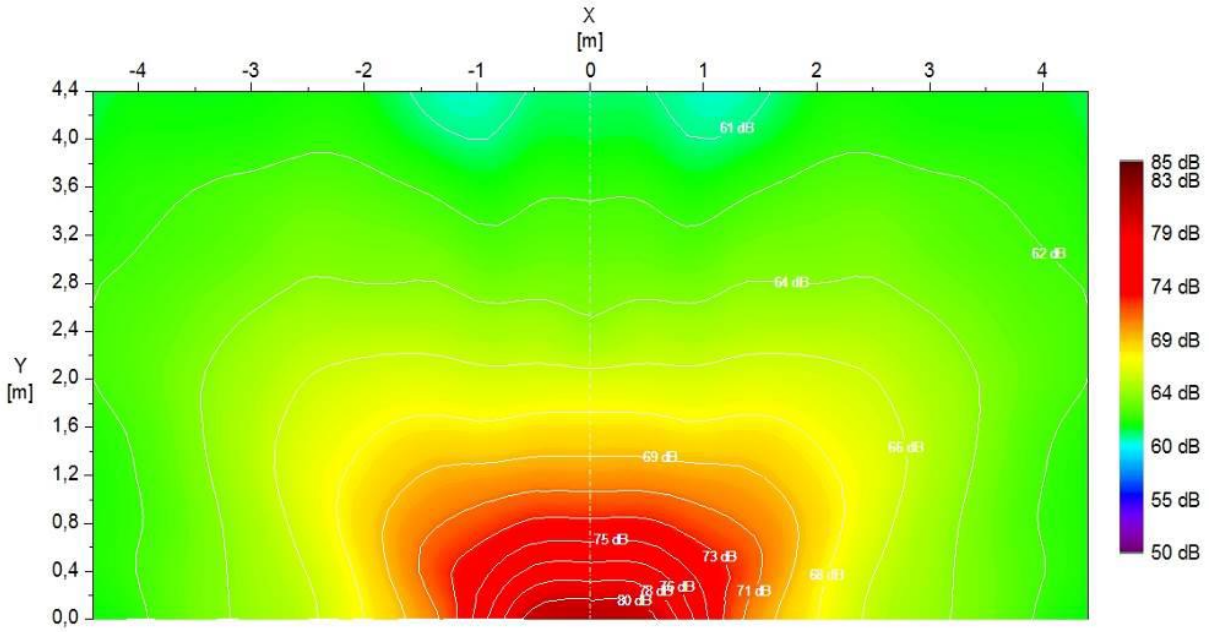

Figure 5.13: Directivity pattern of the fan sound with standard nozzle at 60 Pa (from the FP7_GreenHP Project, Deliverable 7.1)

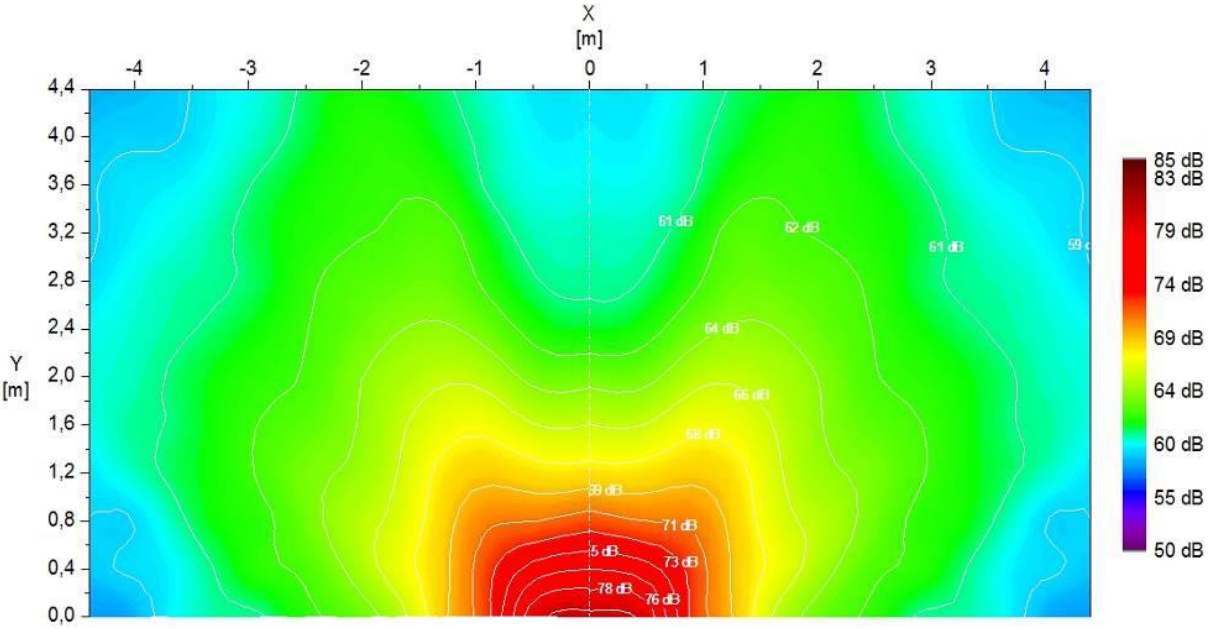

Figure 5.14: Directivity pattern of the fan sound with guide vane unit at 60 Pa (from the FP7_GreenHP Project, Deliverable 7.1)

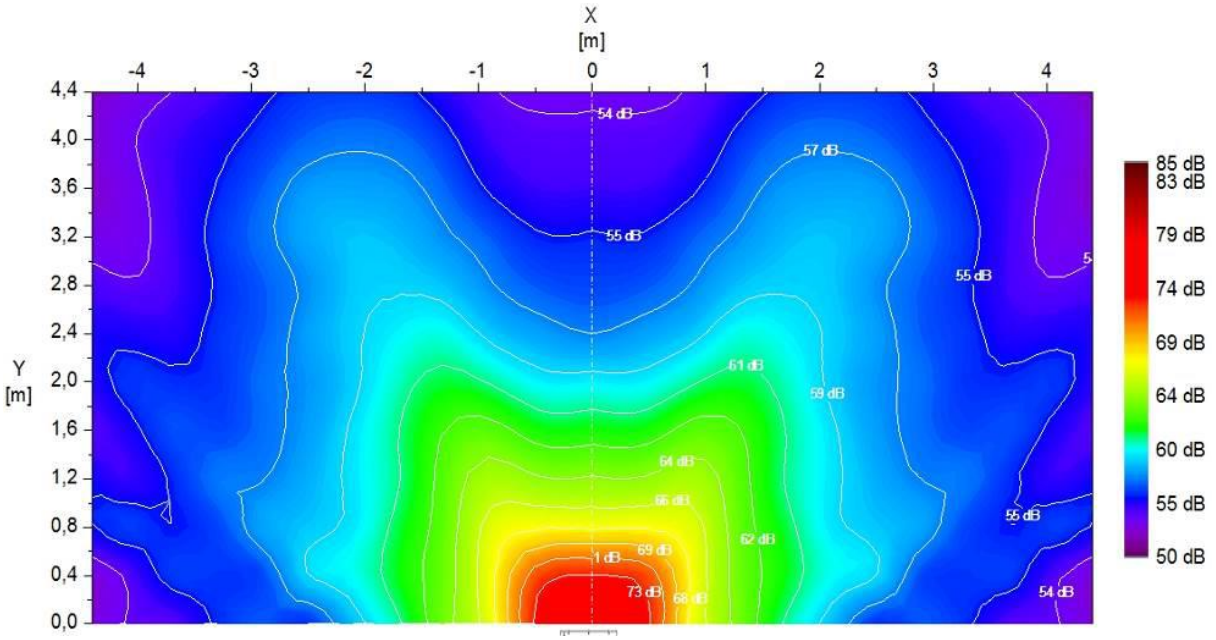

Figure 5.15: Directivity pattern of the fan sound with guide vane unit and diffusor at 60 Pa (from the FP7_GreenHP Project, Deliverable 7.1)

To achieve further noise reduction, the application of sound absorbing material has been investigated (prototype shown in figure 5.16). A further noise reduction of 2-3 dB can be achieved with this method. A problematic issue is however the robustness of this noise absorbing material against environmental and weather concerns.

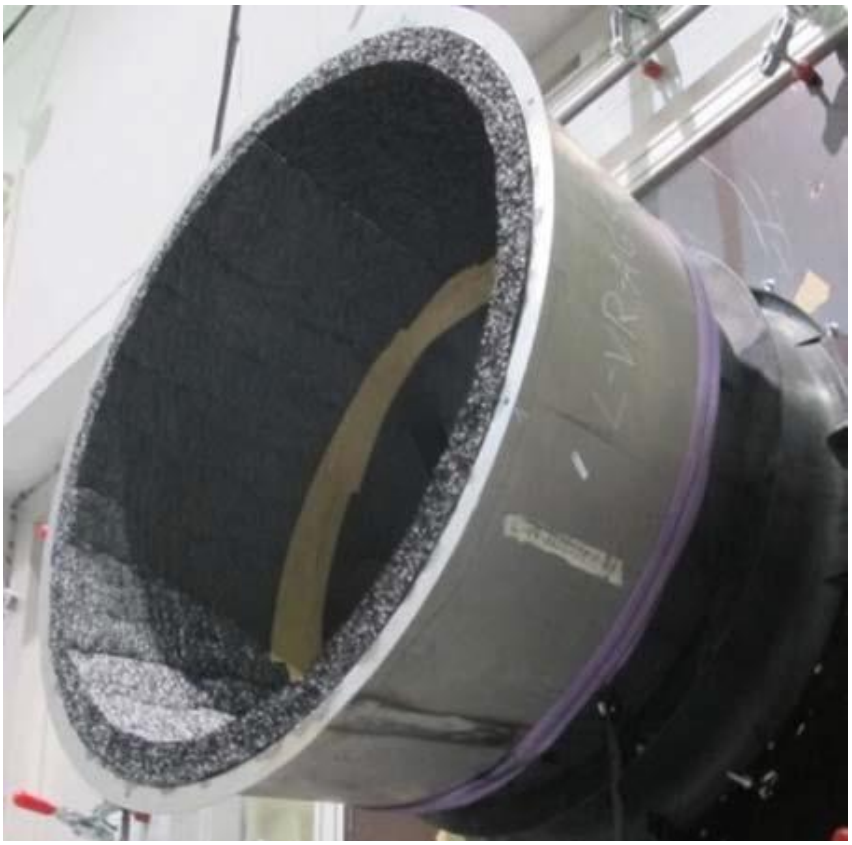

Figure 5.16: Diffusor on guide vane unit with sound absorbing material on test rig (from the FP7_GreenHP Project, Deliverable 7.1)

6. Measurement Service “5ch Acoustics”

The sound power measurement is optimally carried out by determining 5 area scans with an intensity probe in order to be able to take a directional dependence into account in the calculations. A 5 channel measuring system (see figure 6.1) additionally records sound files in 5 directions to enable the heat pump to be made hearable in different operating states.

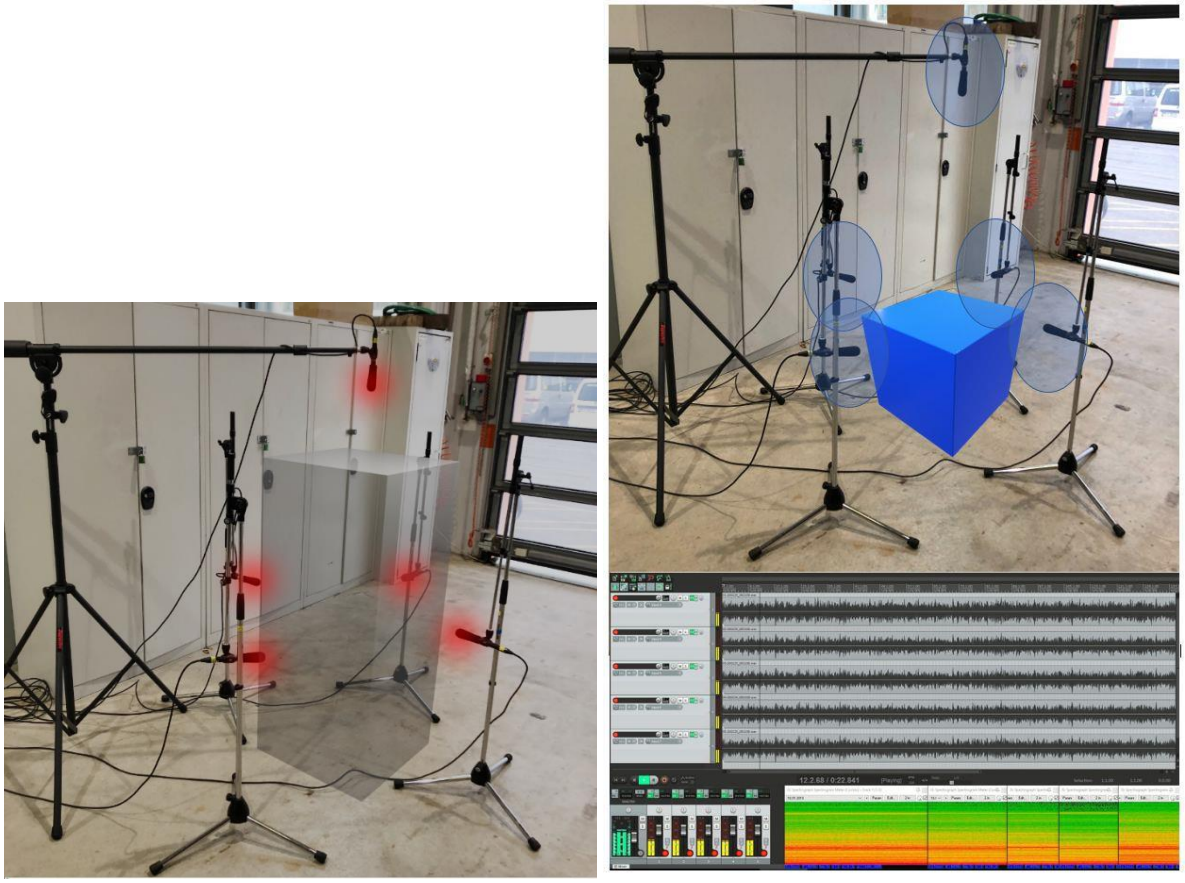

Figure 6.1: 5 microphones are placed around a sound emitting object, one at each side and one from the top. The lower part of the right image shows the 5 five signals and their corresponding frequency content represented in water-fall images. The system is used to generatet he data base for aueralization of heat pumps in the Augemented Reality App.

7. Augmented Reality “HVAC Positioner”

To support the placement of heat pumps or aurelisation of the HVAC component to be newly installed, AIT is developing an app for handheld devices (see figure 7.1). It will allow the virtual placement of a heat pump in the real world and the representation and audibility of sound emissions, taking into account reflections and absorption.

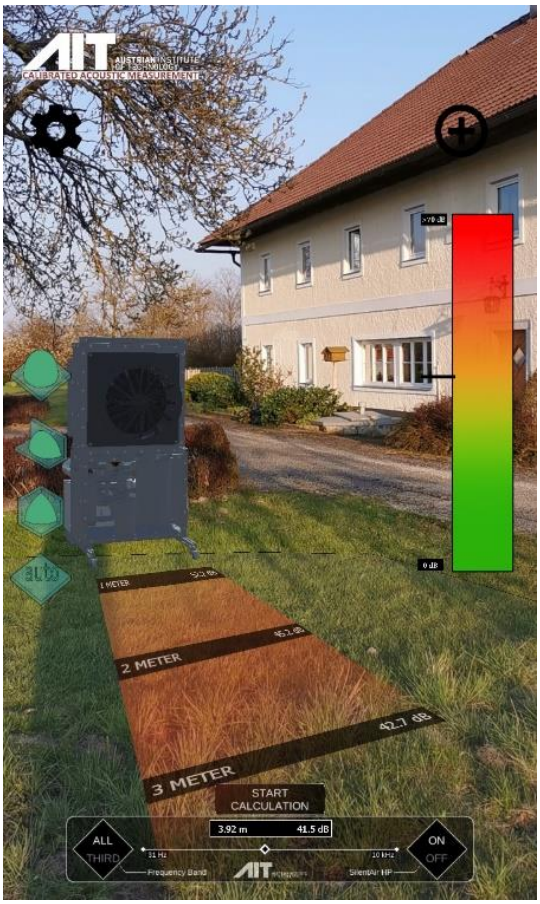

Figure 7.1: Der Laborwärmepumpenprototyp SilentAirHP wird virtuell in eine reale Welt eingeblendet und die Schallemissionen werden sichtbar gemacht.

In the far field of the sound emitter, the best way is to work with half-spheres. Therefore, a methodology has been developed to geometrically calculate 5 sections of a half-sphere, where each sector is attributed to one of the microphones (see Figure 7.2). The sound emitter is presented as a red box (see Figure 3a). Five microphones are placed in a specified distance to this box forming a measurement box (see Figure 3b). Connecting 8 corners of the sound emitter with 8 corners of the measurement box, 8 rays are formed (see orange and green rays in Figure 7.2c) – four on a horizontal place (orange) and four reach-ing to the sky (green). One green and one orange rays are stretching a plane and these four planes are intersected with a sphere (see Figure 7.2d). Finally, the correlation between the 5 parts of the sphere and the corresponding microphone position can be calculated. For this calculation, the following values have to be known: (a) dimensions of the sound emitter, (b) distance between sound emitter and microphone, (c) radius of the sphere.

The aurealisation of the sound emitter is made by a realtime mixing of the 5 wave files (which have been simultaneously recorded) using the position on the sphere. Therefore, one to three signals are used: In the center point of the spheres only one signal is used, on the connection lines between two center points two signals are used, at all other positions three signals have to be mixed. Mixing is performed to ensure that the noise pressure level around the heat pump remains smooth.

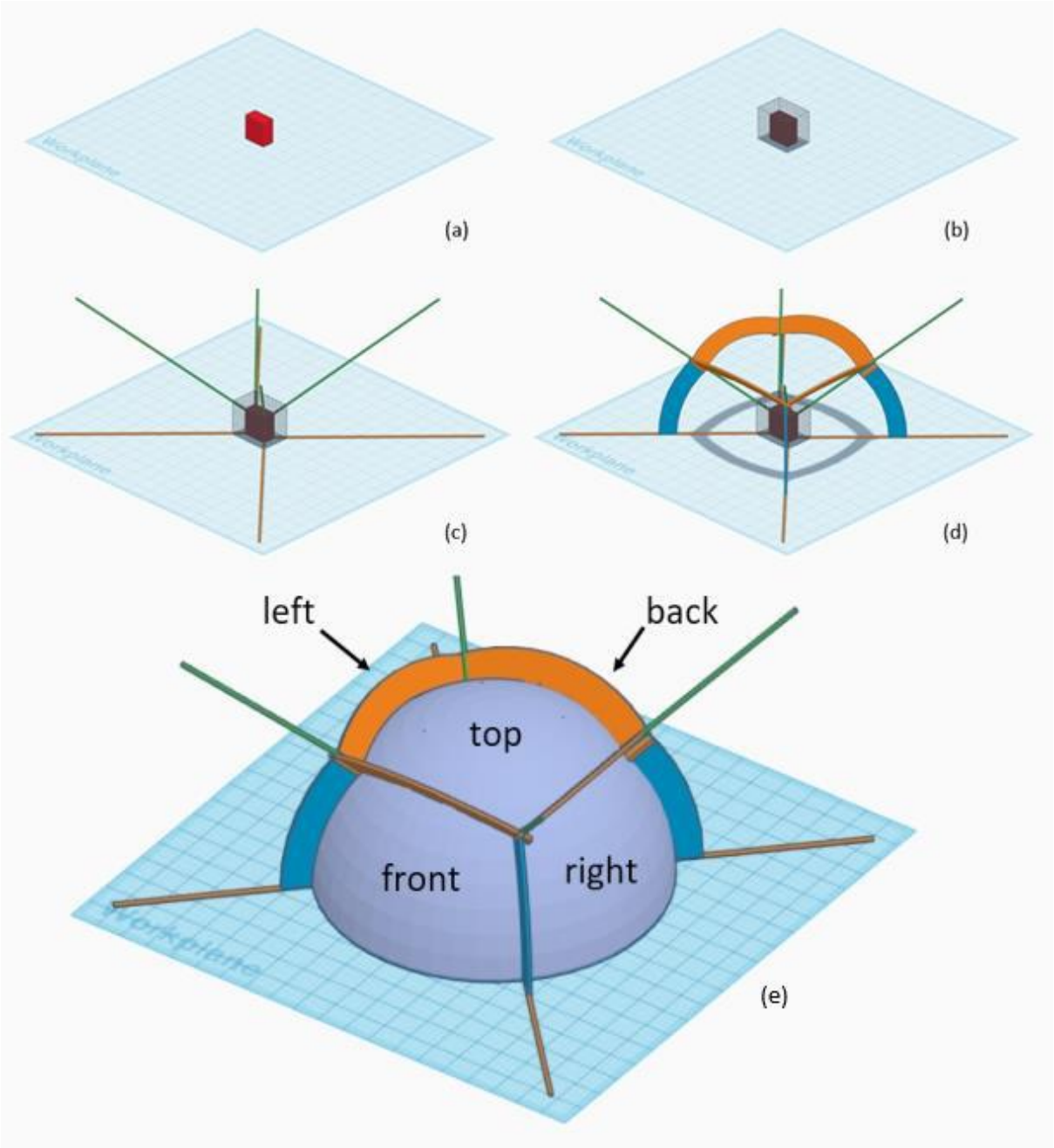

Figure 7.2: Visualization of the directivity aurealisation technique: (a) the red box represents the sound emitting HVAC component (e.g. heat pump); (b) the acoustic pressure is recorded in a specific distance to the emitting surfaces at 5 locations – a measurement surface is formed; (c) rays are generated connecting the emitter's cor-ners with the corners of the measurement surface; (d) parts of the planes stretched by these rays intersected with a sphere; (e) final visualization of the 5 parts of the half-sphere attributed to the 5 microphone measurement po-sitions. (Source: IEA HPT Annex 51 D5)

Various methods are commonly used for calculating sound propagation: Ray tracing, noise mapping, finite element, boundary element, and hybrid methods, among others.

Ray tracing is mostly used for interior problems. This approach is very efficient compared to exact methods such as finite and boundary element method (FEM and BEM, respectively). Sound

propagation in large spaces with many borders can be calculated. Ray tracing is only suitable for outdoor applications if some model for diffraction is included.

Methods of noise mapping can be used when calculating direct sound and first and second reflex-ions. Diffractions are usually only considered approximately based on experiments as well as analytic solutions. The computational effort is relatively low such that these methods can be used on a large scale. However, the efficiency of the analytical approaches is also limited here ([19] Wei et al., 2015). For more complex noise barrier designs, frequency-dependent correction factors can be used to adjust noise mapping calculations ([20] Kasess et al., 2016a). It is however necessary to adjust these values for low heights, short distances and shorter lengths, which are common for the situations considered in this project.

Calculations of the sound distribution using **Finite Element Method** ([21] Bathe, 2014; [22] Reiter, 2017), are limited to small rooms. Radiation can be considered using semi-infinite elements or Perfectly Matched Layers (PMLs). This method can only be used to determine diffraction correction factors behind noise barriers, which is essentially limited to the 2D case.

For noise barriers, the use of the **Boundary Element Method** is usually restricted to mainly 2D or 2.5D calculations, i.e. the cross-section geometry is assumed to be constant in the third dimension, where the latter approach also allows point sources ([23] Duhamel, 1996). Although the efficiency of 2.5D was increased recently ([20] Kasess et al., 2016b), the computational effort required for this does not allow an ad-hoc calculation. Thus, this method is also only suitable for the determination of correction factors. Small geometries allow 3D-BEM calculations, however the frequency range is usually restricted to relatively low frequencies due to the much higher effort.

Following methods were considered additionally in terms of their usefulness in the current project: The use of the **Finite-Difference Time-Domain Method** for outdoor sound propagation modelling is discussed in ([24] van Renterghem, 2014). The **Wave Based Method** ([25] Deckers et al., 2014) is usually used for indoor spaces. **Transformation methods** may be useful in some special cases in this project when only single bordered areas are considered.

The sound propagation of outdoor HVAC units still requires a lot of testing and experimental methods, especially when placed in urban areas. Simulating noise propagation of such units was also re-searched in ([26] Poysat et al. 2019) and noise propagation with a focus on urban areas is discussed in ([27] Ismail and Oldham, 2003).

Here, the following approach was chosen to calculate the values at different positions and distances around the HVAC unit: The recorded sound pressure levels are used as a basis for the simulation of the sound propagation. The directivity of the source is modelled using one monopole and three dipoles, because this assumption simplifies the mapping from source to receiver. The mapping is done mainly as described in ÖNORM ISO 9613-2:2008.This standard includes diffraction, where the diffraction from di-poles is assumed to be identical to the diffraction from monopoles.

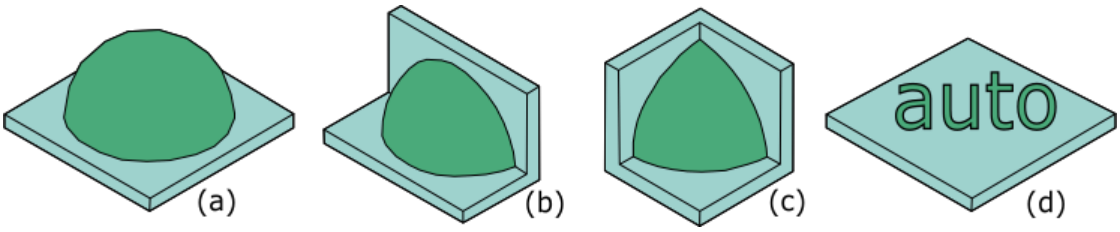

Figure 7.3: Calculation of sound propagation with different options regarding the surrounding environment: (a) free field with floor plane; (b) along a wall; (c) in a corner; (d) automatically detect the surrounding geometry for the simulation (Source: IEA HPT Annex 51 D5)

The reflection from the wall and the ground are simulated using mirror sources. If both are included four sources are needed. If a noise barrier is used also, five sources are needed, since the mirror source behind this barrier is the same for all sources on the source side. Special edges can be calculated with the boundary element method before the real-time session starts, which are performed in 2.5D. The result of this method is attenuation factor depending on the diffraction angle. For deriving a curve, which can be interpolated in real-time, the calculation is repeated. In the developed application the user can select one of four options for the calculation, according to the surrounding environment, as seen in Figure 7.3.

The results of these calculations are visualized for the specific user for clarifying their meaning in an augmented reality environment. There, different visualization options are considered: The measurement values can be projected on the floor or rendered as three-dimensional tags at given distances and directions. The sound pressure level, the user would hear at their current position, can also be visualized using a gradient of traffic light colours according to the effect of the sound pressure level on the human health, which means: green for unproblematic and red for severely damaging sound pressure levels. A textual representation of the current distance to the sound source along with the simulated sound pressure level is another possible approach. A transparent wall or coloured plane that signifies the exceeding of a certain threshold in a given area is another option.

In the developed application, the sound pressure levels are visualized using several of these options, as seen in Figure 7.1.

Various SDKs (Software Development Kits) and development environments are available for developing augmented reality applications. These include vendor-specific solutions, which are only working on their native platforms, like SDKs from [28] BOSE (2020) or [29] Apple Inc. (2020a), as well as solutions working on multiple platforms like Vuforia ([30] PTC, 2020), [31] DeepAR (2020) or [32] Kudan (2020). While some of the toolkits are re-leased as open-source or free projects, others are only available as commercial software or still exist only as beta versions. In [33] Amin and Govilkar (2015) a further categorization according to their overlaying capabilities is discussed. For iOS applications Apple released a native framework, ARKit, in 2017. Google's ARCore ([34] Google, 2020) primarily targets Android devices and became popular after Google's Tango was discontinued in 2017 ([35] Jansen, 2020). Most SDKs rely on third party 3D engines such as Unity Technologies ([36] 2020), Unreal Engine ([37] 2020) or Apple Inc. ([38] 2020b) as development environment ([39] Romilly, 2020).

For this project the Unity environment and Unity's AR Foundation, which acts as a common inter-face for both ARKit and ARCore, are used to develop an app for iOS as well as Android devices.

Calculation and visualization methods of outdoor noise sources, i.e. of HVAC units, were examined and an augmented reality application was developed. These works can help users to evaluate the environmental noise, which is emitted by different noise sources virtually, as well as to find a suitable position before the units are physically placed. The next steps in this project are the automated detection of the environment and including these results into the sound pressure level calculation. Thus, sound-specific properties of the environment are meant to be configurable and considered in the calculation by adding reflexion and absorption.

The current state of the app can be downloaded in

- Google Playstore: HVAC Positioner[6]
- iOS store: iOS HVAC Positioner[7]

8. Sound field simulations

The installation of heat pumps and the acoustic influence on the environment is an essential aspect in understanding the generated sound emissions. The placement of a large number of heat pumps in a terraced housing estate, for example, becomes an acoustic optimisation problem if the aim is to achieve the lowest possible immissions from the countless viewing points (windows) (see Figure 8.1).

[6] https://play.google.com/store/apps/details?id=at.ac.ait.hvacpositioner&gl=AT
[7] https://apps.apple.com/at/app/hvac-positioner/id1462057877

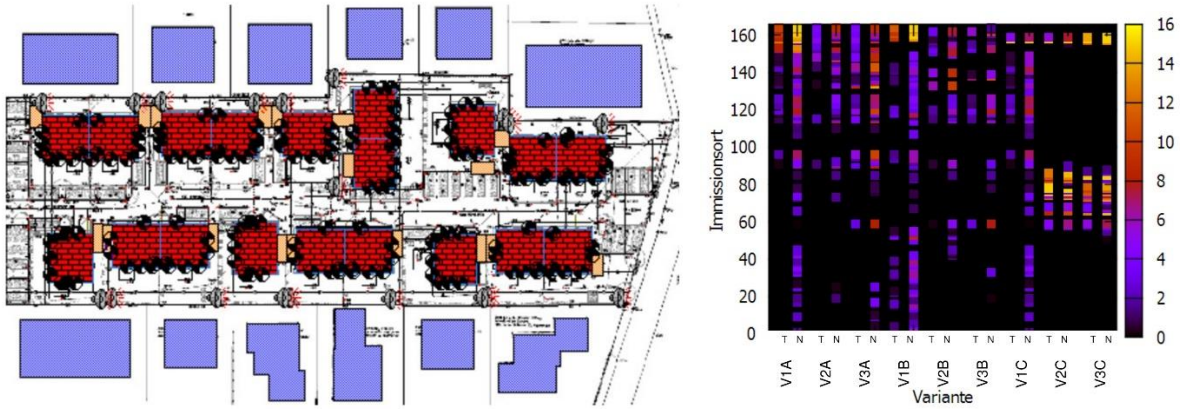

Figure 8.1: Immission points in front of windows (top), heat pump installation locations (bottom left), penalty points for exceeding the limit value (bottom right) (Source: AIT, Austria)

Table 8.1 shows how many penalty points each of the variants, which differ in number and location of the heat pumps, receives. First of all, the penalty points are added up, which are awarded on the basis of the exceedances at the critical immission locations. A distinction is made between day and night, as some of the heat pump models used are operated at night in lowered mode, which results in a lower sound power level. The figures in bold in the table indicate the sum of the penalty points for the periods day and night. The list also contains the maximum and minimum number of penalty points that are awarded for exceeding the limit values at a single critical point of immission. The evaluation of the minimum value is such that only penalty point values that are greater than zero are taken into account. When determining the average number of penalty points, only those penalty point values that are greater than zero are also taken into account. The minimum value of each parameter is highlighted in green, while maximum values are highlighted in red.

Scenario A	Variant 1A		Variant 2A		Variant 3A	
	Day	Night	Day	Night	Day	Night
Sum penalty points	119,71	346,64	33,41	153,08	76,46	239,72
Sum penalty points	**466,35**		**186,49**		**316,18**	
Max. penalty points	12,56	17,56	5,52	10,52	8,93	13,93
Min. penalty points	0,13	0,06	0,37	0,18	0,01	0,15
Mean penalty points	4,13	5,59	2,78	3,93	3,19	4,99
Scenario B	**Variant 1B**		**Variant 2B**		**Variant 3B**	
	Day	Night	Day	Night	Day	Night
Sum penalty points	98,73	341,81	36,89	133,71	30,59	108,86
Sum penalty points	**440,54**		**170,60**		**139,44**	
Max. penalty points	11,32	16,30	5,95	9,95	6,78	11,23
Min. penalty points	0,29	0,40	0,17	0,11	0,53	0,15
Mean penalty points	3,40	4,81	2,46	4,05	2,78	4,19
Scenario C	**Variant 1C**		**Variant 2C**		**Variant 3C**	
	Day	Night	Day	Night	Day	Night
Sum penalty points	57,28	230,82	160,62	198,64	167,65	215,25
Sum penalty points	**288,10**		**359,26**		**382,90**	
Max. penalty points	31,87	33,87	22,44	24,44	22,13	24,13
Min. penalty points	0,13	0,06	1,82	0,04	1,07	0,12
Mean penalty points	2,86	4,44	10,04	9,03	8,38	7,97

Table 8.1: Distribution of penalty points to the nine variants (green shows the best value in a row, red the worst number in a row) (Source: IEA HPT Annex 51 D5)

Due to its low number of penalty points, variant 3B of scenario B scores best when the presented rating system is used as a basis. The reason for the good performance of scenario B is the optimal ratio between the number and sound power level of the heat pumps. Fewer heat pumps are used than in scenario A, which means fewer noise sources in the settlement. In addition, the sound power level of the individual devices is lower than that of the model used when a local heating supply with only two heat pumps is set up for the entire settlement (for a detailled description please download the IEA HPT Annex 51 D5 document here: IEA HPT Annex 51 D5

Since the 3rd variant of scenario B has achieved the fewest penalty points, it is further optimized by building noise barriers around the heat pumps. This protective device can be found above every heat pump. It is 1.70 m high, 1 m long and 1 m wide. As the dimensions of the heat pumps are only slightly smaller, the attached walls are space-saving. Two opposite sides must remain free to allow air to be sucked in and blown out. In this simulation, the openings are oriented either north and south or east and west. Depending on the position of the pump, the direction of the opening that is better suited in

terms of sound insulation is chosen. A minimum distance of 3 m is maintained between the discharge area and the house walls to prevent premature ice formation. This would occur because the air blown out is colder than the ambient air.

The results of the simulation of variant 3B with noise barriers are shown in Figure 8.2. It is shown how high the overshoots or undershoots are when the defined maximum sound pressure levels are used as a guide value. In order to illustrate the comparison with the variant without noise barriers, it is also shown in the diagram. The designations "with" ("mit") and "without" ("ohne"), which are attached to the abbreviation of the variants in the diagram, indicate whether the test results show the case with or without the use of noise barriers. In case of 16 penalty points and more, the marking is in yellow.

The local heating supply scenario has the advantage that the sound is emitted by only two heat pumps instead of 13. Moreover, in the best variant of scenario C both heat pumps are placed next to each other. This means that there is practically one central sound source. The sound power level of this is higher than that of the model of the 13 heat pumps of variant 3B. However, since the sound emanates from a central point, it is obvious to surround this with noise barriers in order to achieve the lowest sound pressure levels at the critical immission points. Three barrier layers are built around the heat pumps from variant 1C. The outermost layer is the highest at 7.75 m. When erecting the walls, care is taken to ensure that the air blown out on one side of the heat pumps is not drawn in on the other side.

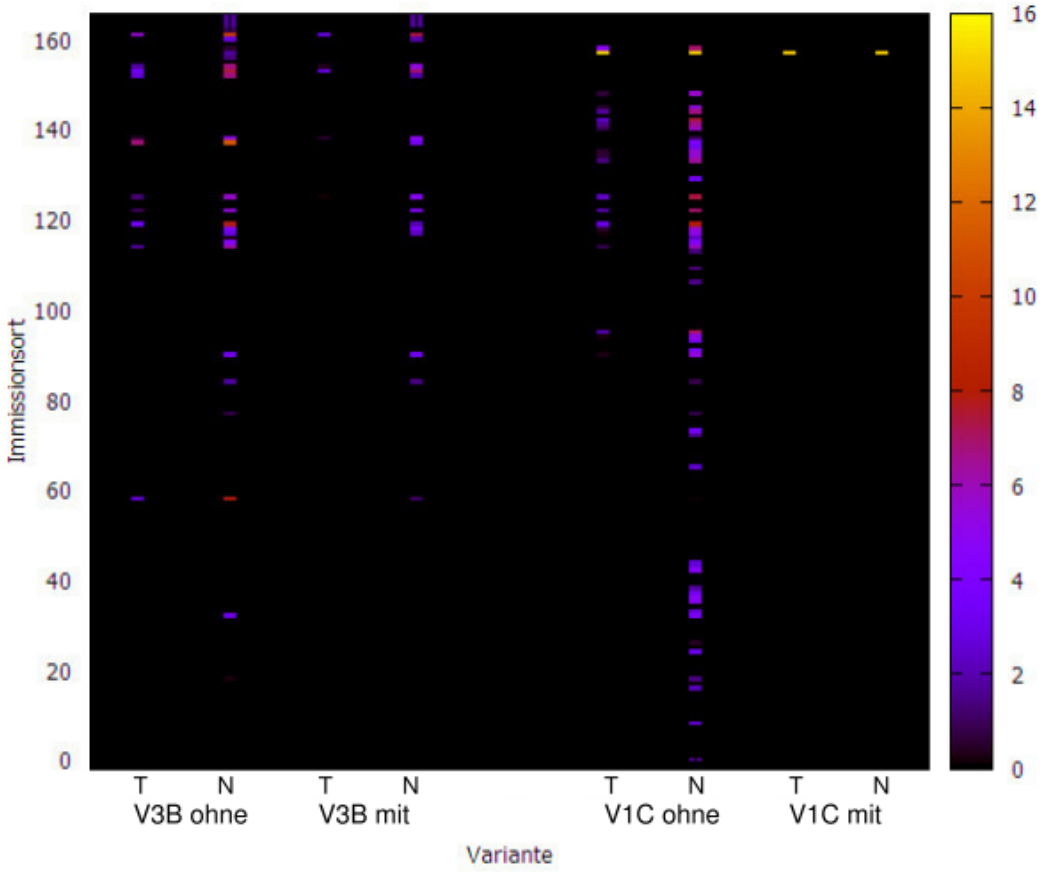

Figure 8.2: : Penalty points at the places of immission for two variants with ("mit") and without ("ohne") noise barriers (Source: IEA HPT Annex 51 D5)

Table 8.2 shows the sum, maximum, minimum and average value of the penalty points awarded for the variants with noise barriers. For comparison, the values of the previous chapter are given again.

Variant 3B	with noise barriers		without noise barriers	
	Day	Night	Day	Night
Sum penalty points	30.59	108.86	6.66	55.37
Sum penalty points	**139.44**		**62.03**	
Max. penalty points	6.78	11.23	3.10	7.30
Min. penalty points	0.53	0.15	0.08	1.10
Mean penalty points	2.78	4.19	1.33	3.46
Variant 1C	with noise barriers		without noise barriers	
	Day	Night	Day	Night
Sum penalty points	57.28	230.82	23.03	25.03
Sum penalty points	**288.10**		**48.06**	
Max. penalty points	31.87	33.87	23.03	25.03
Min. penalty points	0.13	0.06	23.03	25.03
Mean penalty points	2.86	4.44	23.03	25.03

Table 8.2: Distribution of penalty points on two variants with noise barriers (Source: IEA HPT Annex 51 D5)

The use of barriers also leads to impermissible exceeding of the sound pressure level. To ensure that the defined limits are complied with, the heat pump model in variant 1C may emit a maximum of 50.97 dB(A) during the day and 45.97 dB(A) at night. For the model used to heat the individual houses in variant 2B, these maximum values are 49.9 dB(A) during the day and 45.7 dB(A) at night. For the model which, in the same variant, is used to heat the semi-detached houses, these maximum values are 50.9 dB(A) during the day and 45.7 dB(A) at night. This is the result of a simulation in IMMI, in which the sound power levels of the heat pump models are changed so that the defined maximum permissible sound pressure levels are maintained at all critical immission points.

The detailed report can be retrieved at the IEA HPT Annex 51 website:

https://heatpumpingtechnologies.org/annex51/wp-content/uploads/sites/59/2021/10/iea-hpt-annex-51-d5.pdf

9. Dome measurements of a commercial two fan heatpump

As a test system on the market for end customers, a commercial air-water heat pump was acoustically measured. She was part of a round robin test series of the BAM (Federal Institute for Materials

Research and Testing) at AIT. This is a monobloc air-to-water heat pump (see Figure 9.1). These measurements have been performed in the framework of RAARA project (FFG # 873588).

For the calculation of the time-dependent sound power level and for the visualization of the data, the coordination of the microphone positions of the acoustic dome (see Figure 9.2) is essential.

Figure 9.1: Inside part (left) and outside part (right) of the measured air-water heat pump(Source: Heizungsdiscount24.de)

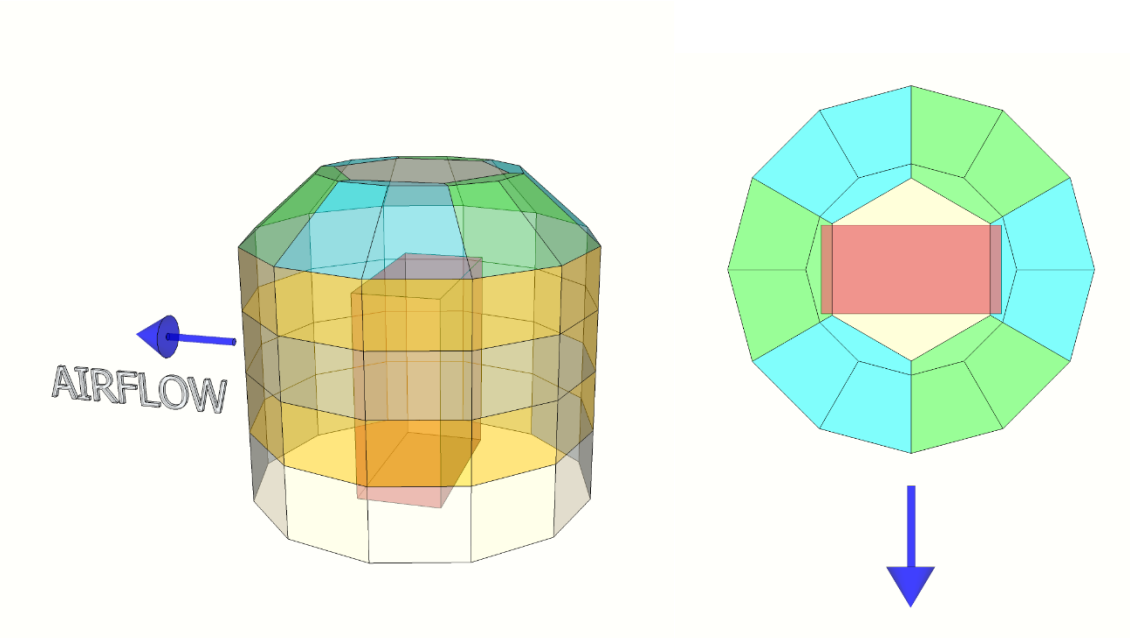

Figure 9.2: Visualization of the structure of the acoustic dome (Source: AIT)

Figures 9.3 and 9.4 show the microphone numbers. Table 9.1 shows the coordinates of the 55 microphones.

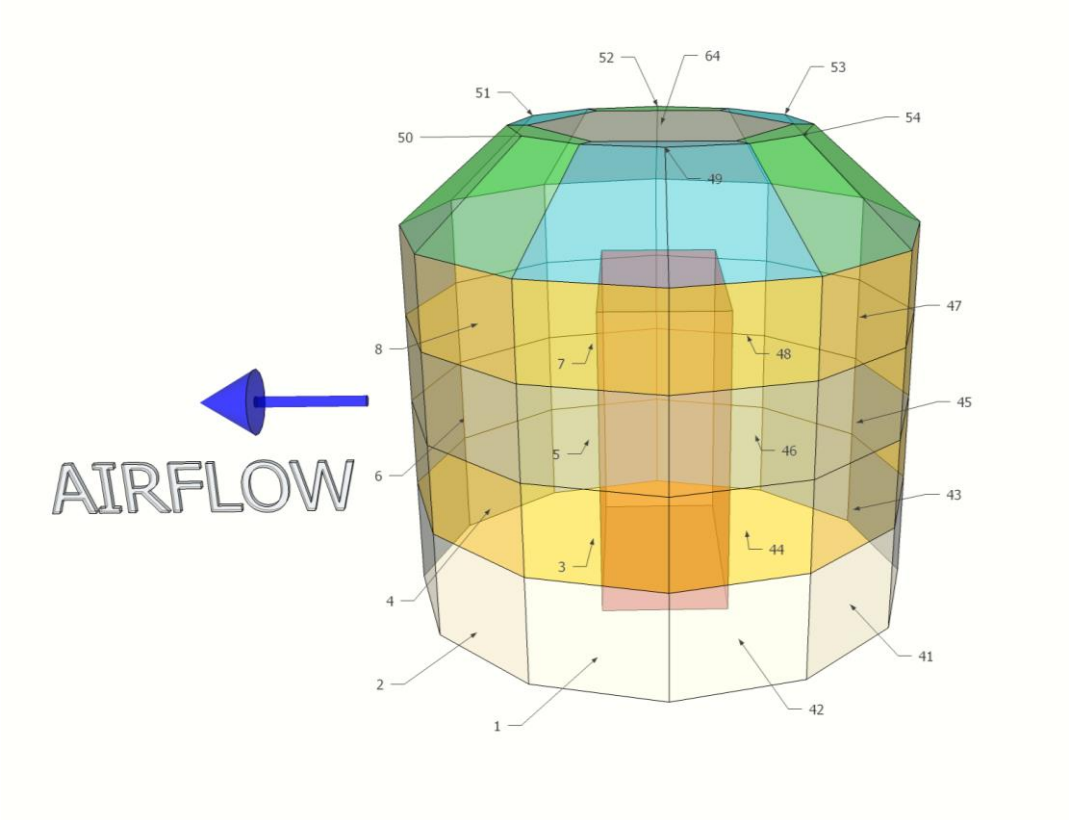

Figure 9.3: Microphone numbers shown in the visualization of the structure of the acoustic dome. The arrow indicates the direction of the flow of the air heat pump (Source: AIT)

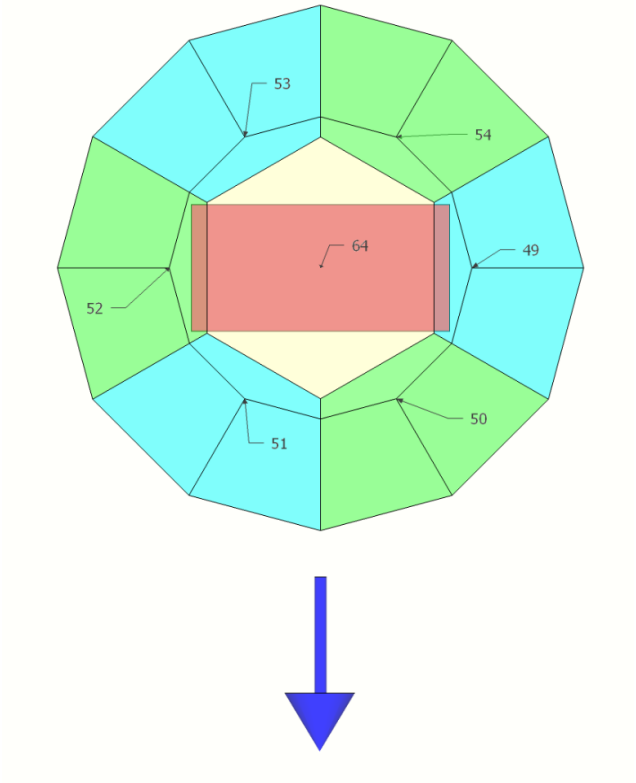

Figure 9.4: Microphone numbers shown in the visualization of the structure of the acoustic dome (Source: AIT)

Mic #	x	y	z
1	-1,063	-0,25	0,28
2	-0,748	-0,796	0,28
3	-1,063	-0,25	0,68
4	-0,748	-0,796	0,68
5	-1,063	-0,25	1,08
6	-0,748	-0,796	1,08
7	-1,063	-0,25	1,48
8	-0,748	-0,796	1,48
9	-0,315	-1,046	0,28
10	0,315	-1,046	0,28
11	-0,315	-1,046	0,68
12	0,315	-1,046	0,68
13	-0,315	-1,046	1,08
14	0,315	-1,046	1,08
15	-0,315	-1,046	1,48
16	0,315	-1,046	1,48
17	0,748	-0,796	0,28
18	1,063	-0,25	0,28
19	0,748	-0,796	0,68
20	1,063	-0,25	0,68

Mic #	x	y	z
21	0,748	-0,796	1,08
22	1,063	-0,25	1,08
23	0,748	-0,796	1,48
24	1,063	-0,25	1,48
25	1,063	0,25	0,28
26	0,748	0,796	0,28
27	1,063	0,25	0,68
28	0,748	0,796	0,68
29	1,063	0,25	1,08
30	0,748	0,796	1,08
31	1,063	0,25	1,48
32	0,748	0,796	1,48
33	0,315	1,046	0,28
34	-0,315	1,046	0,28
35	0,315	1,046	0,68
36	-0,315	1,046	0,68
37	0,315	1,046	1,08
38	-0,315	1,046	1,08
39	0,315	1,046	1,48
40	-0,315	1,046	1,48

Mic #	x	y	z
41	-0,748	0,796	0,28
42	-1,063	0,25	0,28
43	-0,748	0,796	0,68
44	-1,063	0,25	0,68
45	-0,748	0,796	1,08
46	-1,063	0,25	1,08
47	-0,748	0,796	1,48
48	-1,063	0,25	1,48
49	-0,65	0	2,1
50	-0,325	-0,563	2,1
51	0,325	-0,563	2,1
52	0,65	0	2,1
53	0,325	0,563	2,1
54	-0,325	0,563	2,1
55	0	0	2,1

Table 9.1: Coordinates of the 55 microphones of the acoustic dome (Source: AIT)

For the calculation of the sound power level, the corresponding representative areas for the 55 microphones are determined from the coordinates, which together result in a closed enveloping surface. In Table 9.2, the areas are given in square centimeters for the acoustic dome.

Mic #	Area [cm²]	Mic #	Area [cm²]	Mic #	Area [cm²]
1	2807,67	21	2339,72	41	2807,67
2	2807,67	22	2339,72	42	2807,67
3	2339,72	23	2339,72	43	2339,72
4	2339,72	24	2339,72	44	2339,72
5	2339,72	25	2807,67	45	2339,72
6	2339,72	26	2807,67	46	2339,72
7	2339,72	27	2339,72	47	2339,72
8	2339,72	28	2339,72	48	2339,72
9	2807,67	29	2339,72	49	6504,57
10	2807,67	30	2339,72	50	6504,57
11	2339,72	31	2339,72	51	6504,57
12	2339,72	32	2339,72	52	6504,57
13	2339,72	33	2807,67	53	6504,57
14	2339,72	34	2807,67	54	6504,57
15	2339,72	35	2339,72	55	8232,65
16	2339,72	36	2339,72		
17	2807,67	37	2339,72		
18	2807,67	38	2339,72		
19	2339,72	39	2339,72		
20	2339,72	40	2339,72		

Table 9.2: Reference surfaces in square centimeters of the 55 microphones of the acoustic dome and the 5 surfaces of the auxiliary microphones (Source: AIT)

9.1. Transient behaviour data sample

As an example, the evaluation of the one data set of the air-to-water heat pump is shown in Figure 9.5. A breakdown into the different frequency components can be found in Figure 9.6.

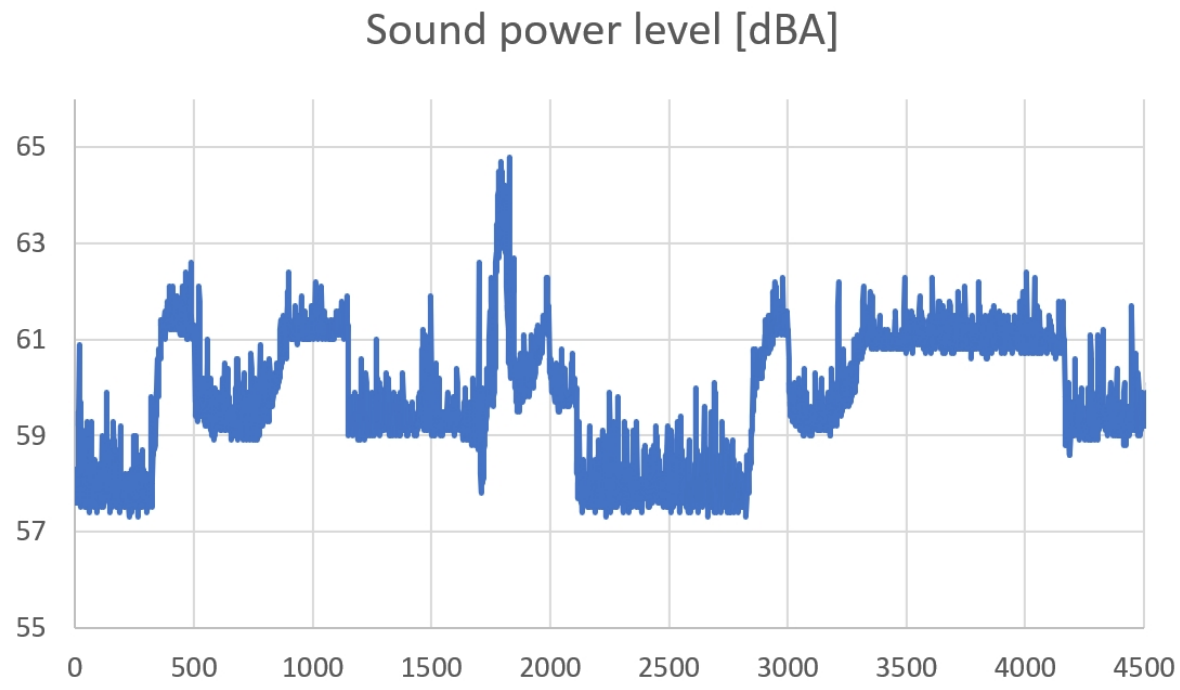

Figure 9.5: Example of a sound power level evaluation of one measurement. Shown is the A-weighted sound power level in dBA. The x-axis is the indication of the running seconds after the start of the measurement. (Source: AIT)

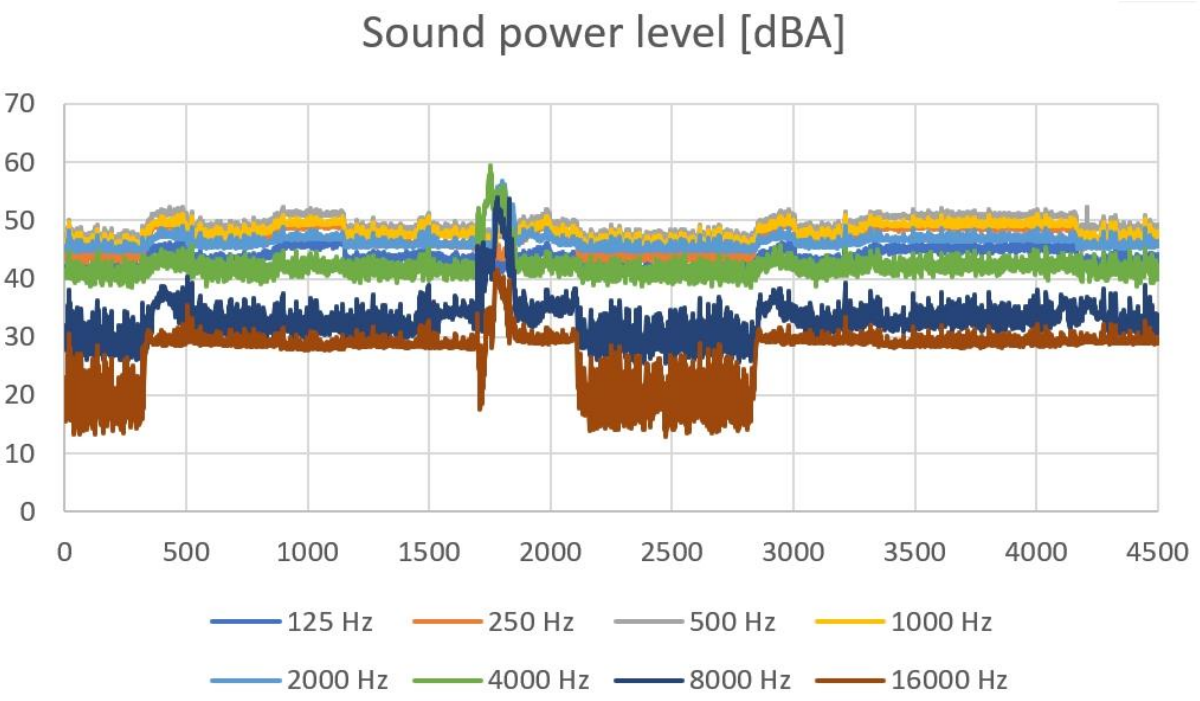

Figure 9.6: Representation of the frequency components of the sound power level of the example measurement - see also Figure 9.5 (Source: AIT)

9.2. Sound power level analysis for different operating points

Table 9.3 summarises the sound power levels at the four different operating points together with the corresponding conditions in the climate chamber. The sound power level increases with decreasing ambient temperature for this heat pump by a total of 8.9 dBA. For this purpose, time sections with steady state conditions for all four measurement points have been extracted from the data set and the mean sound power level has been calculated.

measurement	Temperature [°C]	relative humidity [%]	Sound power level [dBA]
empty (C1)			47.7
M06	-10	70	65.6
M04	2	84	61.1
M10	7	90	59.4
M05	12	90	56.9

Table 9.3: Compilation of measurements on the heat pump at different temperatures and humidities (Source: AIT).

Figure 9.7 to 9.10 show the A-weighted one-third octave band spectra at four different operating temperatures. Figure 9.11 shows the one-third octave band spectrum of a blank measurement without heat pump, using the same calculation algorithm for sound power level determination.

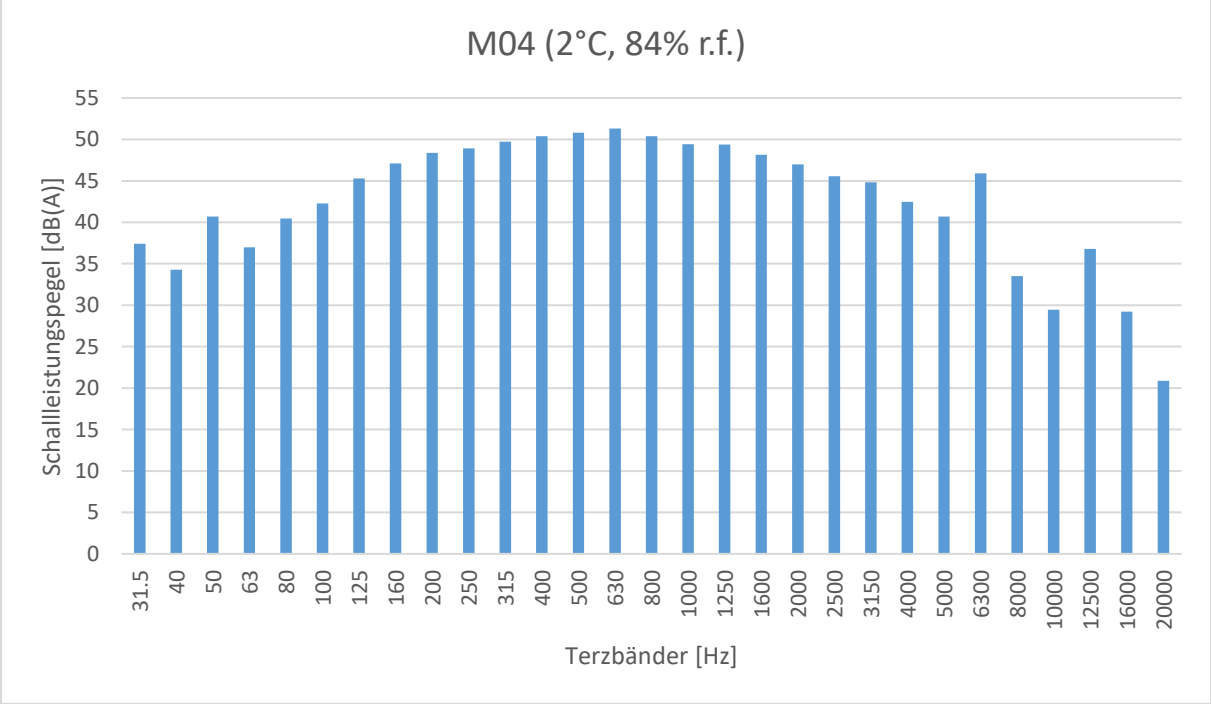

Figure 9.7: A-weighted sound power level of the heat pump at a temperature of 2°C and a relative humidity of 84% (Source: AIT)

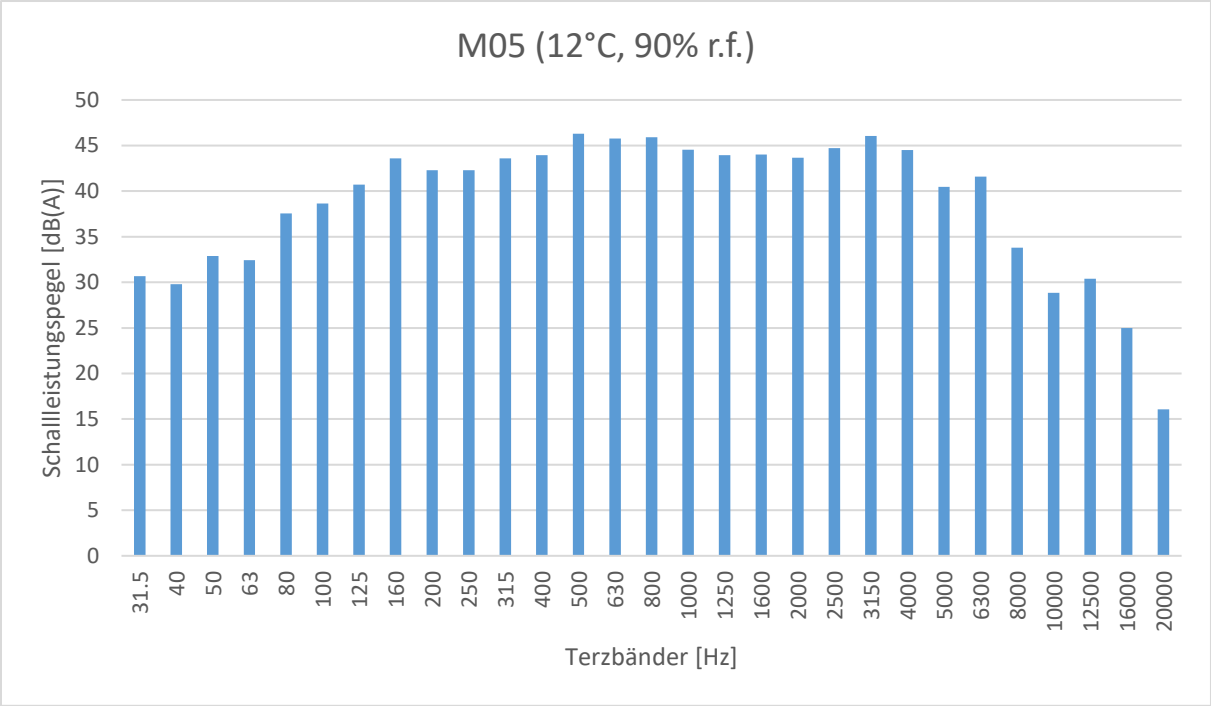

Figure 9.8: A-weighted sound power level of the heat pump at a temperature of 12°C and a relative humidity of 90%. (Source: AIT)

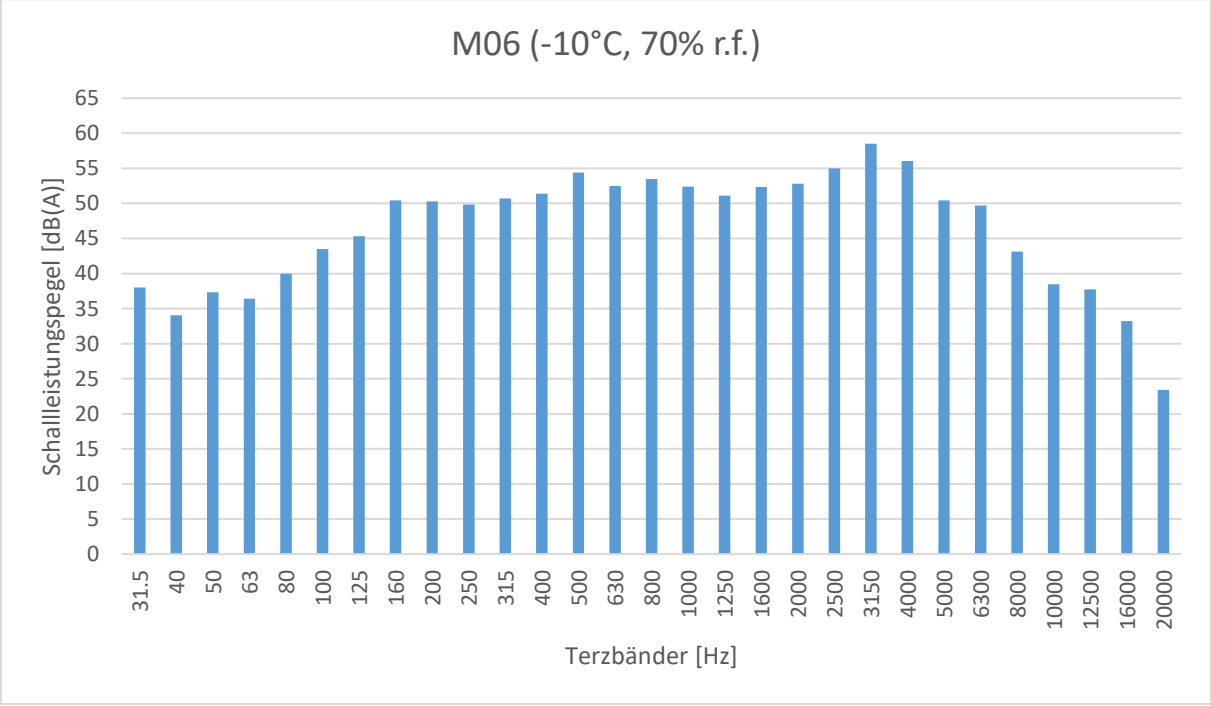

Figure 9.9: A-weighted sound power level of the heat pump at a temperature of -10°C and a relative humidity of 70%. (Source: AIT)

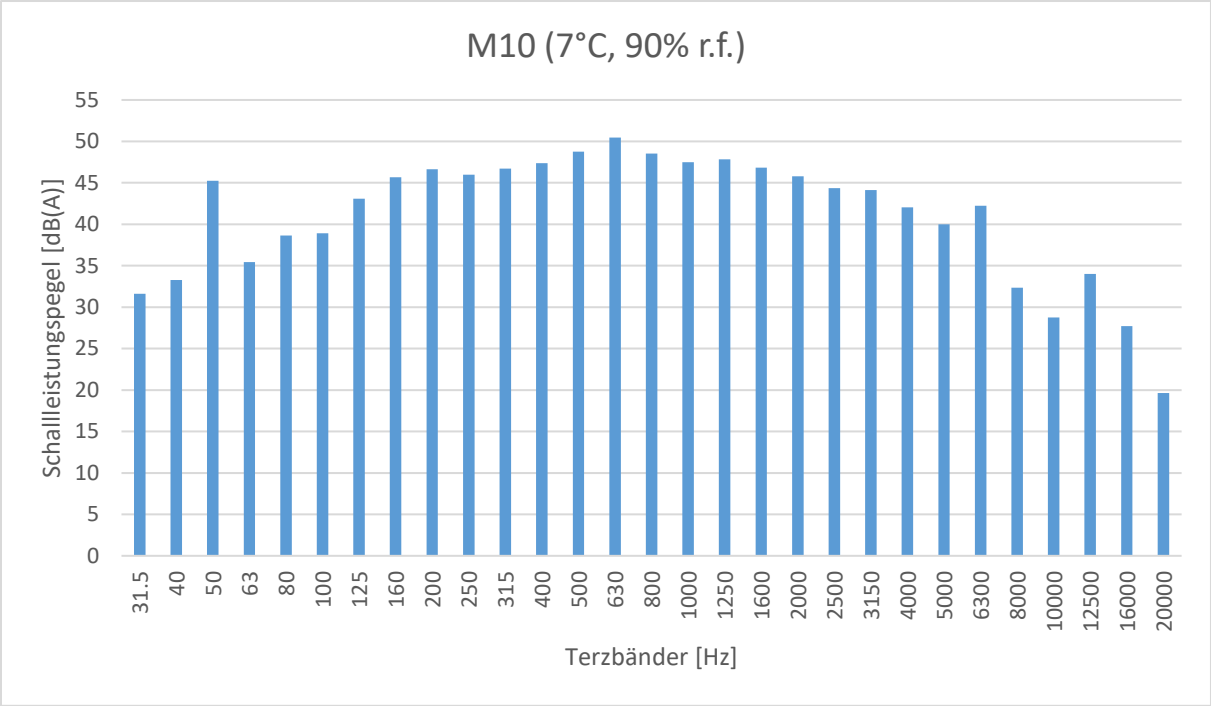

Figure 9.10: A-weighted sound power level of the heat pump at a temperature of 7°C and a relative humidity of 90%. (Source: AIT)

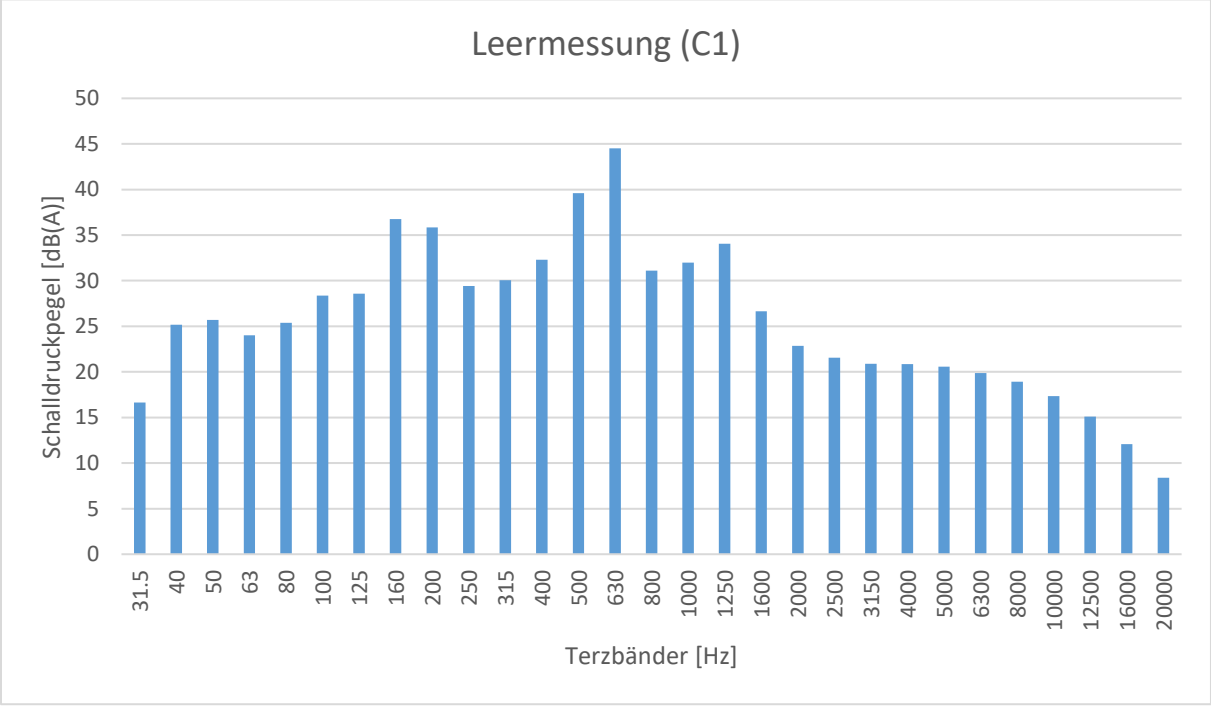

Figure 9.11: A-weighted sound power level of the empty measurement. (Source: AIT)

To analyse the directional dependency, the evaluation of the measurement series M10 at a temperature of 12°C is shown here for 12 microphones in each case at 2 levels (1.48 m and 0.68 m above the floor) as well as microphone 55 (height 2.1 m) mounted centrally at the top.

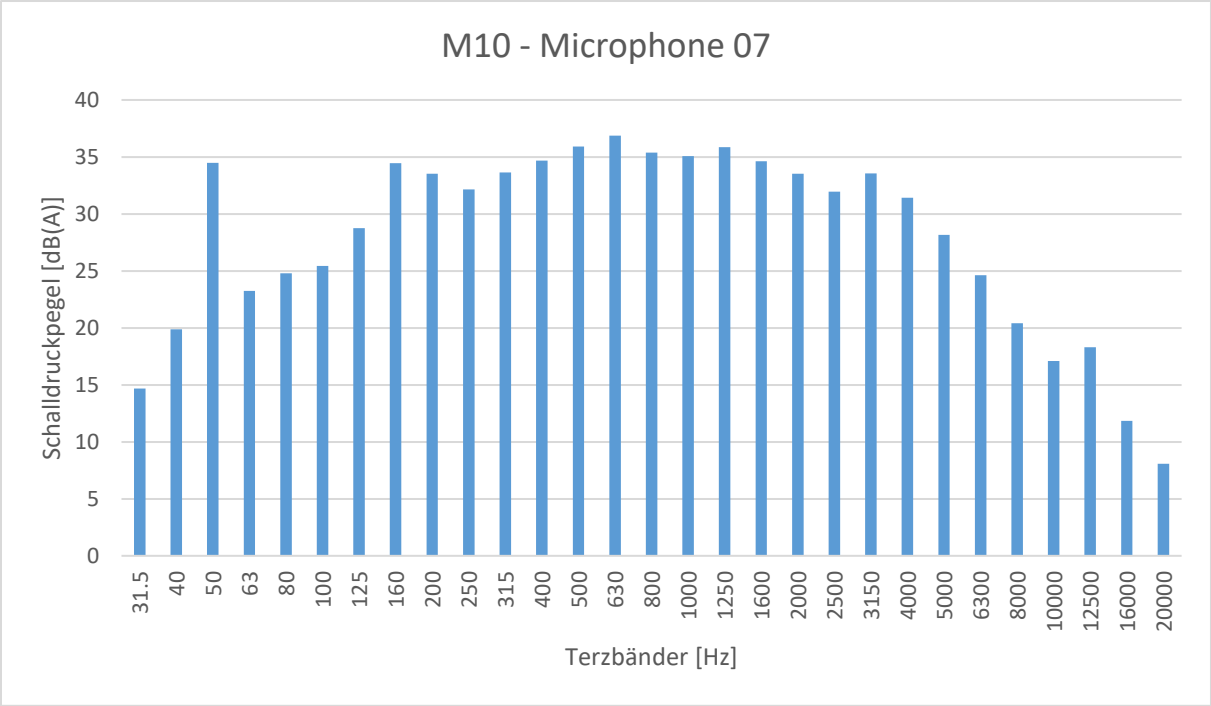

Figure 9.12 A-weighted sound power level of the heat pump measurement at 12°C for microfone 07 (1.48m height) (Source: AIT)

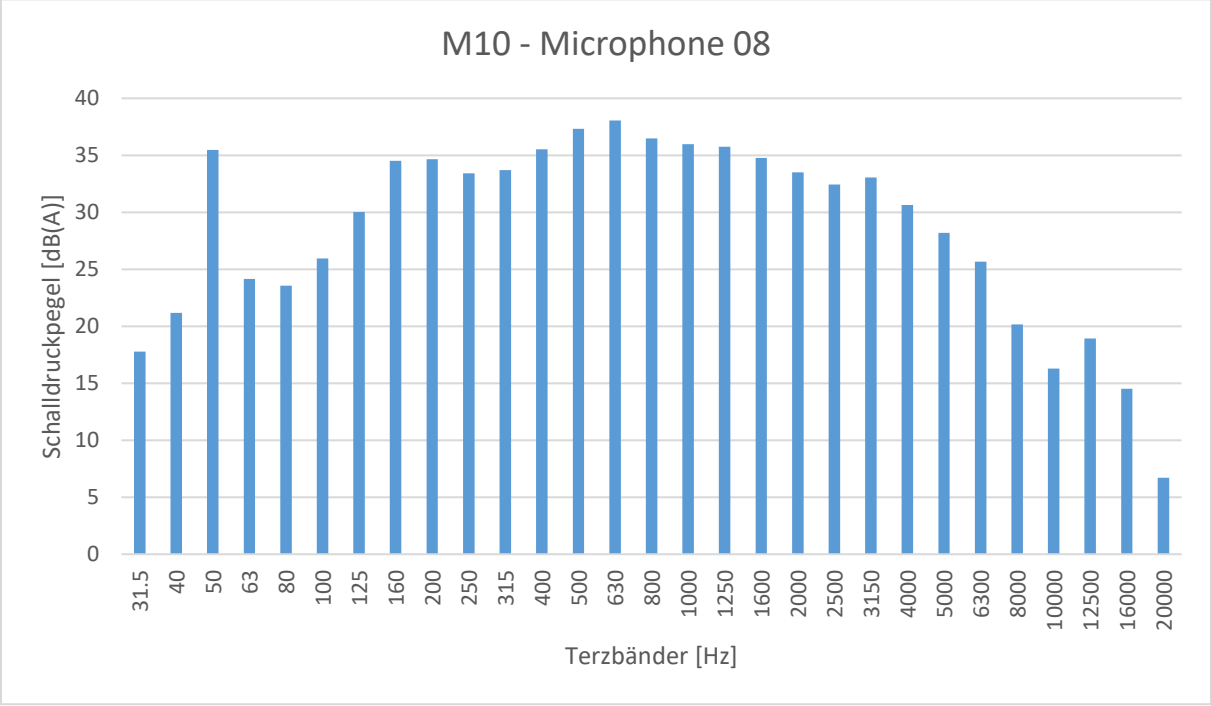

Figure 9.13: A-weighted sound power level of the heat pump measurement at 12°C for microfone 10 (1.48m height) (Source: AIT)

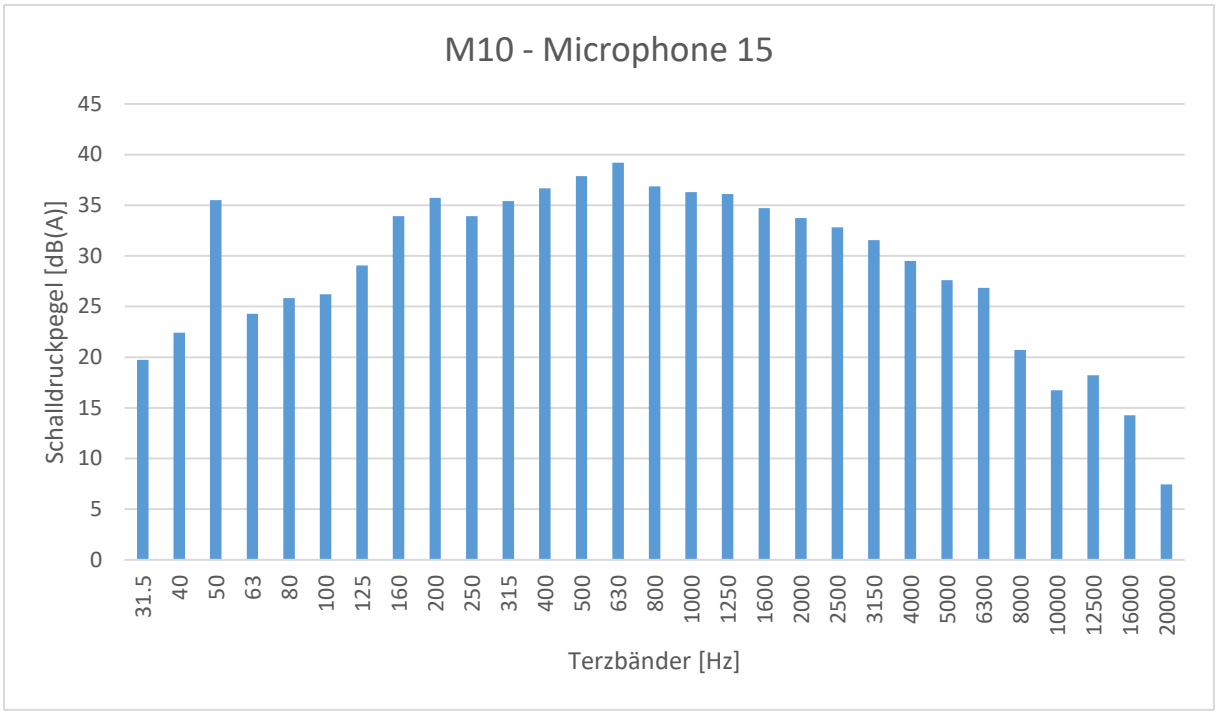

Figure 9.14: A-weighted sound power level of the heat pump measurement at 12°C for microfone 15 (1.48m height) (Source: AIT)

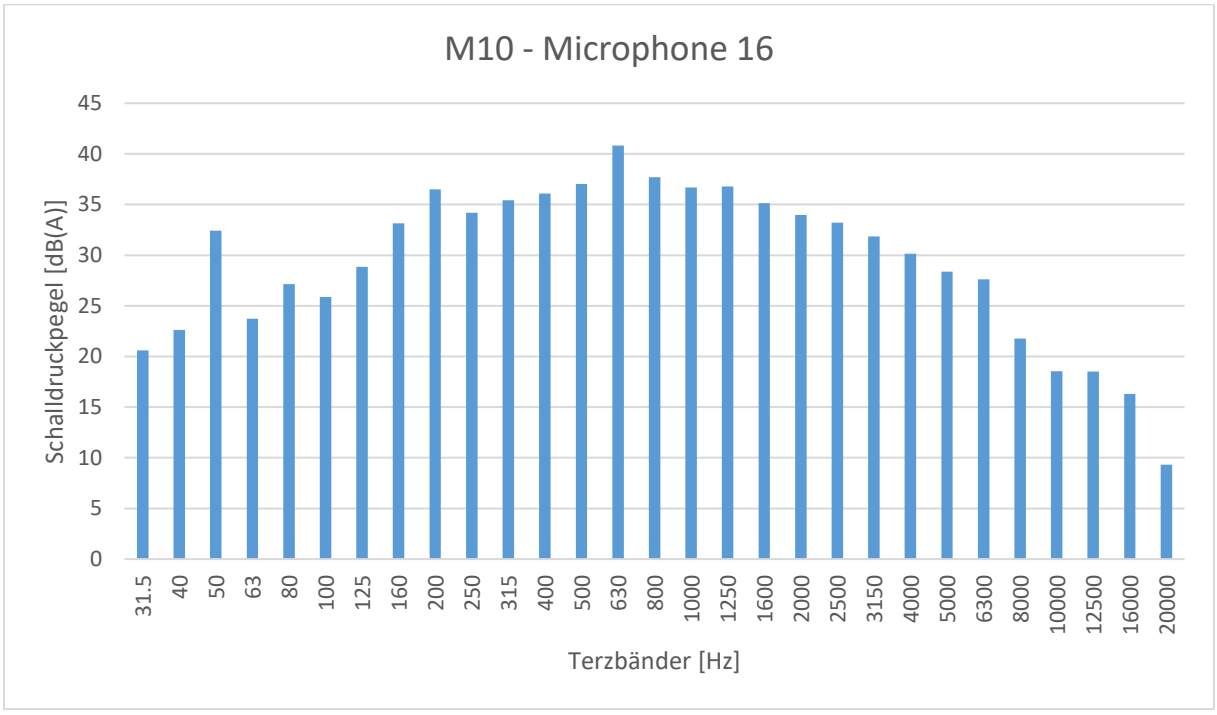

Figure 9.15: A-weighted sound power level of the heat pump measurement at 12°C for microfone 16 (1.48m height) (Source: AIT)

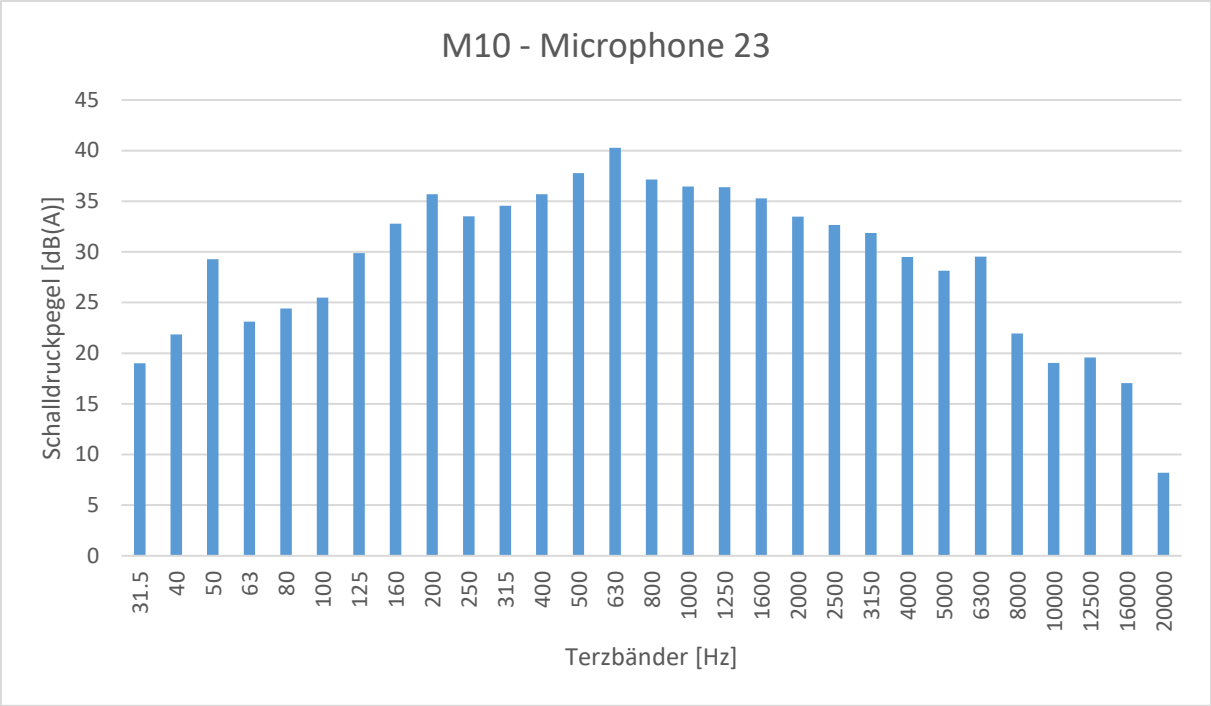

Figure 9.16: A-weighted sound power level of the heat pump measurement at 12°C for microfone 23 (1.48m height) (Source: AIT)

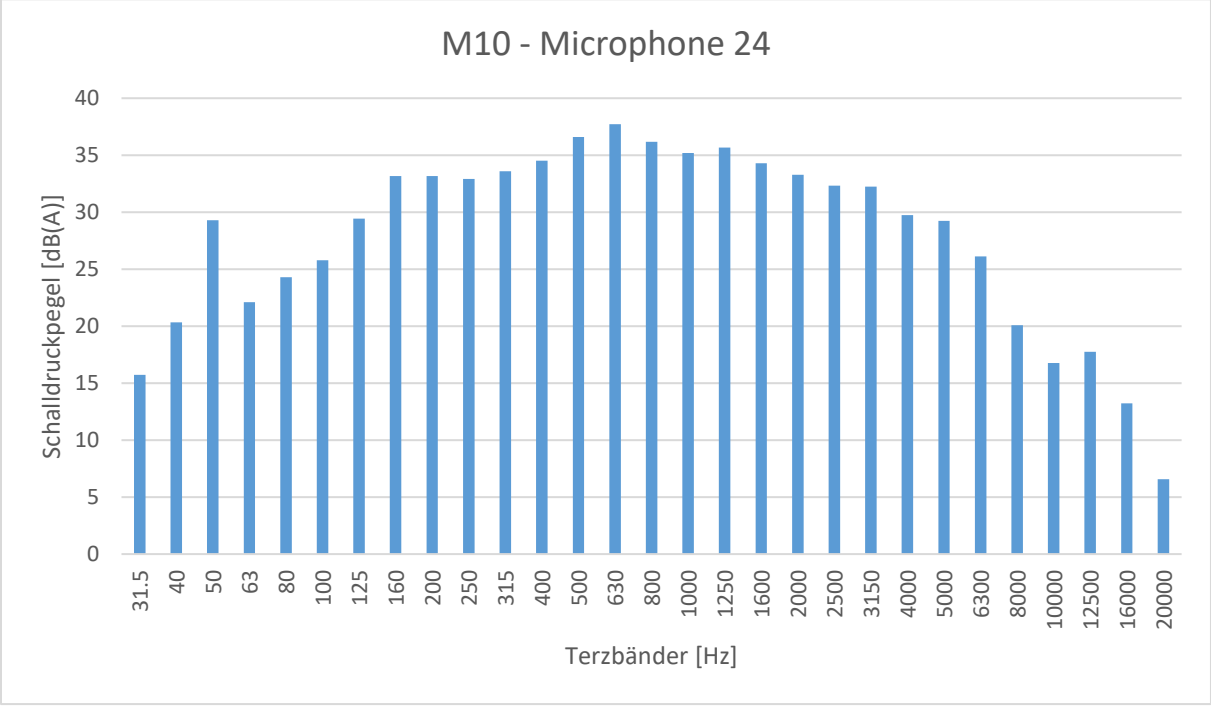

Figure 9.17: A-weighted sound power level of the heat pump measurement at 12°C for microfone 24 (1.48m height) (Source: AIT)

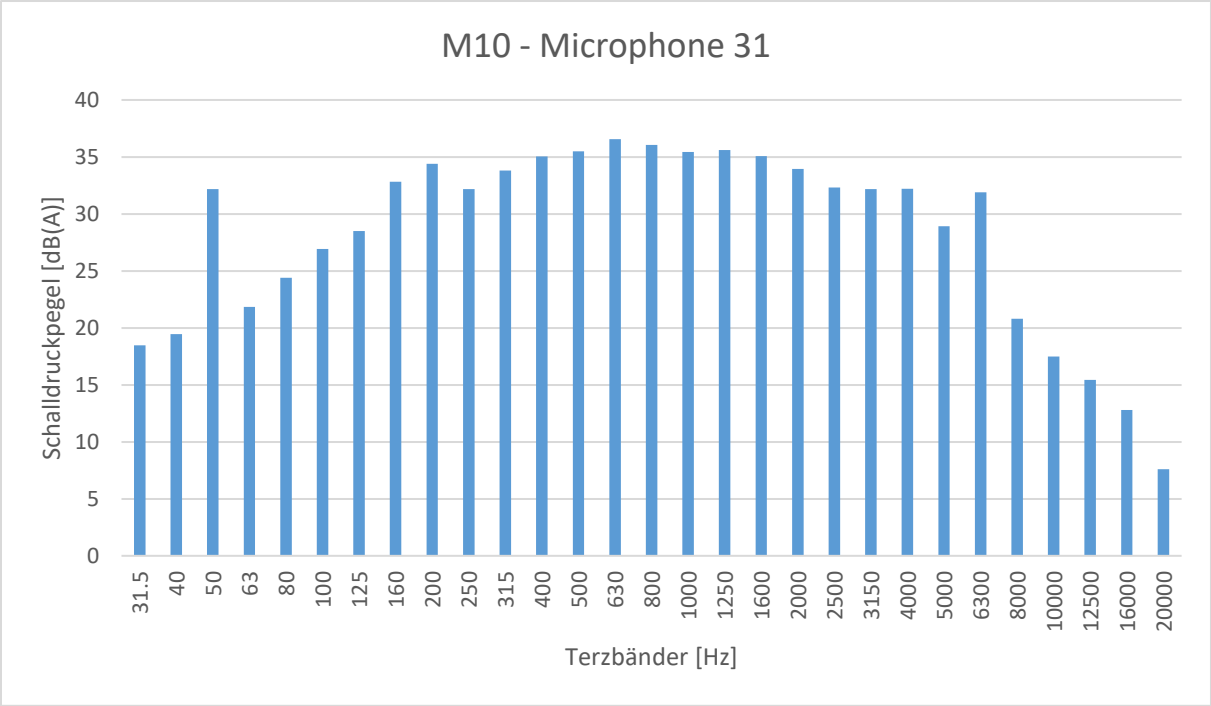

Figure 9.18: A-weighted sound power level of the heat pump measurement at 12°C for microfone 31 (1.48m height) (Source: AIT)

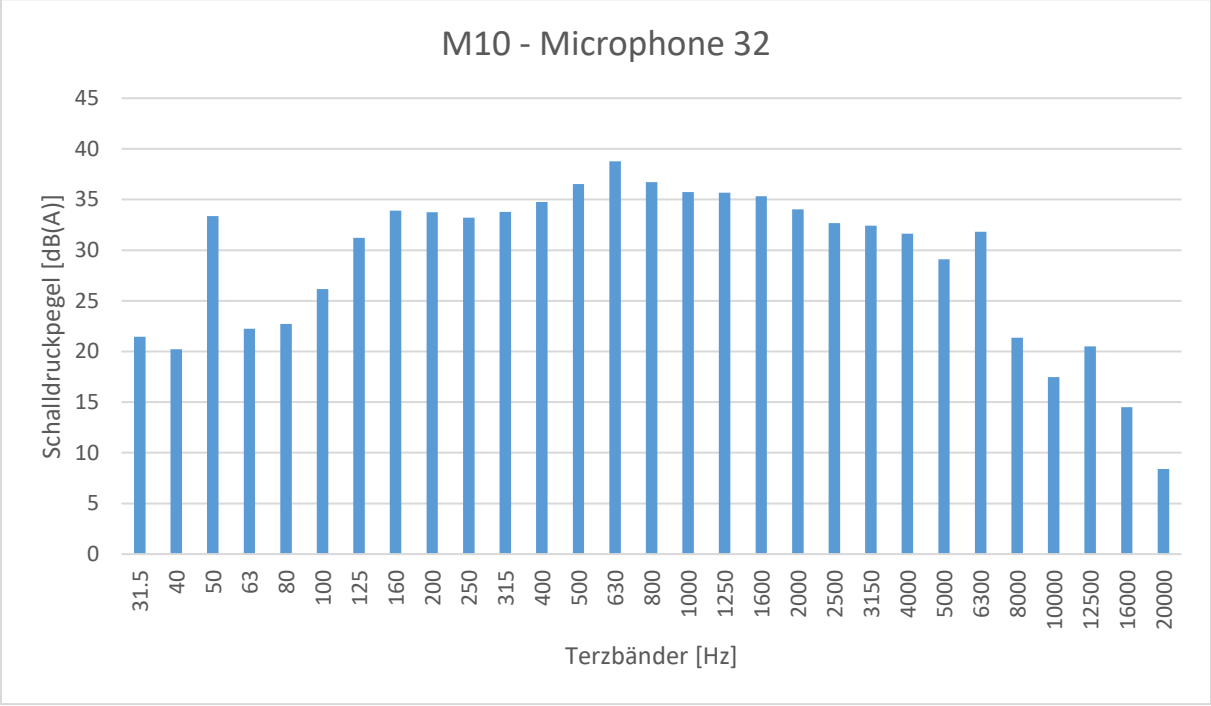

Figure 9.19: A-weighted sound power level of the heat pump measurement at 12°C for microfone 32 (1.48m height) (Source: AIT)

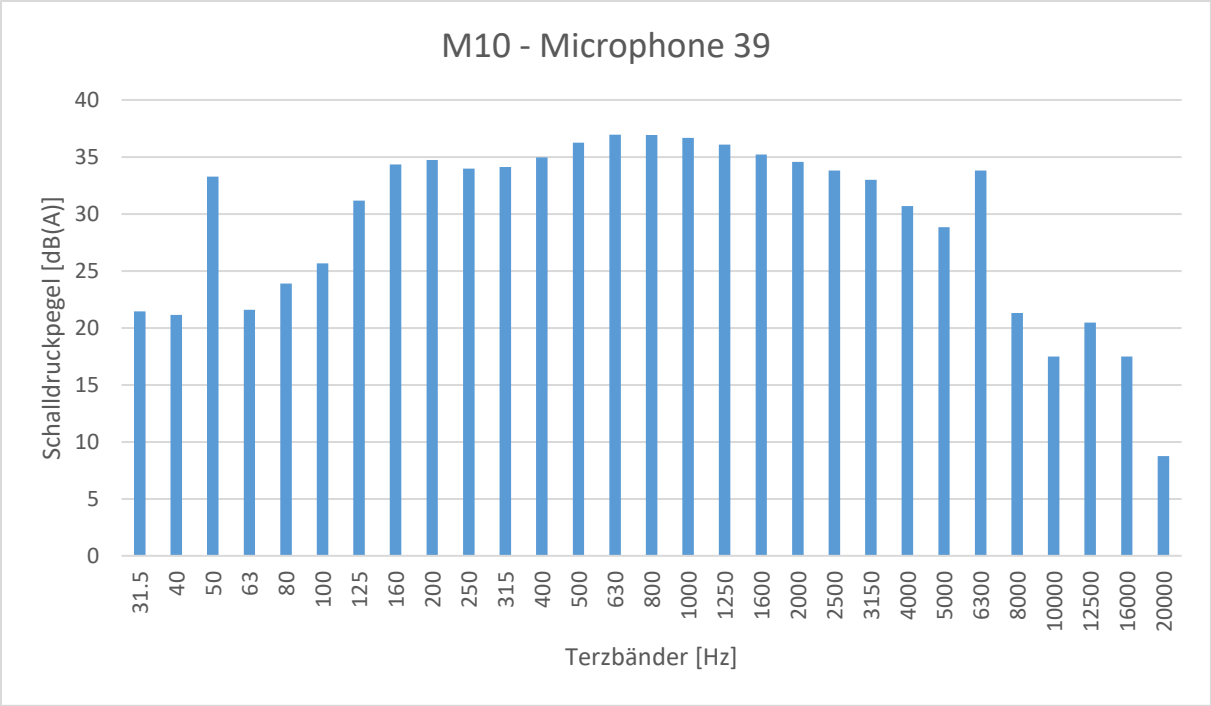

Figure 9.20: A-weighted sound power level of the heat pump measurement at 12°C for microfone 39 (1.48m height) (Source: AIT)

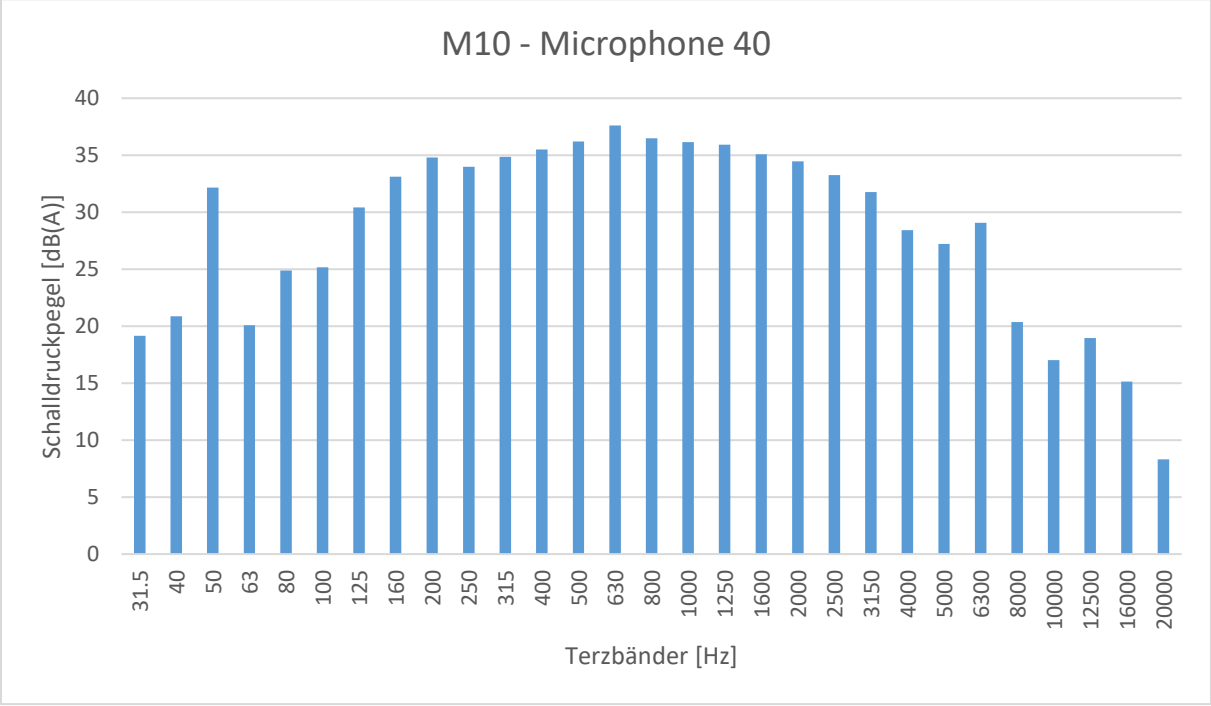

Figure 9.21 A-weighted sound power level of the heat pump measurement at 12°C for microfone 40 (1.48m height) (Source: AIT)

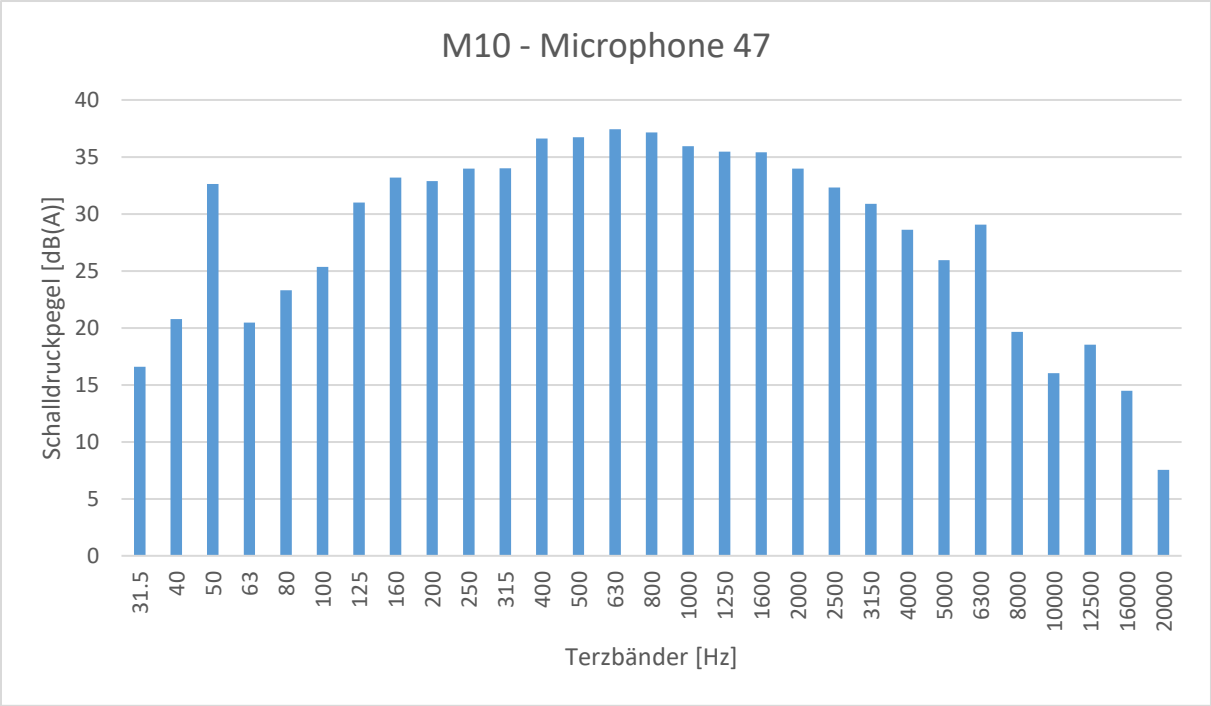

Figure 9.22: A-weighted sound power level of the heat pump measurement at 12°C for microfone 47 (1.48m height) (Source: AIT)

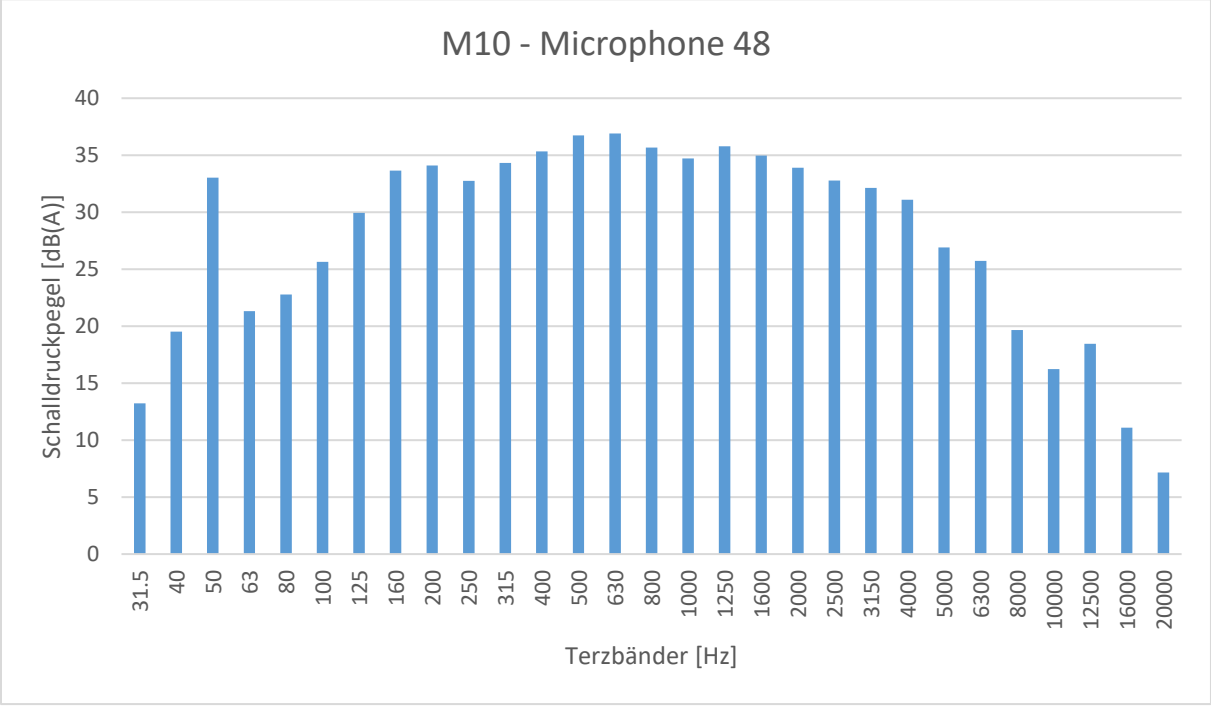

Figure 9.23: A-weighted sound power level of the heat pump measurement at 12°C for microfone 48 (1.48m height) (Source: AIT)

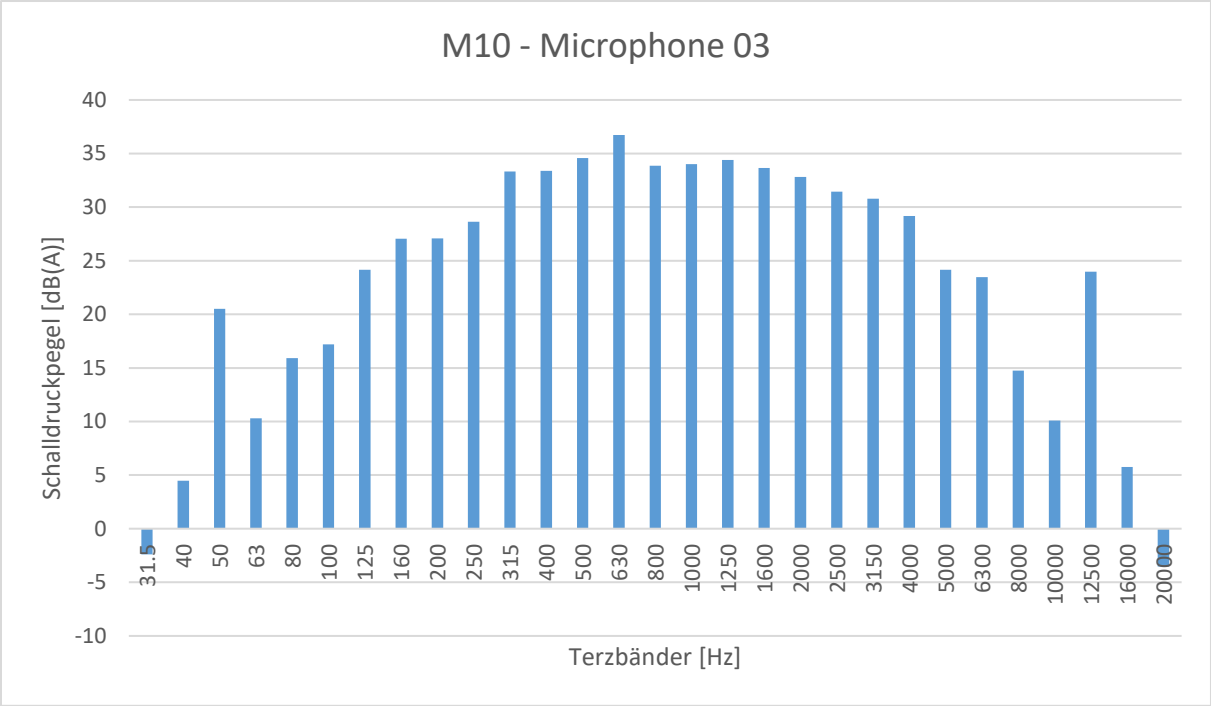

Figure 9.24: A-weighted sound power level of the heat pump measurement at 12°C for microfone 03 (0.68m height) (Source: AIT)

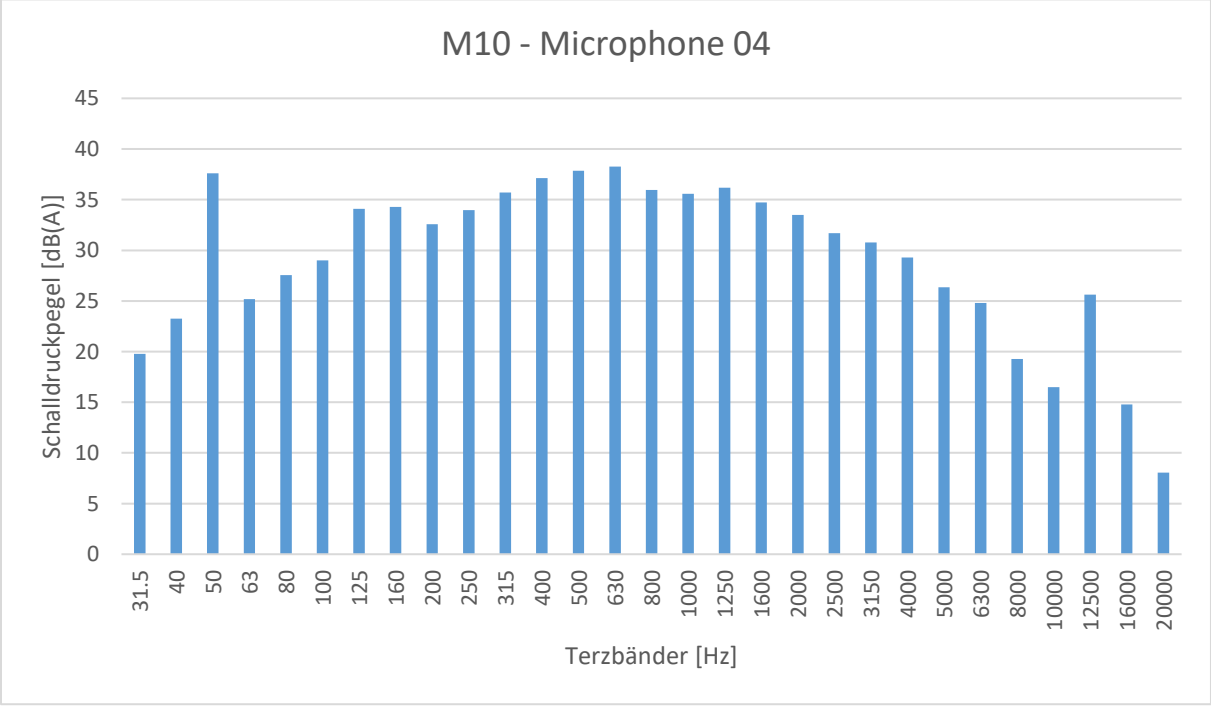

Figure 9.25: A-weighted sound power level of the heat pump measurement at 12°C for microfone 04 (0.68m height) (Source: AIT)

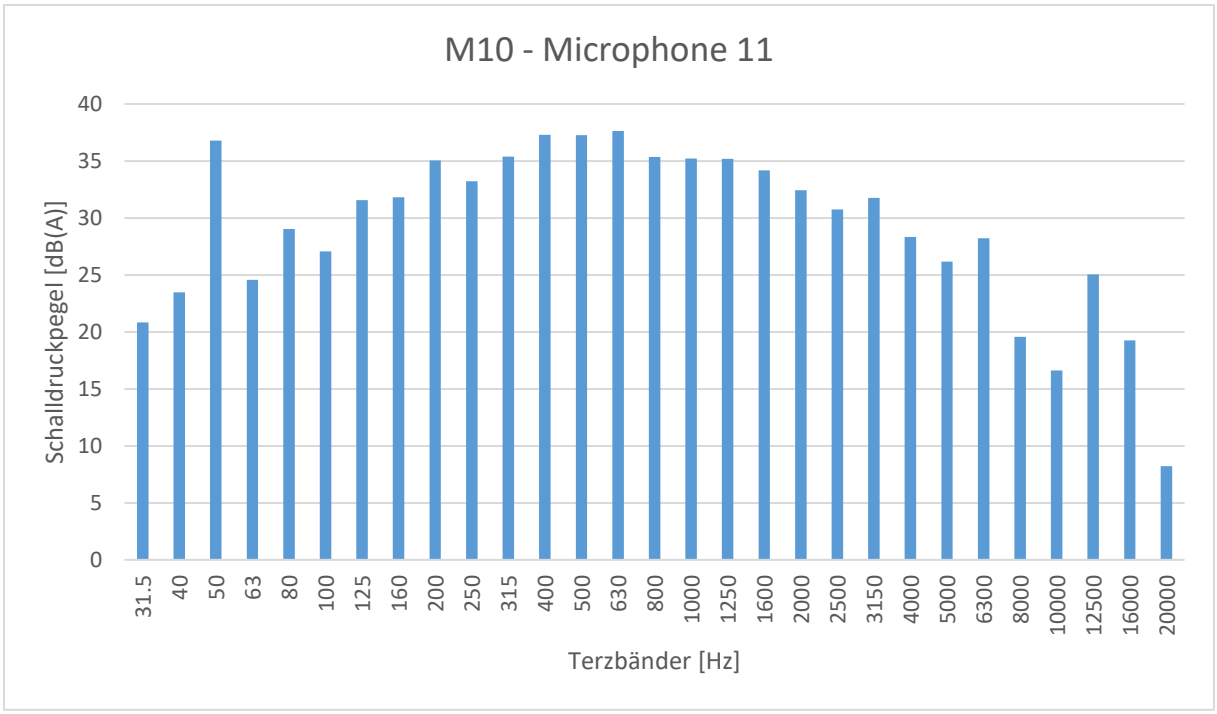

Figure 9.26: A-weighted sound power level of the heat pump measurement at 12°C for microfone 11 (0.68m height) (Source: AIT)

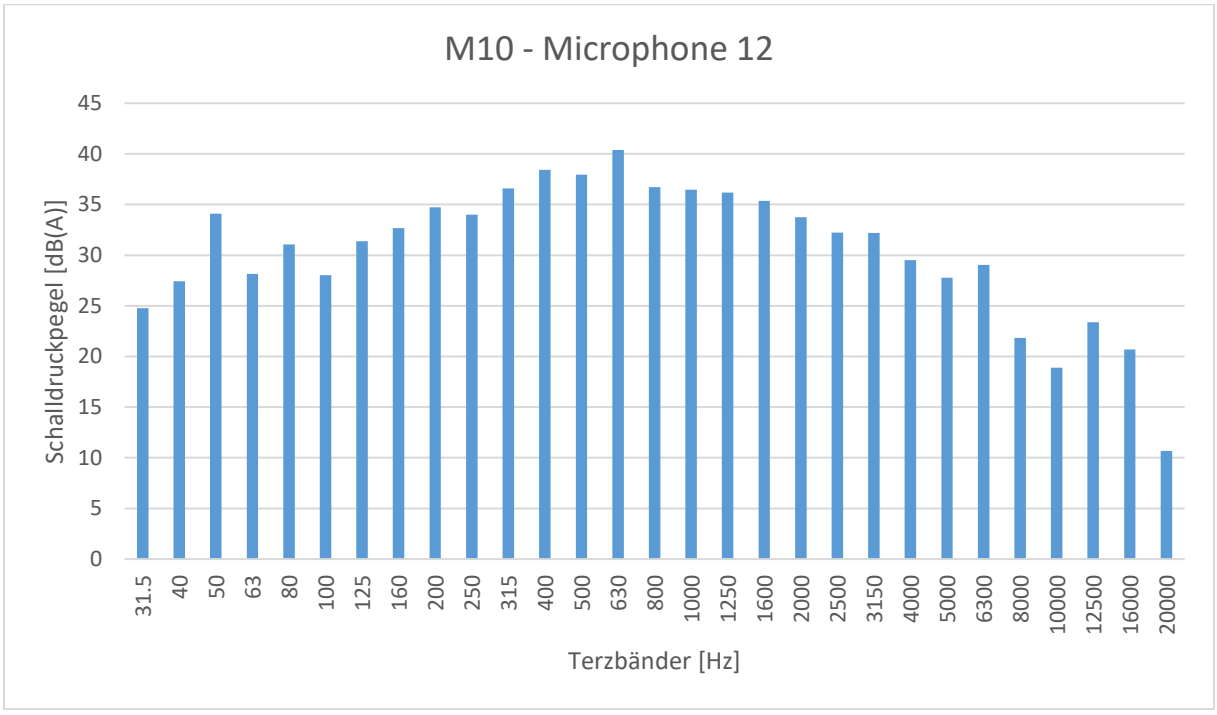

Figure 9.27: A-weighted sound power level of the heat pump measurement at 12°C for microfone 12 (0.68m height) (Source: AIT)

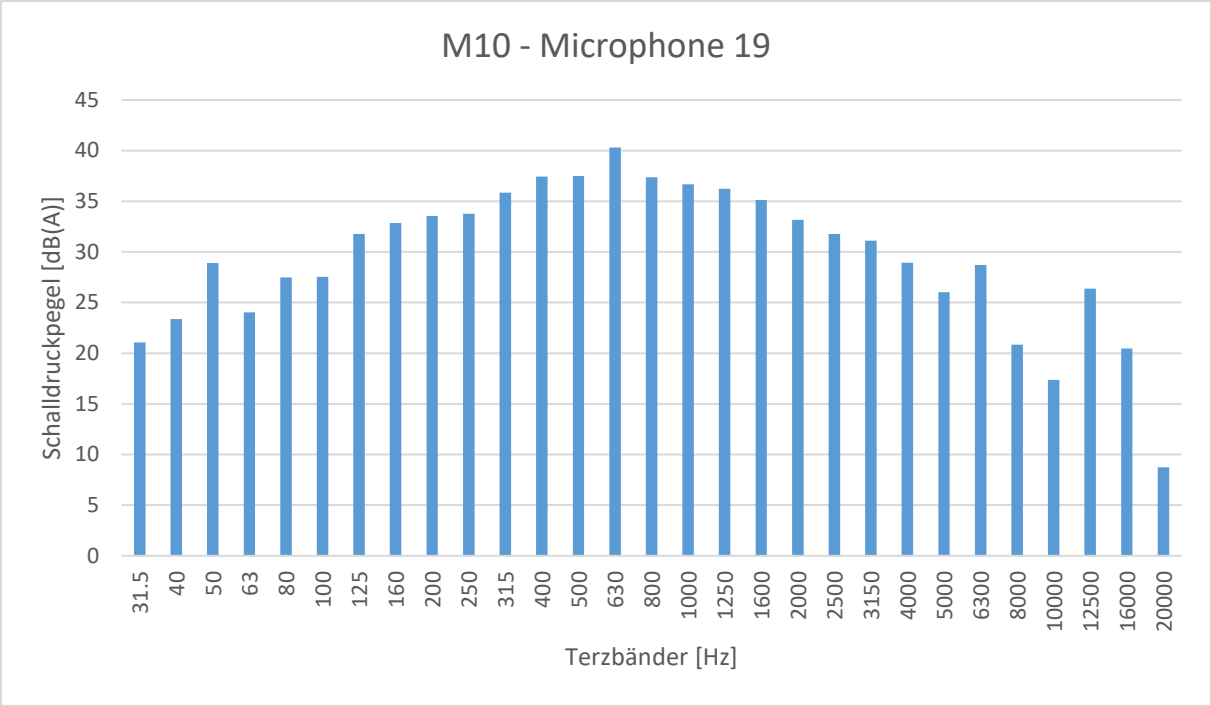

Figure 9.28: A-weighted sound power level of the heat pump measurement at 12°C for microfone 19 (0.68m height) (Source: AIT)

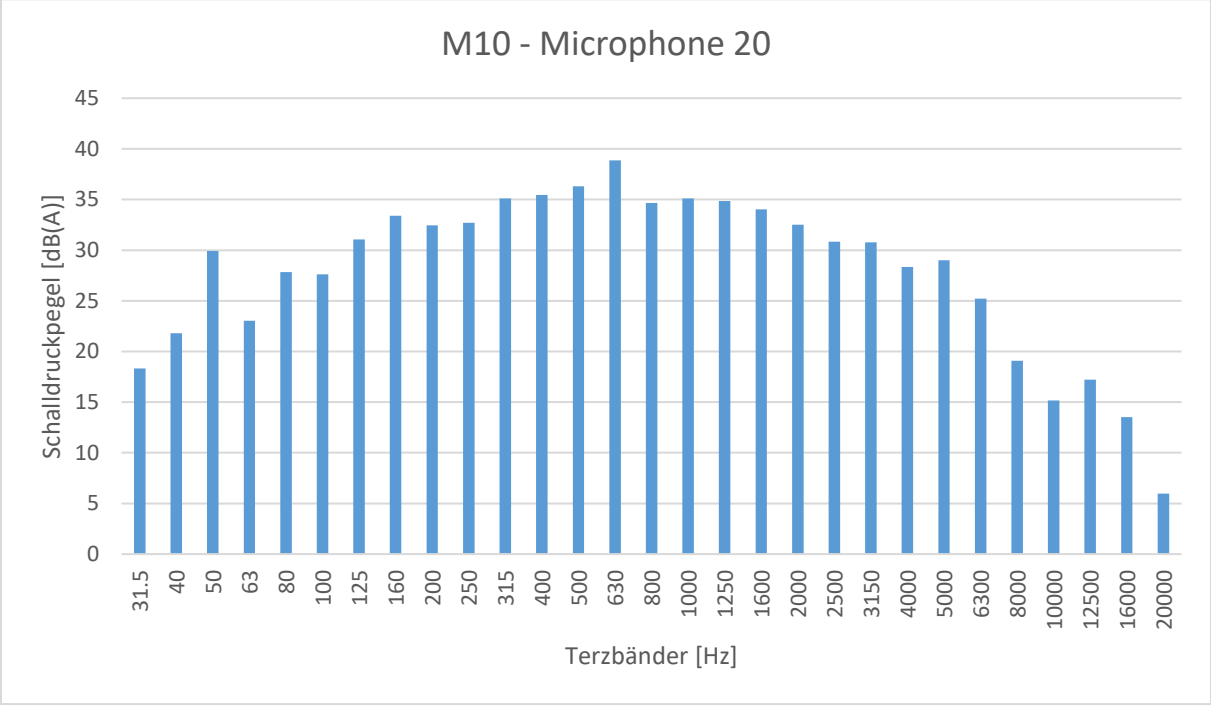

Figure 9.29: A-weighted sound power level of the heat pump measurement at 12°C for microfone 20 (0.68m height) (Source: AIT)

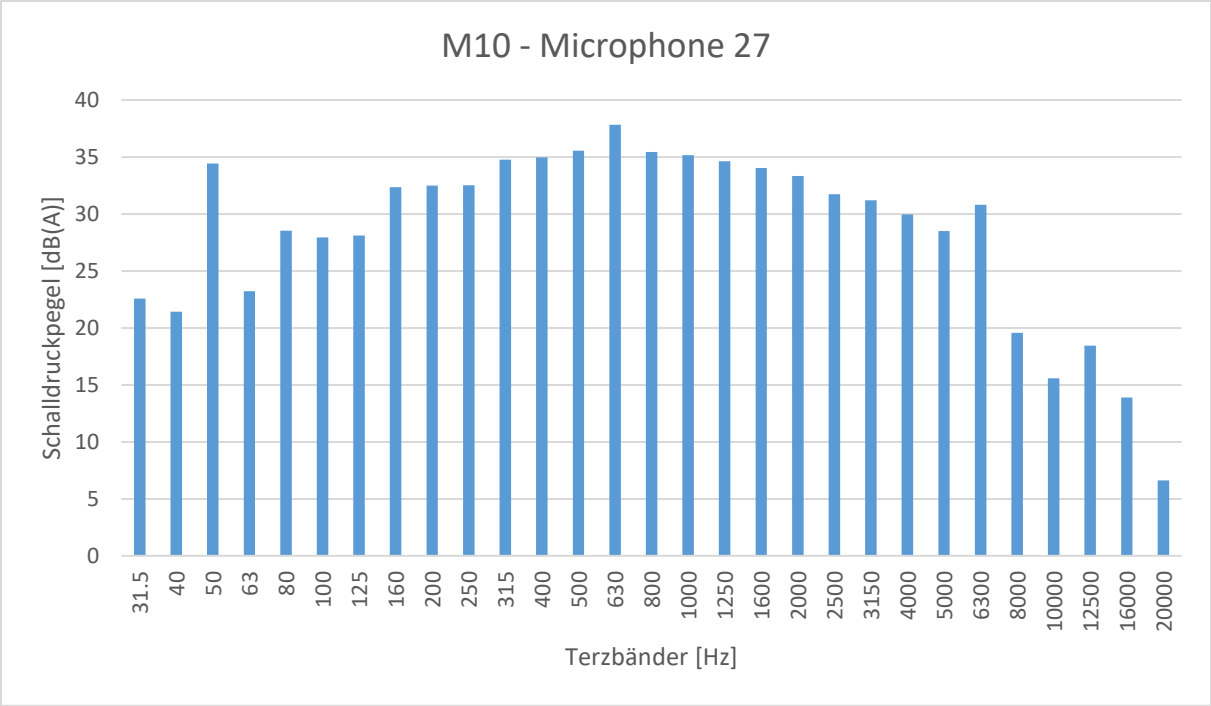

Figure 9.30: A-weighted sound power level of the heat pump measurement at 12°C for microfone 27 (0.68m height) (Source: AIT)

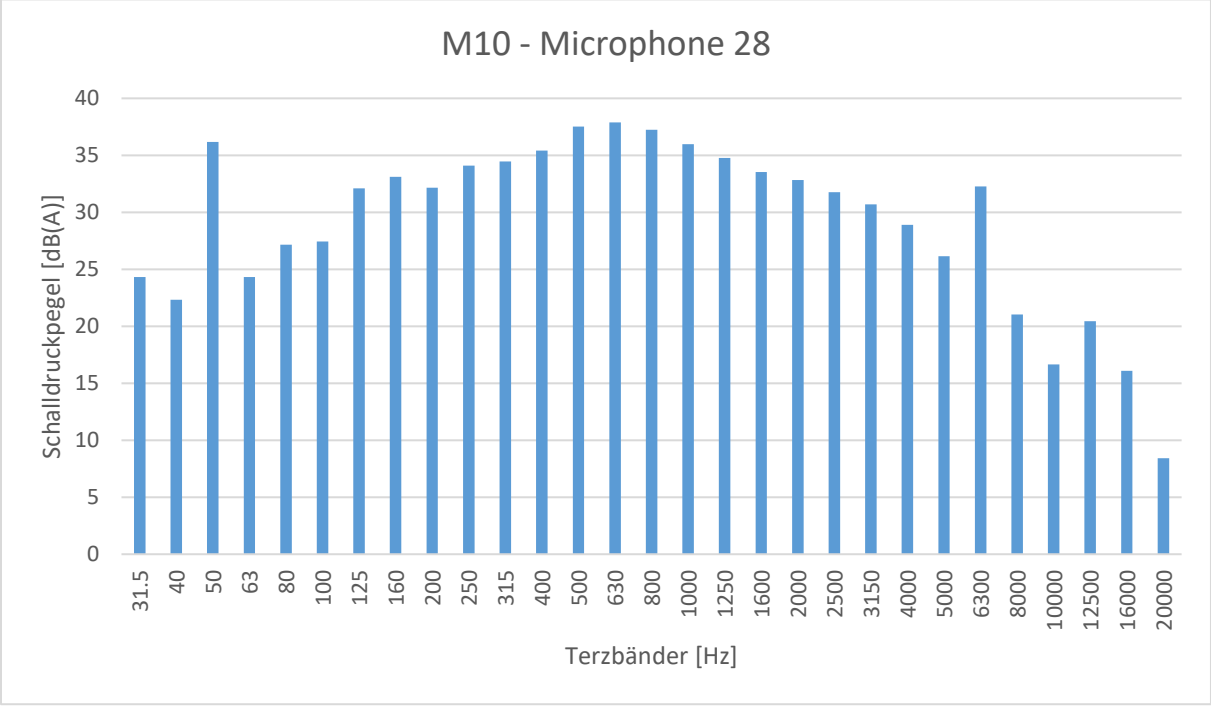

Figure 9.31: A-weighted sound power level of the heat pump measurement at 12°C for microfone 28 (0.68m height) (Source: AIT)

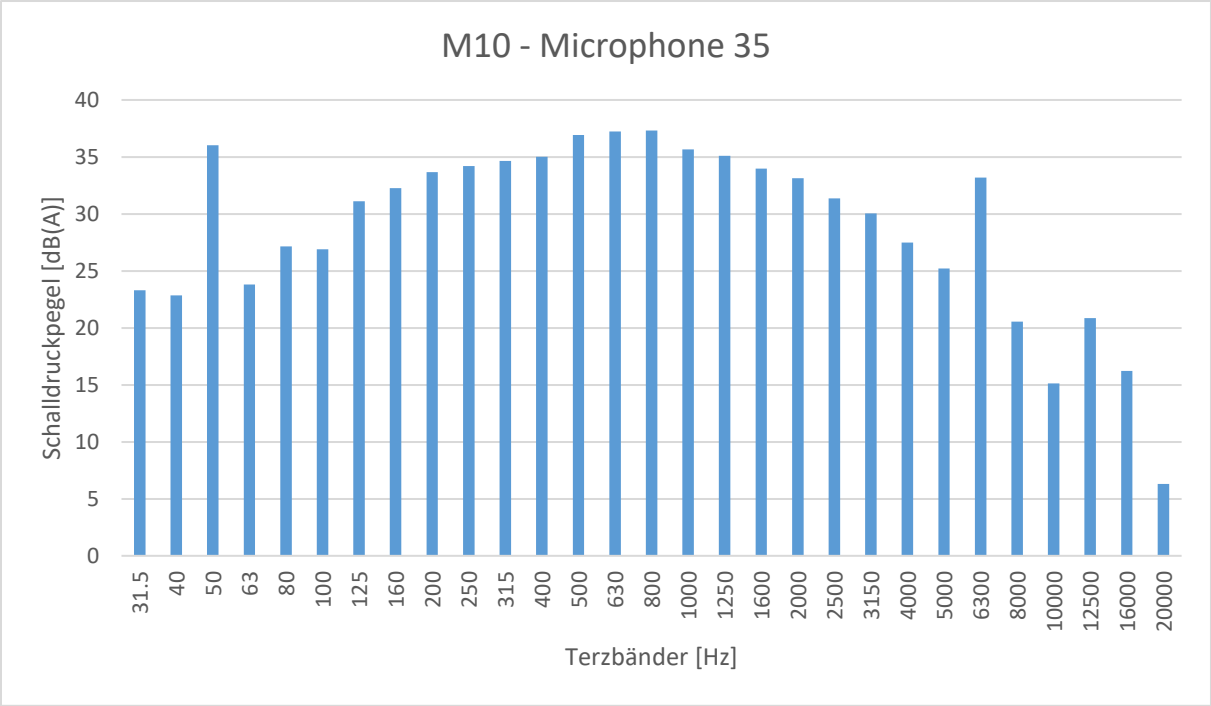

Figure 9.32: A-weighted sound power level of the heat pump measurement at 12°C for microfone 35 (0.68m height) (Source: AIT)

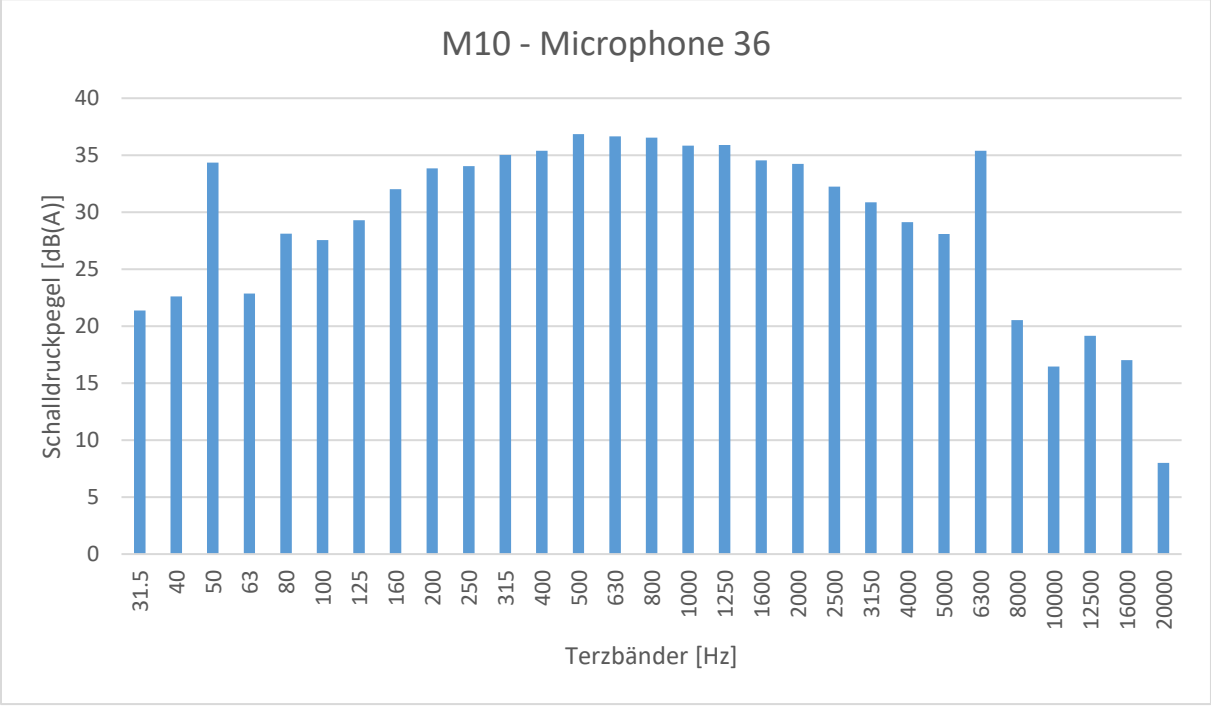

Figure 9.33: A-weighted sound power level of the heat pump measurement at 12°C for microfone 36 (0.68m height) (Source: AIT)

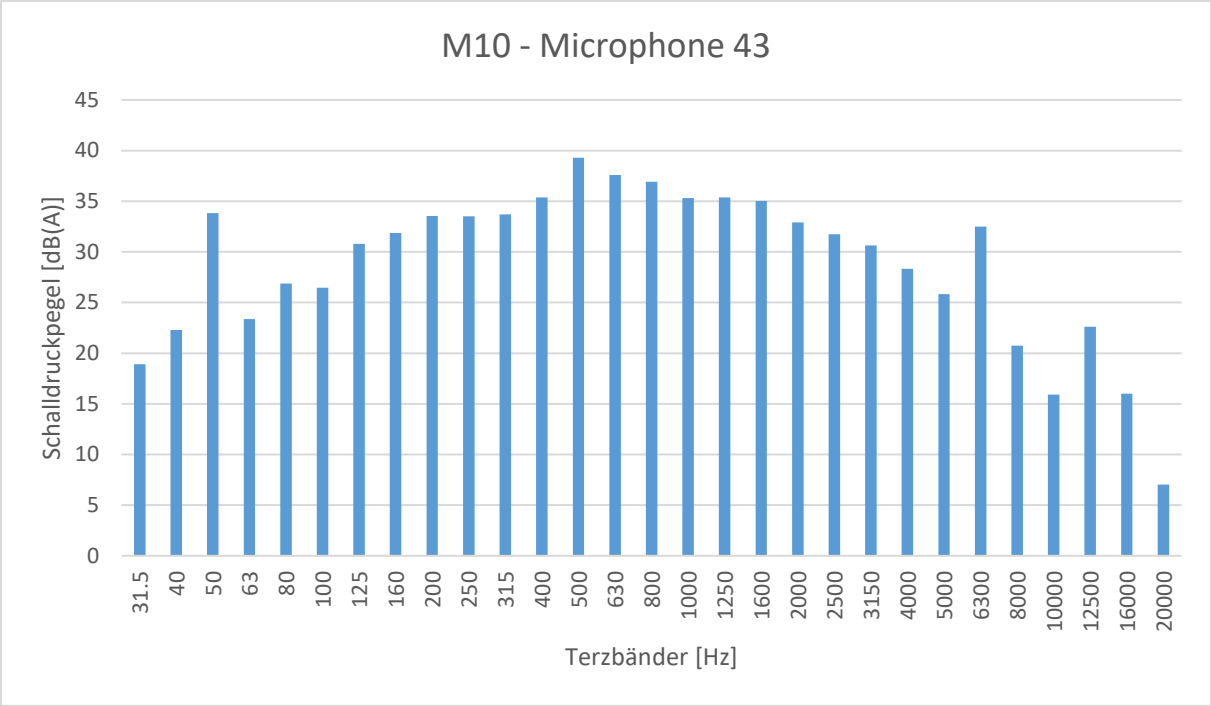

Figure 9.34: A-weighted sound power level of the heat pump measurement at 12°C for microfone 43 (0.68m height) (Source: AIT)

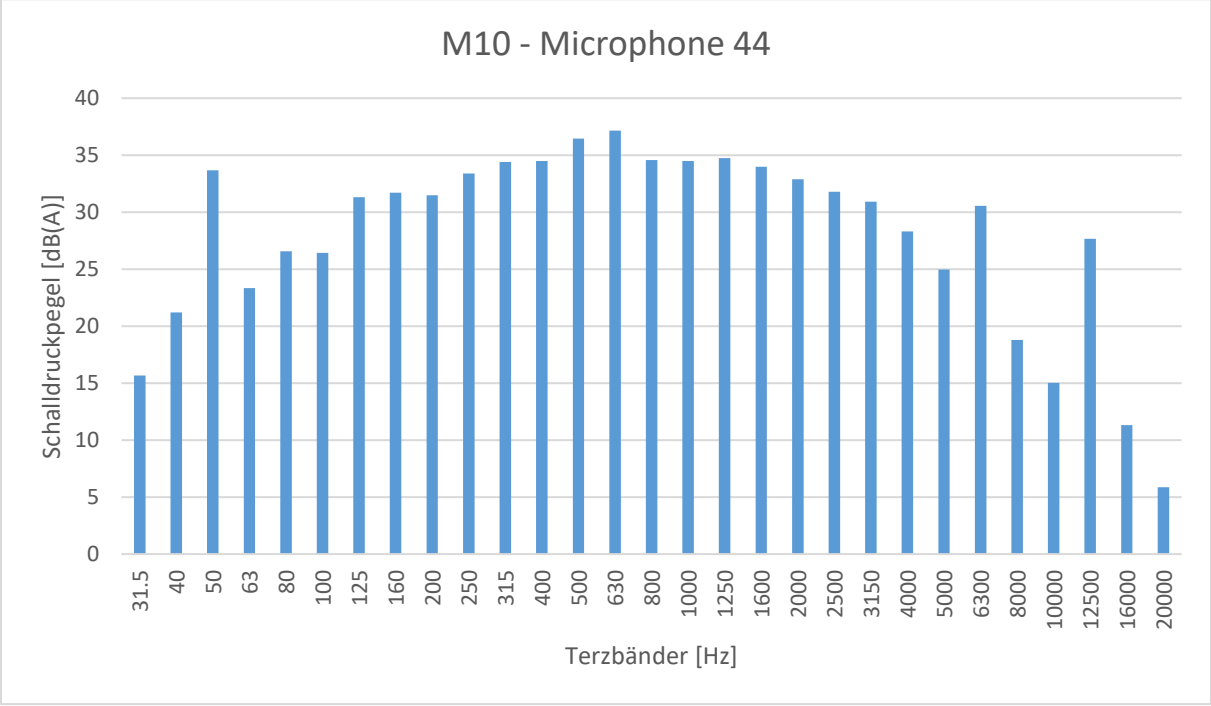

Figure 9.35: A-weighted sound power level of the heat pump measurement at 12°C for microfone 44 (0.68m height) (Source: AIT)

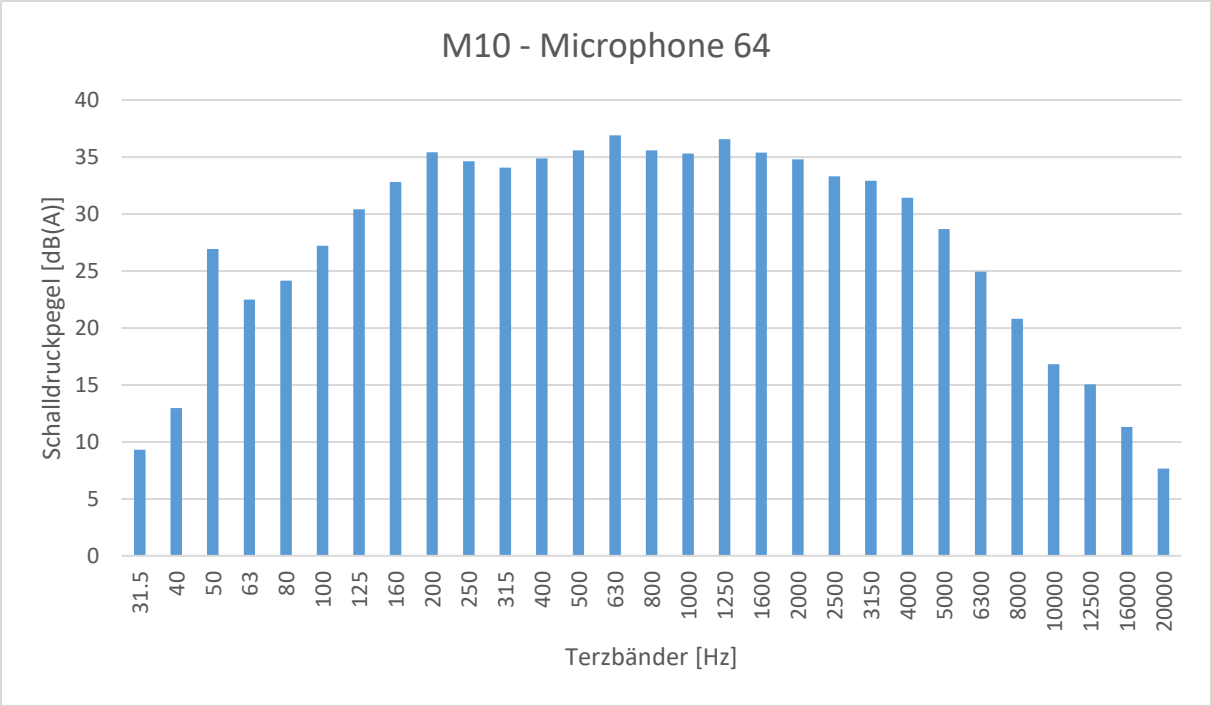

Figure 9.36: A-weighted sound power level of the heat pump measurement at 12°C for top microfone 64 (2.10m height) (Source: AIT)

The third-octave band spectra are given in Figures 9.12 to 9.36. Table 9.4 gives the sound power levels for the microphones. At a height of 1.48 m, the values vary from 46.6 dBA to 48.1 dBA (difference 1.5 dB). At a height of 0.68 m they vary from 44.8 dB to 48.4 dB (difference being 3.6 dB).

Microphone	Sound power level [dBA]	**Microphone**	Sound power level [dBA]
Microphone 07	46.8	Microphone 03	44.8
Microphone 08	47.4	Microphone 04	47.8
Microphone 15	47.9	Microphone 11	47.3
Microphone 16	48.1	Microphone 12	48.4
Microphone 23	47.8	Microphone 19	47.9
Microphone 24	46.6	Microphone 20	46.7
Microphone 31	46.8	Microphone 27	46.7
Microphone 32	47.4	Microphone 28	47.3
Microphone 39	47.5	Microphone 35	47.2
Microphone 40	47.2	Microphone 36	47.3
Microphone 47	47.1	Microphone 43	47.3
Microphone 48	46.8	Microphone 44	46.4
Microphone 64	47.0		

Table 9.4: Compilation of the measurements on the heat pump at a temperature of 12°C and the different microphones to assess the directionality (Source: AIT)

In addition to the measurements with the heat pump, a reference sound source and a dodekaeder have been placed into the middle of the dome. With the help of the dodecahedron, which was swivelled back and forth around the vertical axis, the results could be compared for different noise signals. The type of noise signal resulted in a change of the sound power level from 93.6 dB (white), via 94.5 dB (red-white) to 96.0 dB (pink) at a temperature of 16°C. The effect of additional absorbing material on the inside of the climate chamber was also analysed. The effect of this absorbent material on the inside of the climate chamber door is approx. 0.3 dB. The temperature has only a small influence on the result: with white noise the values are 93.6 dB (16°C) and 93.7 dB (5.5°C).

For the reference sound source, a measurement during a temperature glide between -20°C and 10°C resulted in a change of 1.5 dB in the sound power level. The measurements also showed that the installation of an additional absorbing wall in the area of the inside of the climate chamber door leads to a reduction of the sound power level of 0.3 dB. Switching on the air conditioning, on the other hand, leads to an increase in the sound power level of 0.3 dB.

The measurements of the heat pump were carried out at four operating temperatures between -10°C and 12°C. The sound power level increases with decreasing operating temperature. The sound power level increases with decreasing ambient temperature for this heat pump by a total of 8.9 dBA. The evaluations were also detailed for 12 microphones each at 2 heights: At a height of 1.48 m, the values vary from 46.6 dBA to 48.1 dBA (difference 1.5 dB). At a height of 0.68 m they vary from 44.8 dB to 48.4 dB (difference 3.6 dB).

10. Acoustic Measures to reduce noise

In IEA HPT Annex 51 measures to reduce noise have been studied on component level as well as in view of heatpump placement and additional barriers.

Deliverable 5 of IEA HPT Annex 51 shows an analysis of unit placement, indoor & outdoor sound propagation in chapter 6. Chapter 7 reports on the potential of sound absorption at nearby surfaces and Chapter 8 introduces common "unclever" decisions in heat pump placement including

- Wrong location chosen
- Installation on the roof
- Development of neighbouring property
- Improper sound absorbing measures
- Installation of further units in the neighbourhood

The document can be downloaded here:

https://heatpumpingtechnologies.org/annex51/wp-content/uploads/sites/59/2021/10/iea-hpt-annex-51-d5.pdf

Deliverable 7 of the IEA HPT Annex 51 reports on educational material on acoustics of heat pumps. The document can be retrieved here:

https://heatpumpingtechnologies.org/annex51/wp-content/uploads/sites/59/2021/10/iea-hpt-annex-51-d71.pdf

In this document, four guides are included:

- Control the noise – a guide for installing air for water heat pumps
- Heat pumps & environment acoustics
- Heat pumps & recommendations for installation
- Heat pumps - study of the risk of noise pollution in the vicinity

The first guide is based on a documentation produced for the Danish Energy Agency. The three consecutive documents are based on fiche technquies from AFPAC, the French heat pump association. The original documents are available on the Annex 51 Website https://heatpumpingtechnologies.org/annex51/.

Control the noise – a guide for installing air for water heat pumps covers an introduction to heat pumps discussing noise/sound authority, noise from air to water heat pumps (noise creation, noise measurement, influence of operation conditions, noise regulations), noise distribution (outdoor noise, indoor noise), calculation models (noise data, operating conditions, sound calculation tool), noise reduction, good installation (vibration sources and distribution cannels, rules of thumb regarding vibration isolation), control measurements, npise reduction (noise shields, noise gates, cabinet vibrations, cabinet noise) and examples (unappropriate placement, good and bad placements, control measurment of noise).

Heat pumps & environment acoustics covers definitions of sound power and sound pressure, the calculation method of adding sound sources, recommendations for the implementations (location, reflection of emitted noise, reflection of received noise, directivity of ventilations, distance to property

lines, installation under windows), reminder on the regulation of neighbourhood noise, application examples and emergence calculation (outdoor measurement, measurement inside buildings.

Heat pumps & recommendations for installation covers supports (concrete base, metal frame), network design rules (design principles, wall crossings), the pipes (direct expansion, water pipes), air networks (vibration transmission through ducts, noise transmission through ducts, radiation of noise through the walls of the duct, design principles), acoustic attenuation devices (absorbers on walls, sound barrier, enclosures) and maintenance.

Heat pumps - study of the risk of noise pollution in the vicinity covers measurements of residual noise without heat pumps, acoustic emergence, manufacturer documentation, conversion of acoustic power / pressure, place of installation (location, reflection of emitted noise), location of measurement and the measurement of acoustic emergence (absorbent on wall, sound barrier, enclosure).

Finally, deliverable 3 of the IEA HPT Annex 51 includes a detailed overview on Heat Pump Component Noise and Noise Control Techniques. It can be downloaded here:

https://heatpumpingtechnologies.org/annex51/wp-content/uploads/sites/59/2021/10/iea-hpt-annex-51-d3.pdf

It covers component noise from fan, compressor, secondary sources and heat exchanger in their interaction with fans. After introducing the fundamentals of noise control techniques separating informaiton in airborne and structure-borne noise, concepts for component noise control are described for compressor, fan and secondary sources. Noise emission paths and concepts for noise control are shown for air intake and outlets, casing and structure-borne noise emissions.

11. Conclusion

Air-to-water heat pumps have been analysed with special focus on acoustic characterisation. This report covers results on measurements on the GreenHP heat pump, the IEA HPT Annex 51 air-to-water heat pump and on a two-fan heat pump. In addition to this experimental work a chapter discussing acoustic measures to reduce noise has been added. It covers an analysis of unit placement, indoor & outdoor sound propagation, the potential of sound absorption at nearby surfaces and a introduction to common “unclever” decisions in heat pump placement. The latter is additonaly discussed by introducing the HVAC Positioner and the related 5ch Acoustics system.

12. Acknowledgements

The Austrian Research Promotion Agency (FFG) and the Austrian Climate and Energy Fund (KLIEN) are gratefully acknowledged for funding this work under Grant No. 848891 (program line 'Energieforschung e!Mission 1st call', project 'SilentAirHP') and Grant No 873588 (program line ‘Stadt der Zukunft 2nd call, project ‘RAARA’). We also want to thank the Federal Ministry of the Republic of Austria for Transport, Innovation and Technology for supporting IEA HPT Annex 51 in Austria in the framework of the IEA Research Cooperation.

References

[1] Ch. Reichl, J. Emhofer, Ch. Köfinger, T. Fleckl: “SilentAirHP - Advanced Methods for Analysis and Development of Noise Reduction Measures for Air-to-Water Heat Pump Systems”, 66. Jahrestagung der Österreichischen Physikalischen Gesellschaft, Universität Wien, 27.09.2016

[2] N. Schmiedbauer, J. Emhofer, Ch. Köfinger, P. Wimberger, T. Fleckl, M. Gröschl, Ch. Reichl: “Active Noise Cancelling for Heat Pump Applications”, 66. Jahrestagung der Österreichischen Physikalischen Gesellschaft, Universität Wien, 27.09.2016

[3] P. Wimberger, J. Emhofer, Ch. Köfinger, T. Fleckl, M. Gröschl, Ch. Reichl: “Space-, time- and frequency resolved recording and analysis of sound emissions and sound source localisation using a multichannel measuring system”, 66. Jahrestagung der Österreichischen Physikalischen Gesellschaft, Universität Wien, 27.09.2016

[4] N. Schmiedbauer: “Active Noise Cancelling im Anwendungsfeld der Luft-Wasser-Wärmepumpen“ (Arbeitstitel). Diplomarbeit (in Fertigstellung), Betreuung: Prof. Martin Gröschl, TU Wien, Christoph Reichl, AIT

[5] Dymola: 2

[6] Modelica: https://www.modelica.org

[7] TIL-Library: https://www.tlk-thermo.com/

[8] ThermoCylcle-Library: http://thermocycle.net/

[9] J. Emhofer, R. Zitzenbacher, Ch. Reichl: "Sound Source Extension Library for Modelica"; Vortrag: 12th International Modelica Conference, Prag, Tschechische Republik; 15.05.2017 - 17.05.2017; in: "Proceedings of the 12th International Modelica Conference", Modelica Association, (2017), ISBN: 978-91-7685-575-1; 8 S.

[10] D. Meisl: „Implementierung einer softwarebasierten Regelung einer Luft-Wasser-Wärmepumpe“, Diplomarbeit; Betreuung: G. Grabmair (FH Oberösterreich), J. Emhofer (AIT), 2017; Abschlussprüfung 20.09.2017

[11] Ch. Reichl: "Heat and Mass Transfer in Renewable Energy Systems"; Habilitationsschrift, Technische Unversität Wien, Faculty of Mechanical and Industrial Engineering, Institute of Fluid Mechanics and Heat Transfer, 2018.

[12] M. Popovac, J. Emhofer, E. Wasinger, P. Wimberger, R. Zitzenbacher, D. Meisl, F. Linhardt, N. Schmiedbauer, Ch. Reichl: "OpenFOAM implementation of algebraic frosting model and its applications on heat pump evaporators"; Vortrag: 13th IIR Gustav Lorentzen Conference 2018, Valencia, Spain; 18.06.2018 - 20.06.2018; in: "13th IIR Gustav Lorentzen Conference on Natural Refrigerants (GL2018). Proceedings", IIF/IIR, (2018), Paper-Nr. 1203, 9 S.

[13] N. Schmiedbauer, J. Emhofer, C. Köfinger, P. Wimberger, T. Fleckl, M. Gröschl, C. Reichl: "Aktive Störschallunterdrückung für Wärmepumpenanwendungen"; Vortrag: 43. Jahrestagung für Akustik, Kiel; 06.03.2017 - 09.03.2017; in: "Fortschritte der Akustik - DAGA 2017", Deutsche Gesellschaft für Akustik e.V. (DEGA), (2017).

[14] F. Linhardt: "Simultaneous measurements of sound, vibration, and flow, as well as determination of acoustic transfer functions in the context of air water heat pumps";

Diplomarbeit; Betreuung: M. Gröschl, Ch. Reichl; Technische Unversität Wien, Institut für Angewandte Physik, 2018; Abschlussprüfung: 19.03.2018.

[15] F. Linhardt, K. Alten, J. Emhofer, C. Köfinger, T. Fleckl, P. Wimberger, M. Gröschl, Ch. Reichl: "Charakterisierung der Schallabstrahlung von Luft-Wasser-Wärmepumpen mittels simultaner Hitzdrahtanemometrie, Vibrationsmessung und Schalldruckbestimmung"; Vortrag: 43. Jahrestagung für Akustik, Kiel; 06.03.2017 - 09.03.2017; in: "*Fortschritte der Akustik - DAGA 2017*", Deutsche Gesellschaft für Akustik e.V. (DEGA), (2017), S. 1238 - 1241.

[16] R. Zitzenbacher: *"Schallreduktionsmaßnahmen für Luft/Wasser-Wärmepumpen";* Diplomarbeit, Betreuung: M. Steinbatz, J. Emhofer; FH Oberösterreich, 2017; Abschlussprüfung: 20.09.2017.

[17] http://www.waermepumpe-austria.at/verein-waermepumpe-austria/leitfaden-zur-akustik-von-waermepumpen.html

[18] https://heatpumpingtechnologies.org/annex51/

[19] Wei W., van Renterghem T. and Botteldooren D. (2015) An-efficient-method-to-calculate-sound-diffraction-over-rigid-obstacles. EURONOISE 2015.

[20] Kasess C.H., Kreuzer W., and Waubke H. (2016a). Deriving correction functions to model the efficiency of noise barriers with complex shapes using boundary element simulations. Applied Acoustics;102:88–99, DOI: 10.1016/j.apacoust.2015.09.009.

[21] Reiter P., Wehr R. and Ziegelwanger H. (2017). Simulation and measurement of noise barrier sound-reflection properties. Applied Acoustics;123:133–42, DOI: 10.1016/j.apacoust.2017.03.007.

[22] Bathe K-J. (2014). Finite element procedures. 2nd ed. Englewood Cliffs, N.J: Prentice-Hall.

[23] Duhamel D. (1996). Efficient calculation of the three-three-dimensional sound pressure field around a noise barrier. Journal of Sound and Vibration;197(5):547–71, DOI: 10.1006/jsvi.1996.0548.

[24] van Renterghem T. (2014). Efficient Outdoor Sound Propagation Modeling with the Finite-Difference Time-Domain (FDTD) Method: A Review. International Journal of Aeroacoustics;13(5-6):385–404, DOI: 10.1260/1475-472X.13.5-6.385.

[25] Deckers E., Atak O., Coox L., D'Amico R., Devriendt H. and Jonckheere S. (2014). The wave based method: An overview of 15 years of research. Wave Motion;51(4):550–65, DOI: 10.1016/j.wavemoti.2013.12.003.

[26] Poysat P., Robinet B. and Lenaerts S. (2019). Simulation of noise propagation of outdoor HVAC/R unit in surrounding space. INTER-NOISE and NOISE-CON Congress and Conference Proceedings;259(4):5367–77, 2019.

[27] Ismail M.R. and Oldham D.J. (2003). Computer Modelling of Urban Noise Propagation. Building Acoustics;10(3):221–53, DOI: 10.1260/135101003322662023.

[28] BOSE (2020). Bose AR Beta. Bose Developer Portal. [Online]: https://developer.bose.com/bose-ar. (February 28, 2020).

[29] Apple Inc. (2020a). ARKit 3 - Augmented Reality. [Online]: https://developer.apple.com/augmented-reality/arkit/. (March 27, 2020).

[30] PTC (2020). Vuforia Engine. [Online]: https://engine.vuforia.com/engine. (March 25, 2020).

[31] DeepAR (2020). DeepAR. [Online]: https://www.deepar.ai/augmented-reality-sdk. (March 25, 2020).

[32] Kudan (2020). Kudan. [Online]: https://www.kudan.io/. (March 25, 2020).

[33] Amin D. and Govilkar S. (2015). Comparative Study of Augmented Reality Sdk's. IJCSA;5(1):11–26, DOI: 10.5121/ijcsa.2015.5102.

[34] Google (2020). ARCore, Google Developers. [Online]: https://developers.google.com/ar/ (March 27, 2020).

[35] Janssen J-K. (2020). Googles Augmented Reality: Tango ist tot, es lebe ARCore. heise online. [Online]: https://www.heise.de/newsticker/meldung/Googles-Augmented-Reality-Tango-ist-tot-es-lebe-ARCore-3817226.html

[36] Unity Technologies (2020). [Online]: https://unity.com/. (February 28, 2020)

[37] Unreal Engine (2020). What is Unreal Engine 4. [Online]: https://www.unrealengine.com/en-US/what-is-unreal-engine-4

[38] Apple Inc. (2020b). SceneKit, Apple Developer. [Online]: https://developer.apple.com/scenekit/. (February 28, 2020)

[39] Romilly M. (2020) 12 Best Augmented Reality SDKs. [Online]: https://dzone.com/articles/12-best-augmented-reality-sdks. (March 25, 2020)